Analysis of land cover changes of the Hartebeesthoek Radio Astronomy Observatory environment over five decades

by

Lisa Nyadzua Mbwia

(29386552)

Submitted in partial fulfilment of the requirements for the degree

MASTERS OF SCIENCE IN GEOINFORMATICS

In the

FACULTY OF NATURAL AND AGRICULTURAL SCIENCES
UNIVERSITY OF PRETORIA
PRETORIA

Supervisor: Prof. Ludwig Combrinck
Co-supervisor: Dr. Joel Botai

12 January, 2018

DECLARATION OF ORIGINALITY

This is to certify that the work is entirely my own and not of any other person, unless explicitly acknowledged (including citation of published sources). This work has not been submitted previously to the University of Pretoria or to any other institution for assessment or for any other purpose

Signed:

Date:

Research Supervisors

Supervisor:

- Prof Ludwig Combrinck, Hartebeesthoek Radio Astronomy Observatory (HartRAO), also at Department of Geography, Geoinformatics and Meteorology, University of Pretoria

Signed:
Date:

Co-supervisor:

- Dr. Joel Ondego Botai, South African Weather Services (SAWS) also at Department of Geography, Geoinformatics and Meteorology, University of Pretoria.

Signed:
Date:

ACKNOWLEDGEMENTS

All thanks go to Almighty God for His greatest favours in my life, to my Father: Simeon Arthur K Mbwia, Mother: Irene Lucy Kadama Mbwia, sister: Nelly Medza Nyamvula Mbwia and my entire family for their patience, guidance and always being source of my encouragement.

Supervisor: Prof. Ludwig Combrinck of the Hartebeesthoek Radio Astronomy Observatory (HartRAO), also at Department of Geography, Geoinformatics and Meteorology, University of Pretoria, for his dedication to support, guide and mentor me through my research career.
Co-Supervisor: Dr. Joel O Botai, South African Weather Services (SAWS), also at Department of Geography, Geoinformatics and Meteorology, University of Pretoria for guidance and mentorship.

I would also like to thank Dr. Francis W Nsubuga, Philemon Tsele and Paul Mmtomi Barasa and the entire Faculty of Natural and Agricultural Sciences University of Pretoria, and Anthony Njuguna Matheri (University of Johannesburg) for their mentorship, encouragement and support through my studies, research and technical support.

Much appreciation goes to the Hartebeesthoek Radio Astronomy Observatory (HartRAO), now part of the South African Radio Astronomy Observatory (SARAO) of the National Research Foundation (NRF) for research funding and conference support.

My appreciation is extended to Dr. Cecilia Kinuthia Njenga- Head of UNEP, Southern Africa for internship, consultancy and mentorship, Prof. Moses Azong Cho and Dr. Abel Ramoela at the Earth Observation group, Natural Resources and Environment, Council for Scientific and Industrial Research (CSIR), Dr. Henry Bulley- Assistant Professor of Geography & GIScience at Borough of Manhattan Community College, City University of New York, Dr. George Chirima at Agricultural Research Council (ARC) and Marianna Purnell General Manager at Argbiz Grain South Africa and the Rotary Club of Pretoria East South Africa for their guidance and contribution towards this research.

ABSTRACT

The focus of this research was to determine the multi-temporal land cover changes (LCC) of the Hartebeesthoek Radio Astronomy Observatory (HartRAO) environment over 5 decades. The HartRAO site is a strategic point in the mapping system of South Africa and acts as fundamental reference node in the International Terrestrial Reference Frame (ITRF). In this study, the conducted field assessments determined the land cover type of the study area and its environment. The use of aerial photographs, Google Earth images, satellite images and climate data were platforms to assess the LCC of the area and surroundings. The ENVI 5.1 software package was used to determine the LCC of the area from the Landsat TM and Landsat OLI satellites using image analysis. In addition, ArcGIS 10.2 was used to determine the hydrology of the area from the SRTM DEM file, provide a platform to view aerial photographs, and map out LC images determined from ENVI 5.1. Field assessments and demarcation of the study area were conducted using Google Earth images. The e-Water TREND software proved useful in determining the statistical significance of climate data over 5 the decade period. Microsoft Excel software was used to tabulate, generate graphs and charts from satellite image and climate data analysis.

According to the first objective the delineation of land cover types in the area was done using aerial photographs and field assessments of the study provided pictorial information to interpret land cover changes over the years of the study. Analysis of satellite data for the last 19 years also showed the changes in the land cover type and this was used to delineate land cover types. This was followed by satellite image processing and analysis over the last 19 years involving: image ratioing, image classification, change detection and accuracy assessment. Trends in rainfall and temperature of the area over period in the study area were determined using climatic data. Combining primary and secondary data to provide visual interpretation on the changes in land cover type and the seasonal variability were tools identified for the study. Hence there is a note that there is an increase in woody vegetation within HartRAO and changes in land cover and land use activity which does affect the changes in climate and land cover type.

Image processing: image ratioing of the Landsat TM and Landsat OLI images, the EVI, NDVI, NDBI and NDBaI spectral indices were used to give an overview of the land cover type and coverage in the area using the ENVI 5.1 software. A supervised image classification technique (pixel-based) was the ideal method for the Landsat images in this study this is because of the variability of the land cover type and when analysing will depend

on spectral information. The second and third objective focuses on remote sensing techniques, where there is an importance in removing biasness when comparing of classification algorithms to determine the most suitable algorithm for image classification. Therefore in the study maximum-likelihood (parametric) and support vector machine (non-parametric) classification algorithms were used to determine the extent of the land cover type in the area. Change detection in the study was used to determine the level of changes within and between the land cover type in the area of study. The aim of accuracy assessment is to determine the performance of the classification algorithms based on the land cover type. This proved that both performed well but SVM had a slightly higher accuracy with most land cover types and as part of the study, classification algorithms can be used individually while assessing specific land cover types.

By combining the first three objectives together, the results and discussion draw us to the fourth objective which brings us to what the changes in the land cover are caused by, and the rate of changes. In the results and discussion chapter by interpreting aerial photographs, Google Earth images and field assessment images and data illustrate there is an increase of vegetation within the immediate HartRAO environment. Surrounding areas of HartRAO indicate an increase in the proportion of agricultural land, and an increase of bare-lands due to mining activities within the surrounding areas. Outcomes from climatic data analysis conducted through the Mann-Kendall test using the e-Water TREND software indicated an increasing trend (mean annual temperatures) for the first normal of the years in the study. Climate data analysis of the second normal indicates that MATmax has an increasing trend. While MATmin and TAR are decreasing with a statistical significance at 95% confidence interval of Z = -2.194 and -1.998 respectively.

Utilizing satellite image analysis, image ratioing shows that there is an increase in vegetation ratio results in both NDVI and EVI. The NDVI images have higher values than EVI images for the Landsat TM while EVI have higher values in Landsat OLI as recognized in the summer images and winter images. The NDBI is higher which does not depict what the area is, as the built-up index reflects the milky-quartz rocks as built-up structures. The NDBaI is lower in the study. From the image classification results, the ML classification algorithm classifies forests and grasslands well. In SVM the scattered vegetation and grasslands are classified well. Both classification algorithms provide poor results for the milky-quartz with scattered vegetation and shale-rock with scattered vegetation. In relation to the accuracy of the ML and SVM classification, both had higher accuracies when classifying the Landsat

summer images with values above 90% and overall accuracy for winter images was between 82% - 90%. However, the July 2007 satellite images had the lowest overall accuracies for both ML and SVM classification algorithms. There is a negative annual rate of change for all the land cover types throughout the years (1960 - 2017) the study covers. A higher negative value from the rate of change is illustrated from the grassland cover type for all summer and winter images used in the study. The forestland cover and built-up land cover type has an increase in negative change noted from the classification of the winter images. Comparison of both classification algorithms using Chi-square test illustrate no statistical significance, which concludes that both perform equally well in terms of overall accuracy and land cover.

TABLE OF CONTENTS

LIST OF ACRONYMS

AISA	Airborne Imaging Spectrometer for Applications
ANN	Artificial Neural Network
ASTER	Advanced Space borne Thermal Emission and Reflection Radiometer
CSIR	Council for Scientific and Industrial Research
DEM	Digital Elevation Model
ETM+	Enhanced Thematic Mapper Plus
EVI	Enhanced Vegetation Index
GPS	Global Positioning System
HartRAO	Hartebeesthoek Radio Astronomy Observatory
LC	Land Cover
LCC	Land Cover Changes
LIDAR	Light Imaging, Detection and Ranging
LU	Land Use
MATmax	Mean Annual Maximum Temperature
MATmin	Mean Annual Minimum Temperature
MIR	Middle Infrared
ML	Maximum likelihood
MNDWI	Modified Normalized Difference Water Index
MODIS	Moderate-resolution Image Spectroradiometer
MSS	Multispectral Scanner System
NASA	National Aeronautics and Space Administration
NDBaI	Normalized Difference Bareness Index
NDBI	Normalized Difference Built-up Index
NDVI	Normalized Difference Vegetation Index
NDWI	Normalized Difference Water Index
NIR	Near Infrared
NRF	National Research Foundation
OLI	Operational Land Imager
RADAR	Radio Detection and Ranging
SAR	Synthetic Aperture Radar
SONAR	Sound Navigation and Ranging
SRTM	Shuttle Radar Topography
SVM	Support vector machines
SWIR	Short Wave Infrared
TIR	Thermal Infrared
TM	Thematic Mapper
TAR	Total Annual Rainfall

LIST OF COMPUTATIONAL TOOLS

1. ArcGIS 10.2- Mapping software, location platform and spatial data analytics
2. ENVI 5.1- Image processing
3. e-Water TREND Toolkit- statistical testing for climate data trend in time series
4. Microsoft Excel- Window version support program for visual basic application (VBA) and support charts, graphs and histograms

LIST OF TABLES

LIST OF FIGURES

1 INTRODUCTION

This chapter introduces effects of land cover analysis on a spatial, temporal and magnitude aspect. It focuses on the issues that affect land cover changes and specific land-use activities in an area. The intention is to look at the historical changes and the impact that the Hartebeesthoek Radio Astronomy Observatory (HartRAO) now South African Radio Astronomy Observatory (SARAO) has had on the area. It also focusses on the importance of HartRAO in South Africa and internationally as an observatory and why the land cover change analysis is necessary for the area as noted in the problem statement and the aim and objectives

1.1 Introduction

Multi-temporal land cover change (LCC) analysis has become a vital aspect of resource planning, allocation and development (Yang and Lo, 2002). The function of multi-temporal land cover change analysis is to monitor impacts of land cover (LC) changes that occur with regards to its spatial extent and magnitude (Sakai *et al.*, 2015). The spatial extent of land cover change is usually determined by how much impact there is from anthropogenic or natural activities which gradually have effects on the landscape. The extent and impact of natural and anthropogenic forces on the land cover also determine the magnitude of the land cover change with concomitant effects on terrestrial ecosystems (Abbas, 2012; Badreldin, Frankl and Goossens, 2013). Spatial and magnitude factors influence the original landscape, which leads to land cover transformations, that could be beneficial or detrimental depending on the land use at a given time on a landscape extent (Hlatywayo and Masvosve, 2015). Some land cover transformations can lead to regeneration and degradation of forest landscapes (Southworth, 2004), species movement (Gillespie *et al.*, 2008; Jones *et al.*, 2009), biodiversity and ecological changes (Pettorelli *et al.*, 2005), and socio-economic impacts (Xiuwan, 2002; Butt *et al.*, 2015) just to name a few, which usually have effects on habitats. As suggested, land cover transformations usually result in a local and even global environmental change (Latham, 2008). Researchers, land planners and policy makers have noted that with land cover changes, which leads to environmental change, there is a need to monitor, detect and manage resources through land cover change analysis (Xu, 2007). Thus it is important to carry out land cover analysis on the Earth's surface, for the purpose of observing modifications of the landscape; to evaluate, monitor and plan the resources in the environment (Kennedy *et al.*, 2009).

Numerous multi-agencies have established projects with long-term operational systems for land cover monitoring (Turner II, Lambin and Reenberg, 2007). In addition to acquiring information from these long term operational systems, the data becomes beneficial when predicting natural disasters (Yang, Weisberg and Bristow, 2012) and during ecological studies focussing on the improvement of vegetation growth and re-growth (Nagendra, Munroe and Southworth, 2004). Land cover change monitoring and data capturing also provide more accurate datasets that assist in describing the geographical distribution of the LC at different scales (Tilahun, 2015) while at the same time reducing costs for monitoring land cover locally, regionally and globally (Dwivedi, Sreenivas and Ramana, 2005; Gong *et al.*, 2013).

Techniques and instrumentation of LCC analysis are continuously improving. Two techniques and their continuous development that allowed for major progress in this field have been the evolution and use of aerial photographs and satellite imagery using remote sensing techniques. Capturing land cover images through aerial photography using aircraft and unmanned aerial vehicles (UAV's), and application of photogrammetry have illustrated the use of ancillary data for data collection and evidence based analysis (Chen *et al.*, 2012). In turn, the development of satellite imagery as a logical consequence of aerial photography has helped to form a strong basis for various LCC analyses (Aguirre-Gutiérrez, Seijmonsbergen and Duivenvoorden, 2012).

Using remote sensing techniques and technology, there has been improvement in updating land cover change information analysis, due to availability and the authenticity of more accurate and higher resolution data (Li, Jiang and Feng, 2013; Li and Chen, 2014). Multi-temporal and multi-spectral datasets are used in LCC studies, where satellite imagery varies in terms of the spatial spectral and temporal attributes. Utilisation of different satellite imagery types (hyper-spectral, multi-spectral), have allowed researchers and analysts to derive different classification and change detection algorithms of which each has their own merits and demerits, and there is no single optimal approach that is applicable to all the cases in LCC studies (Wedderburn-bisshop *et al.*, 2001; Lu *et al.*, 2004a; Vicente-Serrano, Pérez-Cabello and Lasanta, 2008). To obtain information with regards to an area, one should consider the land cover of the area, type of analysis envisaged, the availability of satellite data and other resources (Lu *et al.*, 2004a). After this process, remote sensing techniques can be applied and a final product generated to predict the state of the environment (Almeida-Filho and Shimabukuro, 2002; Tewkesbury *et al.*, 2015).

Through routine updates of satellite information and improvement of satellite image data, researchers have been able to develop LCC techniques from pre-to post-classification. Pre-processing techniques include ancillary data collection, field assessment, geometric correction (Vogelmann *et al.*, 2001; Vicente-Serrano, Pérez-Cabello and Lasanta, 2008; Roy *et al.*, 2014), radiometric correction (Song *et al.*, 2001; Schroeder *et al.*, 2006; Roy *et al.*, 2014) and calibration (Vogelmann *et al.*, 2001; Chander, Markham and Helder, 2009; Roy *et al.*, 2014). Classification techniques include unsupervised (computer based and automated) (Duda and Canty, 2002) and supervised classification (computer based but human interpretation/intervention included) techniques and post classification techniques include change detection (Berberoglu and Akin, 2009; Huang *et al.*, 2015) and accuracy assessments (Foody, 2002, 2008, 2010a, 2010b; Foody and Mathur, 2004; Foody, Mathur, *et al.*, 2006).

1.2 Problem Statement

Changes in LC can be attributed to Land Use (LU) changes and climate conditions (Mas, 1999a; Lu *et al.*, 2004a; Chen *et al.*, 2006). Land use activities include agricultural activities (Kalnay and Cai, 2003; Vancutsem *et al.*, 2010; Atzberger, 2013; Latham *et al.*, 2014; Akar and Güngör, 2015), mining, industrial and residential built-up areas (Townsend *et al.*, 2009; Adam, Mutanga and Rugege, 2010), which have both an effect on the livelihood of humans and the ecological footprint of an area (Herold, Scepan and Clarke, 2002; Hlatywayo and Masvosve, 2015; Khaing, Htun and Lwin, 2016). Studies have shown that a change in land use can be beneficial and detrimental (Giordano and Filippi, 1993; Wu, 2008). This of course depends on one's point of view, e.g. an economist and a conservationist will interpret the question whether an increase in food production versus the reduction of natural habitat is beneficial, differently. For example, an increase in agricultural land leads to more production of food and resources to the community (Pinstrup-Andersen, 2009; Godfray *et al.*, 2012), while mining and other industrial activities have increased the economical capacity of an area (Si *et al.*, 2010). Increase in residential and recreational places have provided homes for people in urban and rural areas (Quigley, 1998). However the detrimental aspect is that the use of the specific land use activities and the ability to restore it to the original land cover has proved to be a challenge amongst the land users and land cover resource users (Foley, 2005).

The Gauteng Province contains highly urbanised areas especially within Pretoria and Johannesburg. The vegetation type is mainly Highveld, covered with grassland, acacia trees, and low shrubs. The north-western parts of the province include the Witswatersberg. Towards

the north-west side of the Gauteng Province, the land changes to vast agricultural land. The location of the Hartebeesthoek Radio Astronomy Observatory (HartRAO), a National Research Facility operated under the auspices of South Africa's National Research Foundation and currently the only major radio astronomy facility in Africa, is 50 km west of Johannesburg and north of Krugersdorp, in the foothills of the Witwatersberg. HartRAO is merging with SKA-SA, the South African component of the Square Kilometre Array (SKA) and will be merged to create the South African Radio Astronomy Observatory (SARAO) during 2017.

1.3 Significance of the Research

HartRAO was built in 1961 by the National Aeronautics and Space Administration (NASA) and was then known as Deep Space Instrumentation Facility 51 (DSIF51). It used to be operated by the South African Council for Scientific and Industrial Research (CSIR) on behalf of NASA, and in 1974, after its closure it became a radio astronomy observatory. Before the construction of HartRAO, the land on which the radio astronomy observatory is situated used to be agricultural land. Instead of mainly agricultural use, the use has changed to hosting radio telescopes for astronomy and space geodesy, as well as other equipment. Over the years, the surrounding area (outside the main observatory fenced-in area) has recovered to natural vegetation; however it is composed of woody vegetation mostly comprising the acacia species and natural Highveld grass. There is a reduction of naturally occurring veld fires in this area (burning is now controlled by yearly firebreaks), which may have resulted in more woody vegetation cover and less presence of grassland. Vegetation cover has shifted in some areas from mostly grass to bare-soil and bare-rock in close proximity to woody areas. This paves the way to soil erosion and presence of exposed sedimentary rocks and gully formations along the streams.

Researchers have more often analysed land cover changes on areas where the terrain is fairly level. Hilly landscapes prove to be a challenge in mapping out land cover. There is a need to determine the necessary methods and importance of mapping land cover across all types of terrain. The use of optical sensors has made it easier to study land cover changes due to the spectral resolution of the sensors. Mapping multi-temporal changes also assists planners to know the difference between historical and current land cover. Apart from human induced land cover changes, it is necessary to also know the impact of climatic variables on specific land cover and their effects. Climatic variables such as rainfall and temperature influence the biophysical components of varying land cover types. Determining the land cover changes at

HartRAO in relation to climatic variability, will allow us to ascertain the climatic trends that have influenced the land cover type over five decades. Comparisons of parametric and non-parametric classification algorithms are used to illustrate which classification method best suits the HartRAO specific land cover change study. The study focusses on assessing land cover changes with relation to climate variability as well as human activities and determines the best-suited classification algorithms to delineate and detect land cover changes. This is attained through the aims and objectives listed in Section 1.4.

1.4 Aims and Objectives

1.4.1 Aims

The aim of this research is to determine multi-temporal land cover changes over the period of 5 decades at the HartRAO site. We assessed the land cover changes in relation to climate variability and human induced changes This was done through the comparison of classification algorithms on satellite imagery to determine land cover and using change detection analysis and statistical analytical methods to determine the best classification algorithms. Climate data analysed in the study was to show the effect of climate on the area as land cover changes. The seasonal variabilities also affect the land cover type in the area.The HartRAO site is a strategic point for mapping in South Africa. The position of HartRAO acts as fundamental node in the International Terrestrial Reference Frame (ITRF). The location of the observatory is within the Maropeng area, which has been named the “Cradle of Human Kind”. This area is rich in flora and fauna and considered part of the conservation initiative within the Gauteng region. Mapping the HartRAO provides information about vegetation regeneration within the area.

1.4.2 Objectives

1. Delineate land cover types and their variability, spanning a period of 5 decades, using satellite image analysis and climatic variability.
2. Compare the performance of parametric and non-parametric pixel-based classification algorithms on Landsat TM and Landsat 8 imagery in change detection.
3. Determine which classification techniques used in the study works best for hilly landscapes, as this is the prevalent landscape type of the area of investigation.
4. Establish the relationship between the rate of land cover change in relation to climate and land use at the HartRAO site.

2 LITERATURE REVIEW

This chapter describes what land cover is and defines it contextually according to land cover changes within a remote sensing field. It also establishes the differences between land use and land cover which are terminologies used interchangeably in multi-disciplinary fields. These terms are still discussed on every interdisciplinary level as they are interpreted differently. Thus there is a need to define it according to the research and objectives relating to the remote sensing of the environment. Land cover change analysis subsection provides various studies done to conduct land cover changes and some of the techniques used as a detailed format on how the methodology of the study will be conducted. In the same chapter a detailed outlook of the various remote sensing techniques, the use of other data such as climate, aerial photographs and digital elevation models can be used to do land cover change analysis.

2.1 Land Cover

Land cover is the availability and variability of biophysical and chemical components, on and below the earth's surface (Di Gregorio, 2016). Availability of land cover on the earth surface is considered by its spatial extent (Mumby and Edwards, 2002; Li and Yeh, 2004; Myint *et al.*, 2011), magnitude coverage (Li and Yeh, 2004; Lasanta and Vicente-Serrano, 2012; Badreldin, Frankl and Goossens, 2013) and multi-temporal conditions (Lyle, Lewis and Ostendorf, 2013; Hlatywayo and Masvosve, 2015; X. Li *et al.*, 2015; Sakai *et al.*, 2015). One also has to consider that land cover terminology has been used interchangeably with land use, where land use is the transformation of the land cover for a specific activity at a given moment in time (Turner II, Lambin and Reenberg, 2007; Schneider and Woodcock, 2008; Hlatywayo and Masvosve, 2015). Land cover generally constitutes natural variables such as vegetation, water, soils; and land use terminology can be described through the activities conducted on the landscape which include (Latham, 2008; Latham *et al.*, 2014) agriculture, mining and urban areas (infrastructure, buildings, transport) (Papers, 2007; Latham, 2008; Latham *et al.*, 2014; Di Gregorio, 2016). These two terminologies contribute to the spatial, temporal and magnitude aspect of land cover conversions and transformations (Mcgarigal, 2001; Herold, Scepan and Clarke, 2002; Southworth, Nagendra and Tucker, 2002; Nagendra, Munroe and Southworth, 2004; Kennedy *et al.*, 2009; Uuemaa *et al.*, 2009). Anthropogenic and natural activities have an influence on the attributes of land cover changes (Peters *et al.*,

2002; Kalnay and Cai, 2003; Metternicht, Hurni and Gogu, 2005; Muttitanon and Tripathi, 2005; Foulds and Macklin, 2006; Jobin *et al.*, 2008; Joyce *et al.*, 2009; Santillan, Makinano and Paringit, 2011; Roy *et al.*, 2014). In addition to anthropogenic activities possibly affecting land cover in an adverse manner, land use resulting from human activities could have a positive impact through socio-economic activities generated from land cover. Socio-economic activities include; food security (Cleasby *et al.*, 2014), water conservation (Blignaut and Van Heerden, 2009; Department of Water and Sanitation, 2009) and energy generation (Canadell *et al.*, 2007) just to name a few. There is also an indirect contribution of land use to socio-economical welfare. An example is the establishment of scientific research institutions such as optical and radio astronomy observatories, for research and knowledge generation (Martin and John, 1983; McCray, 2000), which indirectly contribute to economic wellbeing through various products and services.

2.2 Land Use and Land Cover

Nonetheless, if land use and land cover facets are not monitored and evaluated, they could lead to irreversible land cover changes, such as depletion in ecosystem services (Raudsepp-Hearne *et al.*, 2010; Barbero *et al.*, 2016), changes in climate variables (Below *et al.*, 2012; Hollmann *et al.*, 2013), transformation of land cover (degradation of forest to forest patches) (Buyantuyev and Wu, 2010; Swetnam *et al.*, 2011; Lawrence *et al.*, 2012; Romero-Ruiz *et al.*, 2012; Sterling, Ducharne and Polcher, 2013; Barbero *et al.*, 2016) and also to a loss in country revenue (Potapov *et al.*, 2012). Apart from anthropogenic activities, land cover can also be affected by natural activities such as frequency of veld fires, seismic activities, heavy torrential rainfall and floods (Metternicht, Hurni and Gogu, 2005; Joyce *et al.*, 2009; Gitas *et al.*, 2012). Veld fires have a positive impact on plant growth as noted within the fynbos and grass species for it allows for new seedlings to grow if it is in a controlled environment. Uncontrollable veld fires result in species loss (Nyamadzawo *et al.*, 2013). Seismic activities, which could include earthquakes, tsunamis, and volcanic activity also contribute to land transformation (Metternicht, Hurni and Gogu, 2005; Gillespie *et al.*, 2007; Botai, Combrinck and Sivakumar, 2009; Taylor, Pohl and Genderen, 2010, 2010; Yu and Gong, 2012). These areas could develop a distinctive pattern, which is usually used as a point of reference in studies for researchers and may be a tourist attraction site. Negative impacts of seismic activities could lead to a loss in flora and fauna species and richness (Metternicht, Hurni and Gogu, 2005; Botai, Combrinck and Sivakumar, 2009). With proper drainage facilities, water

from torrential rainfall could be a resolve to drought situations (Meek and Hatfield, 1994; Neuenschwander, 2007; Bonan, 2008; Townsend *et al.*, 2009; Bindschadler *et al.*, 2010). This water can be stored in dams. A lack of drainage infrastructure could lead to gully and soil erosion, crop damage, and destruction of infrastructure (Bian *et al.*, 2010). Therefore there is a need to carry out land cover change studies for monitoring, evaluating and decision making (Hansen and Loveland, 2012).

When one considers monitoring land cover changes it is important to note the spatial, temporal and magnitude bearing and impacts (Nagendra *et al.*, 2004; Kuemmerle *et al.*, 2006). Researchers such as (Bucini and Lambin, 2002; Uuemaa *et al.*, 2009; Dingle Robertson and King, 2011; Dupuy *et al.*, 2012)) have investigated landscape fragmentation with regards to the spatial extent of the land cover (Sawaya *et al.*, 2003; Schneider *et al.*, 2008; Butt *et al.*, 2015). Multi-temporal land cover changes such as forest regeneration (Wilson and Sader, 2002; Cingolani *et al.*, 2004; Southworth, 2004; Ruelland, Levavasseur and Tribotté, 2010); urban developments (Mahavir, 2000; Ward, Phinn and Murray, 2000; Xu, 2007; Nairobi, 2012; Butt *et al.*, 2015; Hlatywayo and Masvosve, 2015); conversion of land cover to mining environments (Haibin and Zhenling, 2010; Si *et al.*, 2010; Schueler, Kuemmerle and Schröder, 2011); or inter-land use/land cover conversions (Herold, Scepan and Clarke, 2002; Dewan and Yamaguchi, 2009b; Lasanta and Vicente-Serrano, 2012; Yousefi *et al.*, 2015) have been used to determine land cover changes over years and what could be the reasons behind these changes. Magnitude impacts are described as the extent of the effect land use has on the ecosystem resources, human activities and resource generation (Duro *et al.*, 2007; Zhou, Li and Kurban, 2008). Environmental and climate change are leading drivers which contribute to the magnitude impacts on land cover (Beck *et al.*, 2006; Modarres and de Paulo Rodrigues da Silva, 2007; Serra, Pons and Saur, 2008; Vinukollu *et al.*, 2011; Nsubuga, Olwoch and Rautenbach, 2014). Altogether, these three aspects go hand in hand when monitoring and delineating land cover for change detection.

2.3 Land Cover Change Analysis

Along these lines, monitoring land cover through Land Cover Change (LCC) analysis and reviews have been documented by many researchers worldwide (Singh, 1989; Coppin *et al.*, 2004; Kennedy *et al.*, 2009). The analysis of LCC is done through multi-disciplinary approaches, where there are consolidation of research techniques and studies (Muñoz-Villers and López-Blanco, 2008). Land cover change analysis has resulted in an accumulation of information and exploration of land cover information, which provides a driving force into an

integrated approach (Singh, 1989; Kennedy *et al.*, 2009; Mercier *et al.*, 2012). Likewise, it is important to note that applicability of LCC techniques vary across the globe due to the varying topography, intention of the research and significance to the person carrying out the study (Ruelland, Levavasseur and Tribotté, 2010; Ruelland *et al.*, 2011; Nutini *et al.*, 2013).

Therefore the basics of land cover change analysis encompass field-based assessments (Pradhan, 2001; Ho, Umitsu and Yamaguchi, 2010; Otunga, Odindi and Mutanga, 2014), the use of archived data (Ho, Umitsu and Yamaguchi, 2010; Otunga, Odindi and Mutanga, 2014) and LCC detection techniques. Field-based assessments include: ground-truthing (Yan *et al.*, 2006), validation (Zhu and Blumberg, 2002) and data collection (Wedderburn-bisshop *et al.*, 2001; Sawaya *et al.*, 2003; Lu and Weng, 2007) for investigation. Archived data includes aerial photographs (Mas, 1999b; Blaschke *et al.*, 2000; Herold, Scepan and Clarke, 2002; Calvo, Ciraolo and Loggia, 2003; Xiao and Weng, 2007; Manandhar, Odeh and Ancev, 2009; Hlatywayo and Masvosve, 2015), climate data (Easterling, 2000; Feng, Hu and Qian, 2004; Gong *et al.*, 2013; Hollmann *et al.*, 2013) and multi-temporal satellite imagery (Coppin *et al.*, 2004; Ning *et al.*, 2006; Lu *et al.*, 2007; Wulder *et al.*, 2008; Wasige *et al.*, 2012; Rokni *et al.*, 2015). Land cover change detection techniques such as earth observation, Geographical Information Systems (GIS) and space geodesy play a major role in LCC analysis (Blaschke *et al.*, 2000; Xiuwan, 2002; Benz *et al.*, 2004; Hoffmann and Sander, 2006). Earth observation includes remote sensing techniques such as image preprocessing, classification and post classification (Janzen, Fredeen and Wheate, 2006; Kennedy *et al.*, 2009; Mulder *et al.*, 2011; Mercier *et al.*, 2012; Sharma, Pandey and Nathawat, 2012). The use of GIS techniques include spatial and multi-temporal LC maps (Domenikiotis *et al.*, 2002; Shalaby and Tateishi, 2007; Rozenstein and Karnieli, 2011; El-aziz, 2013).

Examples of field-based assessment using ground-truth estimations are noted in crop growth estimations, analysis of high altitude regions and applications for natural resource planning for managers (Pradhan, 2001; Quincey *et al.*, 2005; Kennedy *et al.*, 2009). Validation of field based data are illustrated in Parker *et al.*, (2003); Kennedy *et al.*, (2009); Foody, (2010); Dingle Robertson *et al.*, (2011) with regards to training data sets for classification. The collection of ground control points for accuracy assessment (Chen *et al.*, 2002; Gorokhovich and Voustianiouk, 2006; Yan *et al.*, 2006; Shalaby and Tateishi, 2007; Dewan and Yamaguchi, 2009; Foody, 2010; Ghorbani, Mossivand and Ouri, 2012; Sun *et al.*, 2013; Bahari, Ahmad and Aboobaider, 2014; Zhu and Woodcock, 2014; Yousefi *et al.*, 2015) and georeferencing is important and this process is also used as a validation method (Foody,

2002; Fonji and Taff, 2014). The process of delineating LC classes uses land cover classification schemes generated from field analytical methods (Baldyga *et al.*, 2007; Abd El-Kawy *et al.*, 2011).

Aerial photographs have also played a major role in LCC mapping (Kamusoko and Aniya, 2009; Gerard *et al.*, 2010), monitoring, and this is usually conducted on a multi-temporal basis, as documented in Baraldi and Parmiggiani (1990); Ridd and Liu, (1998); Hodgson *et al.*, (2003); Guindon *et al.*, (2004); Rocchini and Di Rita, (2005); Ruelland *et al.*, (2011); Hlatywayo *et al.*, (2015).

The current combination and use of climate data for LCC analysis has been a driving factor in improving remote sensing analysis and approaches (Feddema, 2005; McAlpine *et al.*, 2009; Lawrence *et al.*, 2012). Climate data have been used in observational analysis and in depth analysis within the climate modelling aspect (Peterson *et al.*, 1998; Lentile *et al.*, 2009; Hollmann *et al.*, 2013; Mares *et al.*, 2015; Mellor *et al.*, 2015). Analysis of climate data for monitoring land cover changes are noted in Ikeda *et al.*, (1999); Mellor *et al.*, (2015) for grassland estimation and machine learning techniques for forest land cover respectively. As said initially, the use of climate data in remote sensing has been integrated into the core of scientific LCC (Minale and Kameswara Rao, 2012) with basic examples on rainfall and temperature variables. Rainfall and temperature affect the land cover in an area which will show if there is vegetation growth (Nemani *et al.*, 2003; Pettorelli *et al.*, 2005; Helldén and Tottrup, 2008; Nie and Xu, 2013), increase of a dry landscape area, and changes in climate variables which can lead to erosion. The presence of built-up features can affect the micro climate of the area (Herrmann, Anyamba and Tucker, 2005; Helldén and Tottrup, 2008). The use of raw climate data to calculate statistical values assists in determining climatic trends and variability of an area, and in this way shows that climate is a contributing factor to land cover changes.

2.4 Remote sensing techniques for land cover change analysis

Satellite image analysis derives from remote sensing techniques, which is defined as the acquisition of images of the earth's surface through satellite image observation methods (İlsever and Ünsalan, 2012). Remote sensing can be used in a range of disciplines where the satellite images and sensors are optimally used to analyze the changes on the earth's surface including land use and land cover changes (Ji *et al.*, 2015). Remote sensing techniques range from atmospheric studies to deep sea ocean analysis. This process is used in monitoring

(Munyati, 2000, 2004; Collado, Chuvieco and Camarasa, 2002; Metternicht, Hurni and Gogu, 2005), modelling (Blaschke *et al.*, 2000; Blaschke, 2010), future analysis (Weng, 2002) and planning (Bocco, Mendoza and Velázquez, 2001; Li and Yeh, 2004; Martinuzzi, Gould and Ramos González, 2007). There are advantages and disadvantages of using remote sensing techniques. Advantages include collection of in-situ data where there is no direct contact with target area of study (Fingas and Brown, 2014; Jonard *et al.*, 2015; Vander Jagt *et al.*, 2015). Another advantage is that collection techniques can be active, such as (Light Imaging, Detection and Ranging (LIDAR) and Radio Detection and Ranging (RADAR)) and passive (photographic image capture) (Gillespie *et al.*, 2007, 2008; Mulder *et al.*, 2011; Jonard *et al.*, 2015). Therefore systematic data collection of a certain phenomenon is programmed to be acquired by the sensor for a selected period of time (Kim, Evans and Iversen, 2008; Berni *et al.*, 2009). Collection of satellite data provides attribute data, such as height (Hyde *et al.*, 2006), temperature (Small, 2006), moisture (Goward, Xue and Czajkowski, 2002) and biomass (Huete *et al.*, 2002; Flanders, Hall-Beyer and Pereverzoff, 2003; Potapov *et al.*, 2012; Mellor *et al.*, 2015). Satellite image analysis is used to conduct scientific investigations such as environmental changes on large areas (Gupta *et al.*, 2006; Kennedy *et al.*, 2009). This can be analyzed through variance in temporal data (Stefanov, 2001; Kerr and Ostrovsky, 2003; Ning *et al.*, 2006; Röder *et al.*, 2008) and seasonal changes (Inoue *et al.*, 2002; Roerink *et al.*, 2003; Herrmann, Anyamba and Tucker, 2005; Helldén and Tottrup, 2008).

Disadvantages of satellite image analysis and systems include their inherent high costs and accompanying infrastructure which could be too costly (Baltsavias, 2002; Hoffmann and Sander, 2006; Sutton, Elvidge and Ghosh, 2007). Some provided satellite data may not give full details of a particular area with regards to temporal, spatial and spectral resolution which could be economically beneficial. Powerful satellite sensors such as Synthetic Aperture Radar (SAR), RADAR, LIDAR and Sound Navigation and Ranging (SONAR), which emit their own active electromagnetic radiation, can lead to information biases, through additional spectral data on the target phenomenon (Hyde *et al.*, 2006; Aly, Bonn and Magagi, 2007; Marghany and Hashim, 2011; Jia *et al.*, 2012). Considering such sensors, sophisticated equipment and design is usually employed for a specific sensor (Sutton, Elvidge and Ghosh, 2007). There are instances where a sensor system fails to launch, such as Landsat 6, which failed to reach orbit. Another example is Landsat 7 ETM+ that experienced a fault in its scan line corrector; this has led to missing information within a period of time (Markham *et al.*, 2004; Chander, Markham and Helder, 2009). The level of skill development due to

availability of data to produce better results can be hindered due to data cost especially in developing countries (Shevyrnogov, Trefois and Vysotskaya, 2000; Wulder *et al.*, 2008; Chander, Markham and Helder, 2009; Abd El-Kawy *et al.*, 2011; Hansen and Loveland, 2012; Roy *et al.*, 2014; Sakai *et al.*, 2015).

Nonetheless, for LCC analysis to be carried out using satellite data a researcher needs to identify the problem with an area of interest (Weyerhaeuser, Wilkes and Kahrl, 2005; Nagendra, Pareeth and Ghate, 2006). Steps in land cover change analysis includes identification of problem and site for analysis, determining the concept that will be used to carry out the analysis, identifying the satellite data, archived data and field based measurements to determine change, a methodological flow of data analysis used and why and finally an output for the result with recommendations (Lu *et al.*, 2007; Taylor *et al.*, 2010; İlsever *et al.*, 2012; Telcan, 2013).

After the necessary concept note has been developed and relevant field observation techniques illustrated, data is collected for image processing and change detection techniques to be used to highlight LCC (Almeida-Filho *et al.*, 2002; Lu *et al.*, 2007; Hlavac, 2011; Robert A. Schowengerdt, 2012). Conceptually, image processing includes pre-processing as noted in Chen *et al.*, (2006), image classification and post-classification in Muttitanon *et al.*, (2005). Pre-processing methods include editing satellite data by removing any atmospheric or sensor data noise (Munyati, 2000; Weng, Lu and Schubring, 2004; Santillan, Makinano and Paringit, 2011; Butt *et al.*, 2015) through a method called radiometric correction (Muller-karger and Andre, 2001; Weng, 2002; Chander *et al.*, 2006; Xian *et al.*, 2009) and calibration (Rozenstein *et al.*, 2011), and geometric correction (Riaño *et al.*, 2003; Vicente-Serrano *et al.*, 2008; Dewan and Yamaguchi, 2009). Image classification methods include classification algorithms to delineate LC types (Singh, 1989; Eastman, 2001; Otukei and Blaschke, 2010; Faid and Abdulaziz, 2012). This could be through unsupervised (Helmer and Ruefenacht, 2005; Cleve *et al.*, 2008; Butt *et al.*, 2015), supervised (Muttitanon and Tripathi, 2005; Yuan *et al.*, 2005; Zhou, Li and Kurban, 2008; Otukei and Blaschke, 2010) or a hybrid classification (Lu *et al.*, 2007; Xiao *et al.*, 2007; Faid *et al.*, 2012; Butt *et al.*, 2015) The methods that use parametric and non-parametric classification algorithms have been mentioned in (Serpico *et al.*, 1996; Hubert-Moy *et al.*, 2001; Bruzzone *et al.*, 2002; Keuchel *et al.*, 2003; Mondal *et al.*, 2012). Post-classification techniques involve the change detection and accuracy assessment through ground-truthing and validation using field based assessments according to Weng, (2002); Canty and Nielsen, (2006); Lu *et al.*, (2007);

Neuenschwander, (2007); Muñoz-Villers *et al.*, (2008); Wu *et al.*, (2012); Butt *et al.*, (2015). Therefore it is important to carry out image pre-processing for satellite image analysis before image data processing in order to achieve accurate results.

2.4.1 Image processing

The most basic image processing method that provides an overview of LC types is the image ratioing technique. Image ratioing is a qualitative relation of two or more spectral bands to provide a floating value that ranges from -1 to 1 (Weiss *et al.*, 2004). An example of image ratioing is the analysis of vegetation using the vegetation indices; this includes the use of two bands, the red and near infrared (NIR) bands to show changes in land cover through rational numbers (Lunetta *et al.*, 2006). Sequentially, this allows one to view the various vegetative properties of and provides a way to compare the phenology of the vegetation on the land surface (Huete *et al.*, 2002). There are two of the vegetation indices selected for this study; the Enhanced Vegetation Index (EVI) and Normalized Difference Vegetation Index (NDVI) as illustrated in Jung and Chang (2015). According to Gao *et al.* (2000) the EVI quickly picks up quantities of the vegetative canopy structure such as the canopy type, the leaf area index, plant physiognomy and canopy architecture. The EVI index has been used mostly in MODIS data (Beck *et al.*, 2006) for satellite imagery for global LCC studies (Jiang *et al.*, 2008). Whereas NDVI is more suitable for detecting the level of greenness by being sensitive to chlorophyll in the type of vegetation according to Gao *et al.* (2000). Just like any mathematical formula in remote sensing, the performance will vary based on the satellite imagery, its spectral and radiometric resolution and the methods that have been used to compensate for the spatial component of imagery (Jiang *et al.*, 2006; Sesnie *et al.*, 2011). For global LC studies and vegetative studies, EVI and NDVI have proved to be effective tools that complement each other especially in analyzing vegetative changes on a landscape and extracting canopy biophysical parameters (Jackson *et al.*, 2004). The use of vegetation indices has played a major role in monitoring vegetation variations (Pettorelli *et al.*, 2005).

According to the analysis in Pettorelli *et al.* (2005), the use of NDVI is documented for ecological studies to determine environmental changes. This method was detailed to monitor vegetation and plant responses to environmental changes. It is noted that NDVI values increase with healthy vegetation. The NDVI data provides an indication of the spatial distribution of an area, carbon dioxide fluxes and bio-zone. A second method was to determine trophic interaction; this was used to correlate NDVI data to animal species distribution. The third technique was to look at the NDVI method to generate a time series for

ecological measures. The end result was to determine if NDVI could successfully be applied in multi-temporal and spatial analysis as widely used for the tropic interactions within aspects of vegetation dynamics, habitat fragmentation and biodiversity distribution.

Weiss *et al.* (2004) evaluated NDVI in a diverse semi-arid setting, where it was reported that NDVI is influenced highly by the presence of sparse vegetation, where uncertainties of NDVI values can lead to misinterpretation. Results in this document also state the influence of climate variability in inter-annual and seasonal vegetation variability. Ground measurements and NDVI analysis were used to determine the spectral changes in New Mexico which indicated the response to NDVI analysis was higher during spring time and summer, corresponding to the new monsoon climate and El Nino-Southern Oscillations. Ground measurements correspond to the ground measurements.

Work done by Villamuelas *et al.* (2016) evaluated how the EVI can be used as a product to assess the nutritional capacity of the *Pyrenean chamois* and general remote sensing for monitoring and herbivorous populations. Therefore, EVI in the analysis was used for vegetation activity, where a linear relationship was found between the red-infrared ratio and fraction of photosynthetically active radiation intercepted by green vegetation. This was to estimate the available energy amount in vegetation for the herbivorous population. By using EVI it was noted that there is a strong relation between seasonal habitation and dietary components.

Matsushita *et al.* (2007) analyzed the sensitivity of NDVI and EVI on the high density of the Japanese cypress forest. This study was conducted in the Kochi Prefecture, western Japan, an area which is recognized as mountainous. An Airborne Imaging Spectrometer for Applications (AISA) and LiDAR were used for data capturing and coefficient variation used to determine the differences in topographic effect on EVI and NDVI. The EVI showed that it performs better in many applications, but is more sensitive to topographic conditions than NDVI as NDVI can eliminate or weaken topographic effects due to the band ratio.

For land cover changes analysis, it is important to highlight that whenever a landscape changes it could be due to natural or anthropogenic forces. Land use activities such as agriculture and mining, can lead to infrastructure and developments. These land use activities could result in development of urban spaces, such as residential area, farms, houses, recreational facilities and highly sophisticated infrastructure such as development of observatories for research purposes. The Normalized Difference Built-up Index (NDBI) was

developed to determine the spectral reflectivity of built-up areas (Zha *et al.*, 2003; Wu, 2004). Built areas include residential and industrial areas, roads and mines (Waqar *et al.*, 2012). These areas have highly reflective properties in infrared region compared to vegetation and bare soil. Researchers combined bare area and built-up areas due to their similarity in reflective properties. This has changed as it will be discussed according to the bare soil index.

He *et al.* (2010) investigated NDBI and its limitations in mapping urban built-up areas. This approach was to improve NDBI mapping by using the semi-automated segmentation method. It involved the use of Landsat ETM+ images of the National Olympic Park in northern Beijing for analyzing land over changes and IKONOS imagery for accuracy assessment. Continuous NDVI imagery and NDBI was obtained of the Landsat ETM+ imagery and then made into a binary image. The binary imagery of the NDVI was subtracted from the binary image of NDBI to extract the built-up area binary image. The result of the built-up binary image showed positive results of the barren and built-up area. This method eliminates the fact that a positive NDBI should certainly mean that the area is built-up, whereas a positive NDVI should also indicate vegetation thus using this method allows reduction of errors.

According to work done by Bhatti and Tripathi (2014), a new method for NDBI was proposed when using Landsat-8 OLI for the urban areas of Lahore in Pakistan. A built-up extraction method was determined through integration of temperature, NDVI and MNDWI. This method and NDBI were analyzed comparatively to improve the accuracy of built-up index analysis.

Apart from focusing on the built-up areas and its index, one has to recognize that at construction sites there is typically clearance of land cover. The bare-land index is used to calculate the amount of bare-soil exposed on a landscape which depends on the land use activity and the global climatic changes and conditions this bare-land index is known as the Normalized Difference Bareness Index (NDBaI) (Brink and Eva, 2009). Global climatic conditions with extreme temperatures and relatively low rainfall conditions, appeal to desert-like conditions according as illustrated in Chen *et al.* (2006). Changes in the amount of bare-land within an area can be detected by using the NDBaI technique (Zha, Gao and Ni, 2003; Southworth, 2004; Waqar *et al.*, 2012; Li and Chen, 2014).

According to Zhao and Chen (2005), a quick method was developed to map bare areas in the Yellow River delta and to monitor land cover changes in this area. The Yellow River delta area is a coastal region, therefore the normalized difference soil index (NDSI) and NDBaI

were combined to determine bare-areas along the Yellow River delta. The combined two indices produced a higher accuracy with respect to mapping bare-land in the area.

A combination of NDBaI, NDBI, MNDWI, NDVI and other spectral indices were used to determine the land surface temperature of the Guangzhou LULC distribution (Sun *et al.*, 2013). These spectral indices were used to determine the LULC classes by setting a threshold for indices by using Landsat TM satellite imagery. Six land cover classes were determined. The result indicated an increase in bare-land, sparse vegetation and polluted water. Built-up areas revealed higher land surface temperature (LST) values. While water bodies had a negative correlation to LST as LST values were lower. The NDVI values were negatively correlated to LST in areas with high vegetation cover.

All terrain contains water bodies above or below the land surface. The Normalized Difference Water Index (NDWI) was developed to determine the changes in water zones. The purpose of this index is to maximize the reflectance of an open delineated water surface (Xu, 2006), in relation to areas that show moisture content specifically. This is unlike NDVI which provides both moisture and vegetative components as illustrated by Gao (1996). Later on the NDWI ratio was modified according to Xu (2006) to enhance the accuracy of the water values by computing them to higher values than when using NDWI, and this technique is now known as the Modified Normalized Difference Water Index (MNDWI).

Image ratioing is the most basic classification technique, which leads one to the complexities of image processing that involve classification algorithms. Image classification algorithms can be used in both pixel and object-based methods and have been widely used by researchers depending on the spatial, spectral and radiometric resolutions of satellite imagery (Yan *et al.*, 2006). Pixel-based classification is a process where pixels containing spectral information are selected to define a phenomenon (Dingle Robertson *et al.*,2011; Myint *et al.*,2011; Whiteside *et al.*, 2011; Duro *et al.*, 2012). Object-based classification clusters a group of pixels emitting a specific spectral reflectance while combining both the spatial and spectral similarities and has a higher advantage over pixel-based classification (Darwish, Leukert and Reinhardt, 2003; Benz *et al.*, 2004). This encompasses the aggregation of image pixels into homogeneous objects that occur in one or more dimensions according to Blaschke, (2010). After this process an image segmentation algorithm is used to group the aggregated pixels in the satellite imagery (Im, Jensen and Tullis, 2008) and finally categorizes them into a land cover class (Mallinis *et al.*, 2008). These two types of classification provide a

guideline that further molds the essence of the remote sensing methods applied by an analyst and researcher. By using pixel and object-based classification methods, appropriate use of supervised and unsupervised means of classifying the data can be used to determine changes.

2.4.2 Unsupervised and supervised classification

Unsupervised methods of classification requires minimum involvement of the expert to carry out satellite image processing (Canty and Nielsen, 2006). The basic requirement is the selecting specific inputs into a computer interface in order for the computer to learn the data and hence process the data with the built in algorithms specifically stated for the unsupervised classification methods (Duda and Canty, 2002). It is usually used to give an impression of what the unknown phenomenon or study area would represent (Muttitanon and Tripathi, 2005). In the process, the user defines the number of classes that could possibly represent the data and then selects a classification algorithm from the software (Giada *et al.*, 2003). The computer program groups pixels and uniquely clusters them according to the mean, standard deviation and probability in which a pixel will be defined into a class (Canty and Nielsen, 2006). Clustering of the pixels depends on how well the clusters are sorted and the number of clusters represented in the data set (Maulik and Bandyopadhyay, 2002). Unsupervised classification can assist in collecting ground reference data in order to acquire optimum information for the selection of training data that can be used for supervised classification of the satellite imagery. According to Duda *et al.*, (2002) and Maulik *et al.*, (2002) the analyst must be able to choose a classification good algorithm and determine how relevant the clusters and the clustering techniques are to the satellite imagery used.

The main requirement in supervised classification in image processing is the analyst's expertise. This means that the user selectively identifies the training data (training sites) that will be used for the analysis and evaluation for a predefined number of classes (Cingolani *et al.*, 2004; Rahman *et al.*, 2013). The level of classification is determined by how well the user is able to model the target class distribution (Cingolani *et al.*, 2004; Foody *et al.*,2004; Agrawal *et al.*, 2007; Rahman *et al.*, 2013). Prior to the analysis the RS specialist needs to have experience in identifying the variables and locating training data on the image that needs to be classified (Ahmed *et al.*, 2013). Primary and secondary ground truth data measurements are used to compare the training data collected from the satellite image (Hodgson *et al.*, 2003). Three steps are carried out in supervised classification. Firstly, the user has to define the number of classes and the information that needs to be collected to give a representation of your training data (Abdulaziz *et al.*,2009). Secondly, the user must be able to know which

statistical or non-statistical parameters are suited for training the data set (Lu *et al.*, 2007; Rogan *et al.*, 2008). Finally, a decision must be made to select the appropriate classification (Otukei *et al.*, 2010; Myint *et al.*, 2011; Rahman *et al.*, 2013; Idol *et al.*, 2015). Supervised methods are divided into two classes of algorithms; the parametric and non-parametric classifiers (Bruzzone *et al.*, 2002; Otukei *et al.*, 2010).

2.4.3 Parametric and non-parametric classification algorithms

Parametric classifiers are mostly based on statistical analysis of data that has a normal standard probabilistic distribution (Kumar and Sahoo, 2012). This means the satellite imagery portrays a homogeneous type of landscape (Lu *et al.*,2007). The disadvantage of parametric classifiers is that it assumes the Gaussian distribution (normal distribution of spectral data). That means if satellite image is provided from a complex or heterogeneous surface the classification will produce "noise" or misclassified information (Lu *et al.*, 2007). Some parametric classifiers contain supervised classification algorithms and they include the Parallepiped algorithm, Mahalanobis distance, minimum distance and maximum-likelihood classification to name a few (Kumar *et al.*, 2012). These algorithms are standard representations of what a normal distribution is and hence no need for further additional parameters (Kumar and Sahoo, 2012). The parallepiped algorithm uses the Boolean logic AND/OR (Foody *et al.*, 2004; Santillan *et al.*, 2011). The performance of this algorithm solely depends on the number of spectral bands within satellite imagery, where the determining factor is the threshold standard deviation of the mean values of the classification belonging in each category (Xu and Wei, 2012). The Mahalanobis distance algorithm uses the distance measure of one classifier to influence the closeness of one pixel to a distribution cluster (De Maesschalck *et al.*, 2000; Xiang *et al.*, 2008). It has a common factor with the parallepiped classification algorithm, which is the variation of the number of standard deviations of the classifiers relating to the mean of the class distribution (De Maesschalck, Jouan-Rimbaud and Massart, 2000; Carrão, Gonçalves and Caetano, 2008; Xiang, Nie and Zhang, 2008; Perumal and Bhaskaran, 2010).

The minimum distance algorithm belongs to a category called sample classifiers (Toth and Aach, 2001; Zhang, Chen and Zhou, 2006). This method uses a group of vectors or pixels which are estimated to narrowly look like each other and then categorized together (Zhang, Chen and Zhou, 2006).

The maximum likelihood classification algorithm is widely used in supervised classification and displays high accuracy and is widely recommended. This algorithm applies the use of the

Gaussian probability density function model for each class that is selected and determined (Strahler, 1980; Jia and Richards, 1994; Paola and Schowengerdt, 1995; Erbek, Özkan and Taberner, 2004; Shuying, Deren and Jingwen, 2005; Otukei and Blaschke, 2010; Dingle Robertson and King, 2011; Liu, Shi and Zhang, 2011; Mondal *et al.*, 2012; Sun *et al.*, 2013). It is based on the probability of a pixel belonging to a certain spectral class that will be assigned the highest likelihood and is closely linked to the normal distribution of the spectral bands analyzed in a satellite image (Strahler, 1980; Jia and Richards, 1994; Paola and Schowengerdt, 1995; Erbek, Özkan and Taberner, 2004; Shuying, Deren and Jingwen, 2005; Otukei and Blaschke, 2010; Dingle Robertson and King, 2011; Liu, Shi and Zhang, 2011; Mondal *et al.*, 2012; Sun *et al.*, 2013).

Apart from the parametric classification algorithms that assume the normal distribution of data, the non-parametric classification algorithms are classifiers that do not rely solely on assumption of statistical data (Bruzzone, Cossu and Vernazza, 2002; Kumar and Sahoo, 2012). Likewise the probalistic function of the distribution is also not expected to be normal (Lu *et al.*, 2004; Lu *et al.*, 2007). Well known non- parametric classifiers include: random forest, neural network and support vector machine. A random forest composed of random vectors in a tree classifier are independent of the training set (examples that can be used to fit paraemeters) of the input vectors (Breiman, 2001). For the analysis to run a tree classifier casts a unit vote for the popular class in which to place a given input vector (Breiman, 2001; Gislason *et al.*, 2006). Its most popular method of data analysis is bagging according to Breiman, (1996) and boosting according to Gislason *et al.*, (2006) . In bagging the method is used to collect many classifiers and trains them in a training set to be able to improve classification accuracy and avoid over fitting (Breiman, 1996; Gislason, Benediktsson and Sveinsson, 2006). Whereas, boosting as suggested by the name helps improve the algorithm (Breiman, 2001; McIver and Friedl, 2001; Kim, 2013; Ji *et al.*, 2015) by re-training a component of the random forest. This in turn allows for incorrectly classified samples to be given a weight as much as the re-training process continues (Gislason, Benediktsson and Sveinsson, 2006). Boosting assists in improving the performance of the algorithm by reducing both the variance and bias of a classification and hence promotes the accuracy of an algorithm. This process has a slight disadvantage because it can make the analysis slightly slower (Breiman, 2001; Gislason *et al.*, 2006).

The ever-evolving process of the artificial neural network (ANN) is also another non-parametric classifier in solving pattern recognition problems. The ANN development was

motivated by the design of the human brain according to Atkinson and Tatnall, (1997) and Mas and Flores, (2008). Same as the Random Forest method, it does not rely on the assumption of the statistical distribution (Benediktsson, Swain and Ersoy, 1990; Gopal and Woodcock, 1996) of the data, however it works on the performance of how well trained a data set is (Pal, Maxwell and Warner, 2013). Artificial neural networks is known as a learning machine, where the outputs are independent of the input (Gopal and Woodcock, 1996). The process involves " learning" the training the data through recognizing any regularities in the data and then builds rules on data that seem to be unknown to the process (Pal, Maxwell and Warner, 2013; Kumar *et al.*, 2015). However the architecture of the neural network needs a user to define the parameters such as the learning rate and momentum rate in order to improve its performance (Atkinson and Tatnall, 1997). The most common neural network fundamental that is used in remote sensing is the multi-layer perceptron (a class of feedforward artificial neural network) with back error propagation (Serpico *et al.*, 1996; Kavzoglu and Mather, 2003).

A fairly unexploited non-parametric classification algorithm in remote sensing is the support vector machine (SVM) algorithm as documented in Mountrakis *et al.*, (2011). It is slightly different from the rest, because it is based on a statistical learning method (Huang, Davis and Townshend, 2002). The SVM method provides decision boundaries that will be used to separate different classes as illustrated in Pal and Mather, (2005) and Mountrakis *et al.*, (2011). The decision boundaries for the chosen classes are selected by calculating the optimum hyperplane used to separate the classes (Huang *et al.*, 2002; Pal *et al.*, 2005; Mountrakis *et al.*, 2011). The SVM method is sensitive to the training data and the dimension in which the data is projected (Kumar *et al.*, 2015). It is able to minimize the probability of misclassifying a class or pixel from a random or unseen data point (Foody *et al.*, 2004) and reduce classification errors (Pal and Mather, 2005) at the same time solving the RS classification problem (Foody *et al.*, 2004). Originally, SVMs were used for binary classification problems (Foody and Mathur, 2006) For multi class problems, the analyst must generate a number of hyperplanes to be able to optimize the technique for the generation of each class categorized (Foody *et al.*, 2004).

Satellite image processing and change detection techniques entail a wide range of methods which include image differencing. Image differencing involves two satellite images, either unprocessed or classified, obtained at different times but within the same season to determine the change in the area (Ridd and Liu, 1998; Rogerson, 2002; Rosin, 2002; Alphan, 2003;

Coppin *et al.*, 2004; Berberoglu and Akin, 2009). It is done through subtracting pixels from the latest image to the older one (Bindschadler *et al.*, 2010) The result is a third image that consist (as illustrated in Rosin, (2002)) of the numerical difference obtained between the pairs of pixels. Another change detection technique is image ratioing, where the ration of two co-registered images determined pixel by pixel in each band, the smaller the difference the closer the ratio is to 1 (Singh, 1989). The coefficient yields a result of numbers ranging from -1 to 1. It is an effective method to give a general overview of changes in a study with regards to the appearance of surface features mostly used in vegetation, water, impervious surface and bare-soil analysis (Singh, 1989).

These methods serve a different purpose, such as; to create and improve some RS methods, to be able to develop new functions, for analysis in earth observation for a multidisciplinary purpose such as applied mathematics, computer sciences, geographical sciences, biological, physical sciences and social sciences to find solutions to a recurring problem. Land cover change analysis is one of the aspects that have applied all these concepts of remote sensing.

3 RESEARCH METHODOLOGY

The research methodology is a breakdown of how the research was conducted. The focal point is HartRAO and its environment. There is a small overview of the study area the use and significance of type of primary and secondary data used in the study.

3.1 Study Area

The Hartebeesthoek Radio Astronomy Observatory (HartRAO) is located north-west of Johannesburg, in the heart of Mogale City, Gauteng province, within a valley of the Witswatersberg hills. Local vegetation type is a combination of Mixed Bushveld and Rocky Highveld. The Doringspruit River flows near the observatory. Radio astronomy, space geodesy and science awareness are the current land use activities of the area, while the surrounding regions are mainly farmlands and game reserves. The daily maximum summer and winter temperatures range from 28°C to 35°C and 20°C to 25°C respectively, and the minimum summer and winter temperatures range from 13°C to 20°C and 4°C to 11°C. Average summer rainfall is 275 mm and average winter rainfall is 16 mm. The summer season is hot and wet with scattered thunderstorms while winters are cold and dry. Figure 3.1 provides a topographical aspect of the study area.

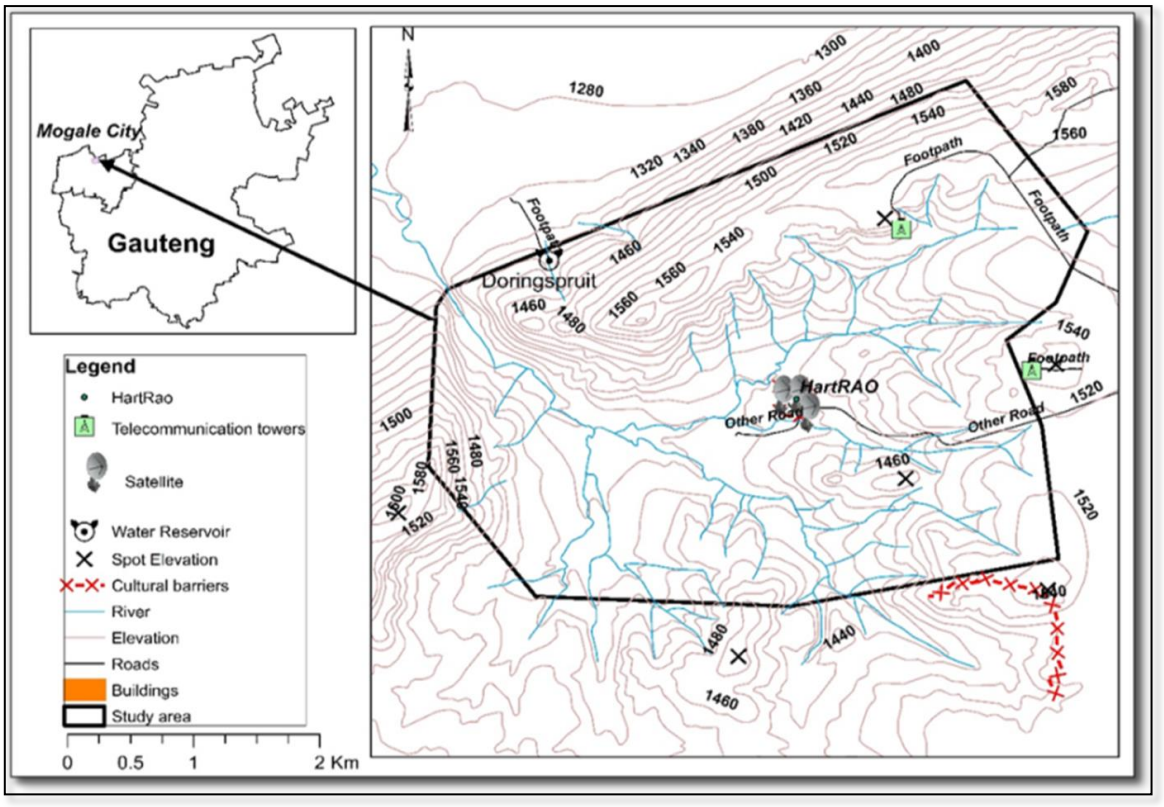

Figure 3.1: Topographical map of HartRAO and environment. The facility is located in a valley, surrounded by hills.

3.2 Data and Methods used for Analysis of Land Cover Change

As illustrated in Figure 3.2, the data and methods used for monitoring land cover changes at HartRAO and its environment are described. Primary and secondary data were used in the land cover change analysis. The primary data involved field work to do land cover validation by noting areas that could not provide substantial information of the land cover description according to the satellite imagery. Secondary data such as aerial photographs informed which land cover was more predominant and which changes occurred in the area over time. Climate data included rainfall and temperature that were used to determine the annual trends in seasons. The climate data from South Africa Weather Services (SAWS) assisted in pointing out the effects of seasonal variability on the land cover type. The use of Landsat imagery and digital elevation models assisted in delineating the land cover to develop a land cover map. The significance of the use of Landsat imagery to delineate land cover is due to the fact that it has been producing satellite images for a long time. It is also important to note that the selection of the optical data was to determine the various land cover changes using spectral data. Synthetic aperture radar data would be significant when focusing on one land cover type dominant in the area whereas in HartRAO there is a variability in land cover type.

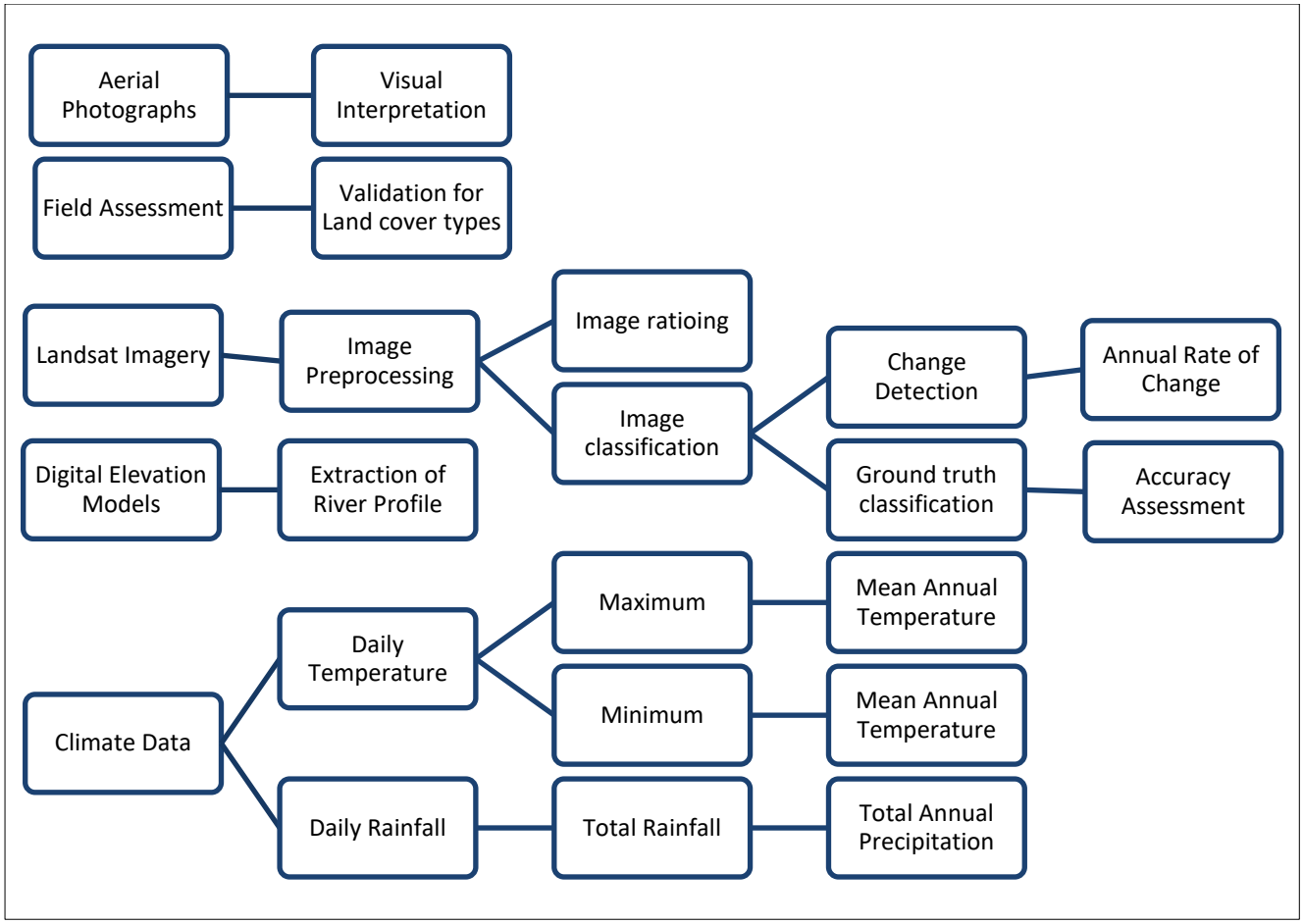

Figure 3.2: Methodological framework used in the LCC analysis of HartRAO and environment.

3.2.1 Satellite imagery

3.2.1.1 Landsat imagery

The focus of this study was to use optical sensors to delineate land cover. Optical sensors are useful when delineating spectral reflectance of land cover through colours. In this study, Landsat imagery from the Landsat 5 Thematic Mapper (TM) and Landsat 8 Operational Land Imager and Thermal Infrared Sensor (OLI/TIRS) were the main satellite images used. The Landsat TM is a multispectral scanning radiometer, with a whiskbroom instrument, that takes multi-spectral images across its ground track (see https://earth.esa.int). Landsat (OLI) carries two push-broom instruments; the Operational Land Imager (OLI) and the Thermal Infrared Sensor (TIRS) (see https://landsat.usgs.gov). When comparing the data quality and radiometric quantization of the Landsat 8 (OLI/TIRS) and Landsat 5 (TM), the signal to noise ratio is better in Landsat8 (OLI/TIRS) compared to Landsat5 (TM) (see https://landsat.usgs.gov).

Both Landsat satellite images have a spatial resolution of 30 by 30 metres per pixel size (http://landsat.usgs.gov/band_designations_landsat_satellites.php). This was useful when comparing the different classification methods in addition to knowing the diversification of different satellite imagery over the years. The increase in the number of different band wavelengths created an improvement in land cover change studies due to better sampling. The Landsat satellite imagery selected was according to seasonal basis over a period of 20 years. This included the peak summer season, which included December, January and February and peak winter seasons that are from June, July and August. Table 3.1 contains the band designations of Landsat imagery and Table 3.2 provides information on the Landsat images used for this study.

Table 3.1: Landsat 5 TM and Landsat 8 OLI bands

Bands	Wavelength (nm)	**Bands**	Wavelength (nm)
Band 1- Blue	0.45-0.52	**Band 1-Coastal**	0.43-0.45
Band 2- Green	0.52-0.60	**Band 2 - Blue**	0.45 -0.51
Band 3- Red	0.63-0.69	**Band 3 - Green**	0.53-0.59
Band 4- NIR	0.76-0.90	**Band 4 - Red**	0.64 – 0.67
Band 5- MIR	1.55-1.75	**Band 5- NIR**	0.85-0.88
Band 6- TIR	10.40-12.50	**Band 6 - SWIR 1**	1.57-1.65
Band 7- SWIR	2.08-2.35	**Band 7 - SWIR 2**	2.11 -2.29
		Band 8- Panchromatic	0.50 -0.68
		Band 9 – Cirrus	1.36 – 1.38
		Band 10- TIRS1	10.60- 11.19
		Band 11 –TIRS 2	11.50 -12.51

Table 3.2: Landsat images metadata

	Date	**Path/Row**	**Cloud cover (%)**
Landsat 5 (TM)	28th Feb 1998	171/078	0
	06th Jul 1998	171/078	0
	04th Jan 2007	171/078	0
	31st Jul 2007	171/078	0
Landsat 8 (OLI)	16th Jan 2014	170/078	1.72
	02nd Jul 2014	171/078	0.04

3.2.1.2 Digital elevation models

A digital elevation model (DEM) is a 3D representation of the surface which is created from terrain elevation data (see https://lta.cr.usgs.gov/DEMs). A DEM file was used to extract the hydrology of the Doringspruit stream, and to detect its flow and tributaries. The data were obtained from the Advanced Space borne Thermal Emission and Reflection Radiometer (ASTER) from NASA and MET imagery and Shuttle Radar Topography Mission (SRTM). Onboard the SRTM shuttle, the C-band Space borne Imaging Radar and X-band Synthetic Aperture Radar (X-SAR) are used to collect information of the Earth's surface (see

https://lta.cr.usgs.gov/SRTM). The SRTM 1 Arc Second Global elevation data set provides elevation data. The data used was SRTM 1, with latitude (south) of -26 degrees and longitude (east) of 27 degrees dated the 25th of September 2014 (see https://earthexplorer.usgs.gov/).

3.2.2 Archived photographs

Archived aerial photographs were used to verify the land cover over the period of the study. Aerial images were used through visual interpretation to determine changes over time. Provision of this data was from the Department of Rural Development and Land Reform (DRDLR) of South Africa, which comprised aerial photographs, orthophotos and topographical maps as shown in Table 3.3.

Table 3.3: Archived data for land cover changes for DRDLR

Type	**Date**
Aerial Photographs	1963, 1964, 1968, 1985, 2013
Analogue	2004
Topographical	1943, 1968, 1985, 1996, 2010
Orthophotos	2004, 2013

3.2.3 Climate data

Climate data used in the study were obtained from the South African Weather Service (SAWS) Kroningspark Station in Krugersdorp, which is the closest station to HartRAO. The data set includes the daily rainfall, as well as maximum and minimum temperature from 1960 to 2014.

3.3 Methodology

3.3.1 Software

To carry out the image analysis, satellite images were stored on a hard drive, image processing was done in EXELIS (ENVI 5.1) (see http://www.harrisgeospatial.com), and some of the outputs were displayed and saved using ENVI 5.1 while the map outputs were made using ESRI (ArcGIS 10.2) (see https://www.esri.com/en-us/home). Analysis of climate data was done using TREND, a toolkit (*eWater*) for hydrological statistical applications (see https://toolkit.ewater.org.au/Tools/TREND) and Microsoft Excel 2013.

3.3.2 Field assessments

Google Earth PRO was used to identify sites where it was problematic to differentiate sites which are difficult to measure. The Global Positioning System (GPS) was utilized for field-based assessments to identify the mixed land cover locations pointed out from Google Earth. A Magellan Meridian Gold GPS (handheld device) and Google Earth PRO were used for storage and of verification of the sampled ground control points of some parts of the study areas. Images taken during the study period are contained in Figure 3.3 to illustrate the method used to take ground control points for the study and the validation process.

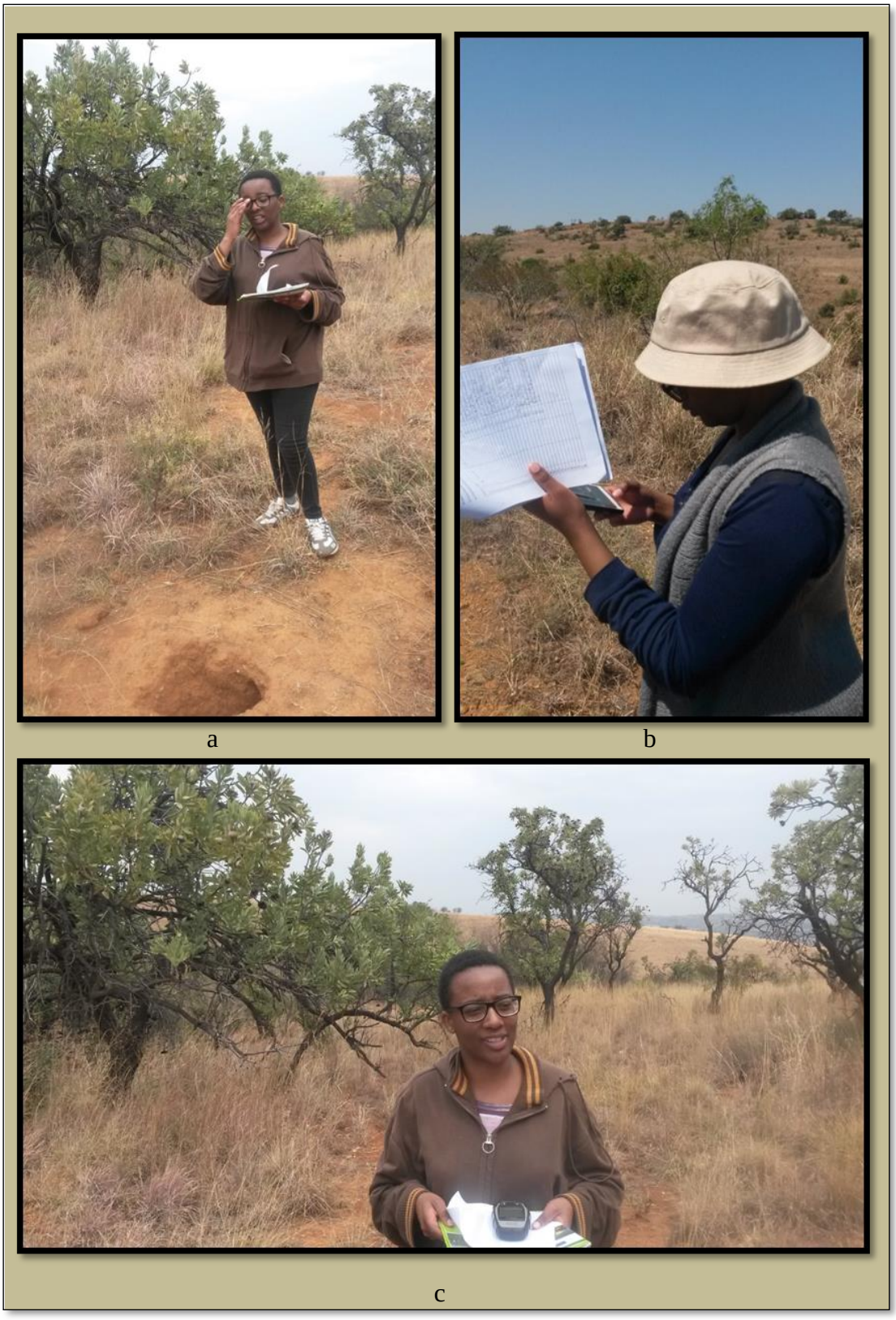

Figure 3.3 (a, b, c): Field assessment carried out to determine land cover types in the area

Therefore, as depicted in Figure 3.3a, Figure 3.3b and Figure 3.3c, this process comprised data collection, which was used to determine land cover. The GPS coordinates collected and data sampled at that point were used to verify mixed pixels in the satellite imagery.

3.3.3 Image analysis

Concurrently with field based assessments, Landsat data used were pre-processed through radiometric and geometric correction. Pre-processing encompasses removal of any distortions and noise caused by the sensor or atmosphere which occurred during the collection phase of the satellite imagery (Xiao and Weng, 2007). After pre-processing of the satellite data and converting it into land surface reflectance, image classification was used to delineate aspects of the land cover. This method is carried out by selecting features through clustering land cover which has similar mean spectral reflectance (Foody, 2002). It is also dependent on the land cover type, as well as the spectral, spatial and radiometric resolution of the satellite imagery (Lu *et al.*, 2007). From image-classification, one must conduct a post-classification assessment which encompasses change detection and accuracy assessment (Skelsey *et al.*, 2003; Muttitanon and Tripathi, 2005). Change detection signifies land cover areal change and rate of change per annum. Whilst accuracy assessment is useful to verify how well the training data and ground control points perform after image classification. It is used to determine how well a classification algorithm is on a specific land cover type (De Roeck *et al.*, 2008).

3.3.3.1 Radiometric calibration

The Landsat imagery was radiometrically calibrated using the Landsat calibration tool in ENVI 5.1. The Metadata file was uploaded into the ENVI 5.1 interface as illustrated in Figure 3.4, where the “Available Bands List” menu is used to access the Landsat Metadata file (MTL).

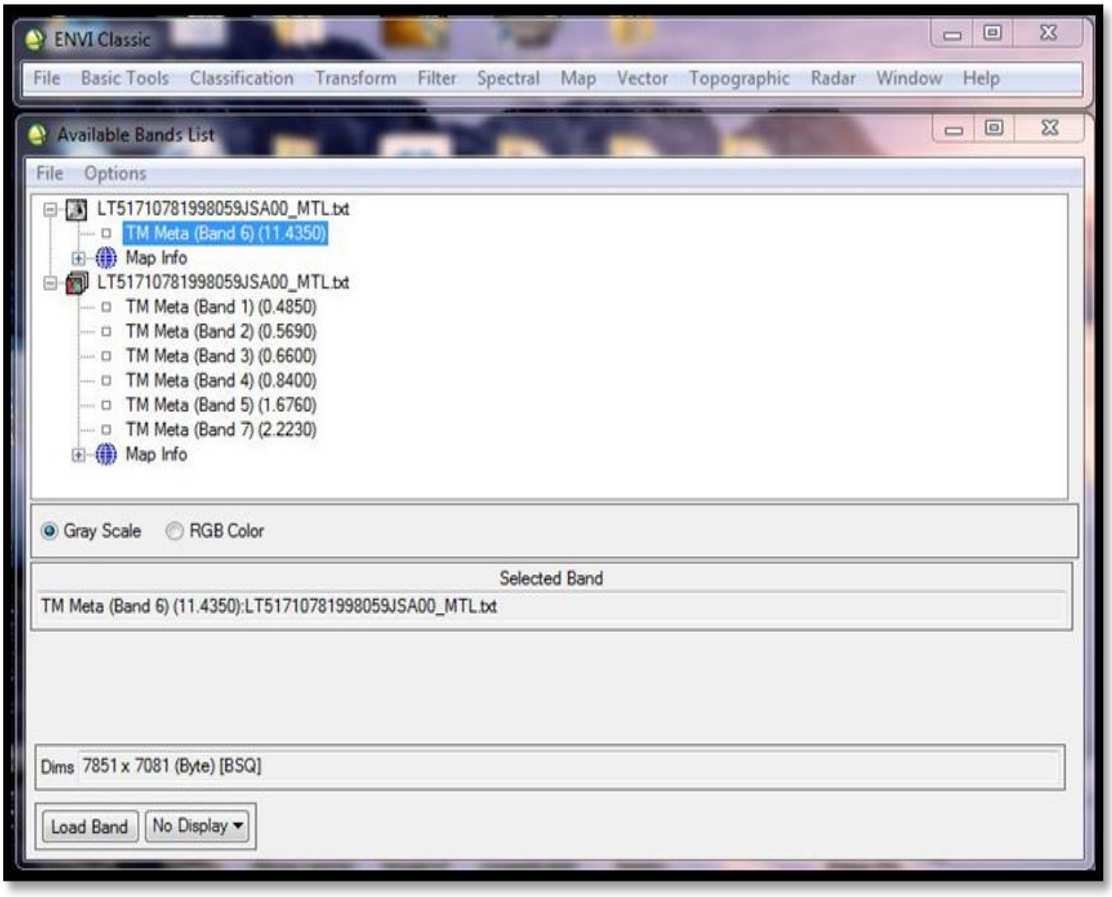

Figure 3.4: Radiometric calibration in ENVI 5.1 step 1

Headers of the images were edited to contain the wavelength of each band before processing (for the purpose of recognising the contents of the file directly from the file name). This was done by averaging the wavelength range, updating the information into a text file and uploading it into the Metadata file as demonstrated in Figure 3.5.

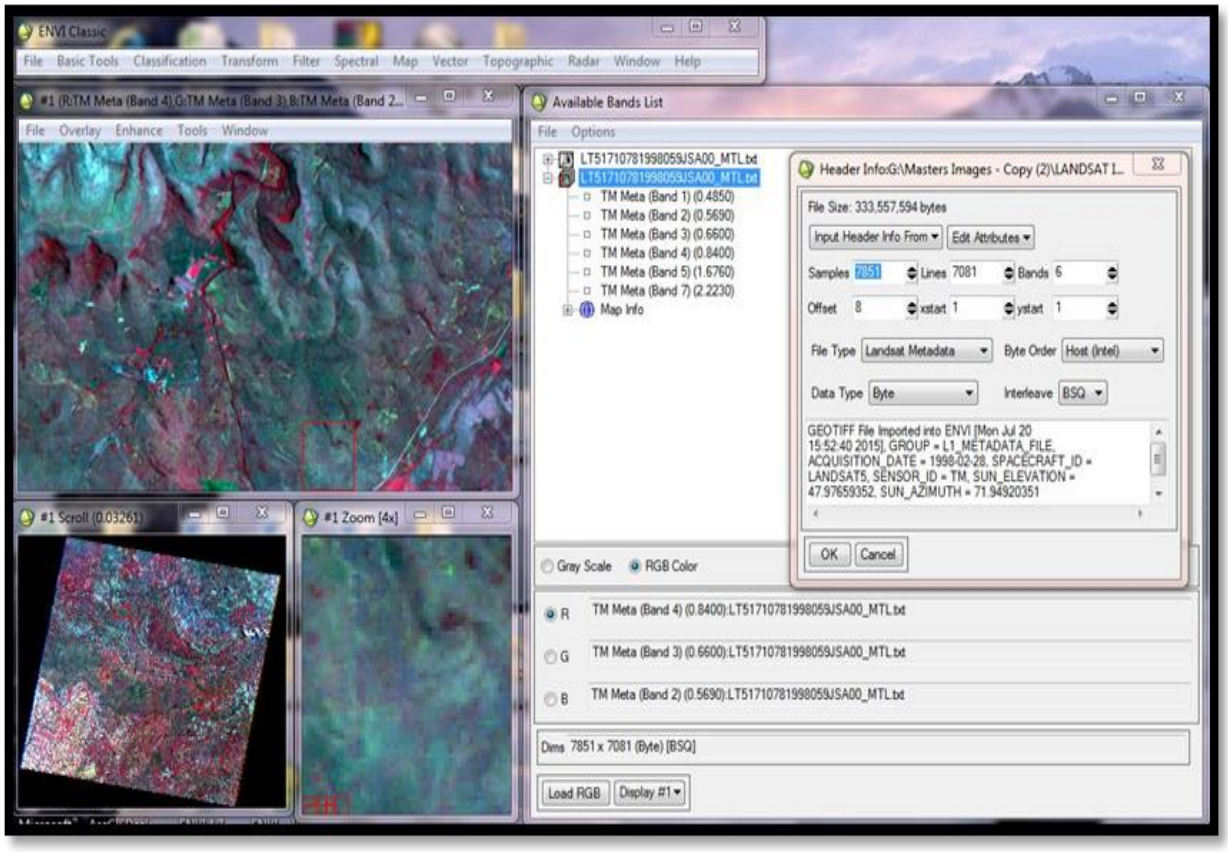

Figure 3.5: Radiometric Calibration step 2

The calibration utility tool was selected and the images were calibrated to radiance values using Equation (1), then calibrated to reflectance values as illustrated in Equation (2) as documented in Coppin *et al.*, (2004). This whole process for the conversion of radiance values to reflectance values is illustrated in Figure 3.6.

$$L_\lambda = \left(\frac{LMAX_\lambda - LMIN_\lambda}{QCALMAX - QCALMIN} \right)(QCAL - QCALMIN) + LMIN_\lambda . \quad (1)$$

Where:

L_λ = Spectral Radiance at the sensor's aperture in Wm^2ster^{-1} μm^{-1}

QCAL = the quantized calibrated pixel value in DN

$LMIN_\lambda$ = the spectral radiance that is scaled to QCALMIN in $Wm^2ster^{-1}\mu m^{-1}$

$LMAX_\lambda$ = the spectral radiance that is scaled to QCALMAX in $Wm^2ster^{-1}\mu m^{-1}$

QCALMIN = the minimum quantized calibrated pixel value (corresponding to $LMIN_\lambda$) in DN

QCALMAX = the minimum quantized calibrated pixel value (corresponding to $LMAX_\lambda$) in DN.

$$\rho = \frac{\pi d^2 L}{E_0 \cos\theta}. \qquad (2)$$

Where:

ρ = unit less planetary reflectance at the satellite (this takes values of 0-1)

π = 3.141593

L = Spectral reflectance at sensor aperture in $mWcm^{-2}\,ster^{-1}\mu m^{-1}$

d^2 = Square of the Earth-Sun distance in astronomical units (au)

E_0 = Mean solar exo-atmosphere irradiance in $mWcm^{-2}\mu m^{-1}$

$Cos\theta$ = Sun zenith angle in radians when the scene is recorded

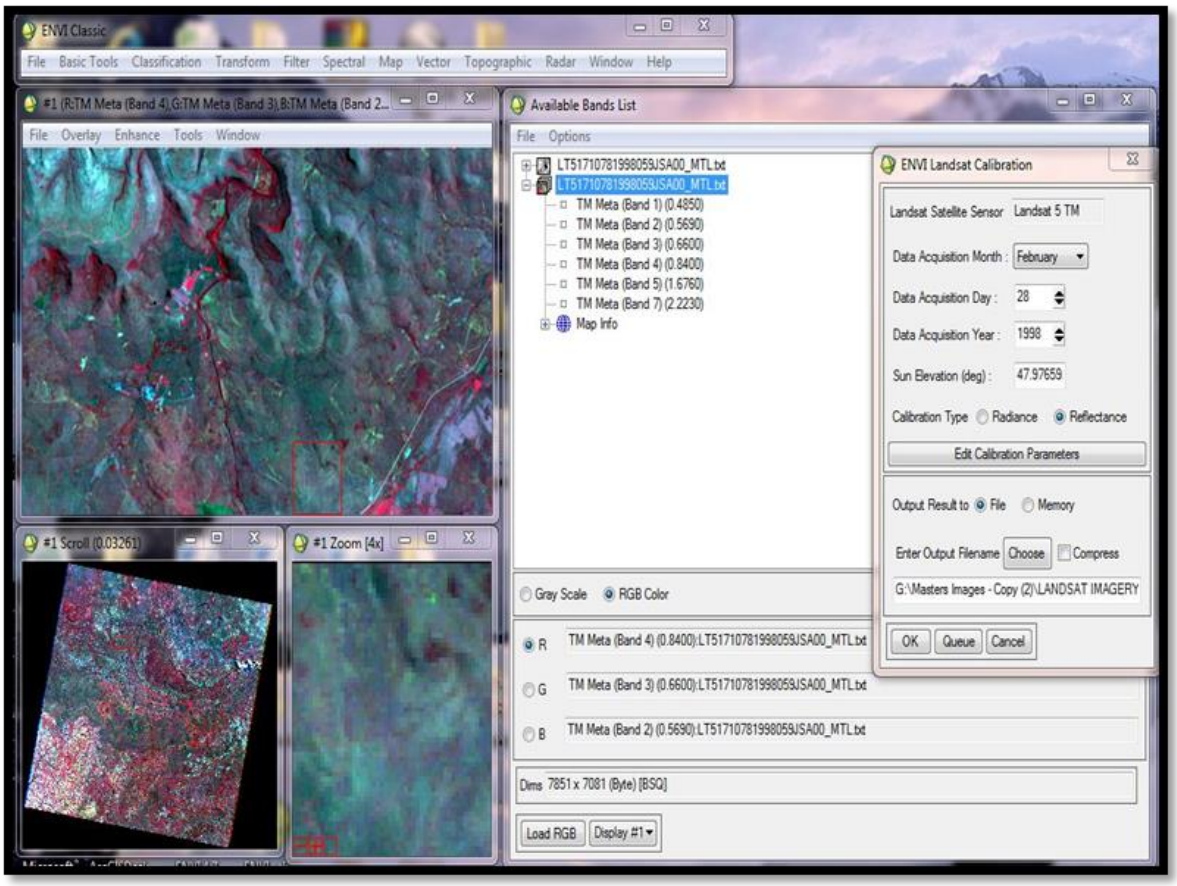

Figure 3.6: Conversion from radiance to reflectance.

3.3.3.2 Geometric correction

After radiometric correction, the data were aligned to the most recent satellite imagery (Yang *et al.*, 2002). The method used for geometric correction was Image-to-Image registration (Santillan, Makinano and Paringit, 2011). Image-to-Image registration involves having the most recent image as a base map, and the older images as warp images (Lu *et al.*, 2007). This method is important, because the earth rotates on its own axis and there is a shift in geographical location caused by the rotation of the axis. It is also necessary to correct any geographical distortion. Using ENVI 5.1, twenty ground control points were selected to warp the images to the base map for this method as documented in Li *et al.*, (2015). A root-mean-square error (RMSE) was determined, though nearest neighbourhood, as illustrated in Figure 3.7 and Table 3.4. Studies indicate that the lower the RMSE is the better the geometric correction. For Landsat imagery RMSE values should not exceed 0.5 as supported in Shalaby *et al.*, (2007) and Li *et al.*, (2015).

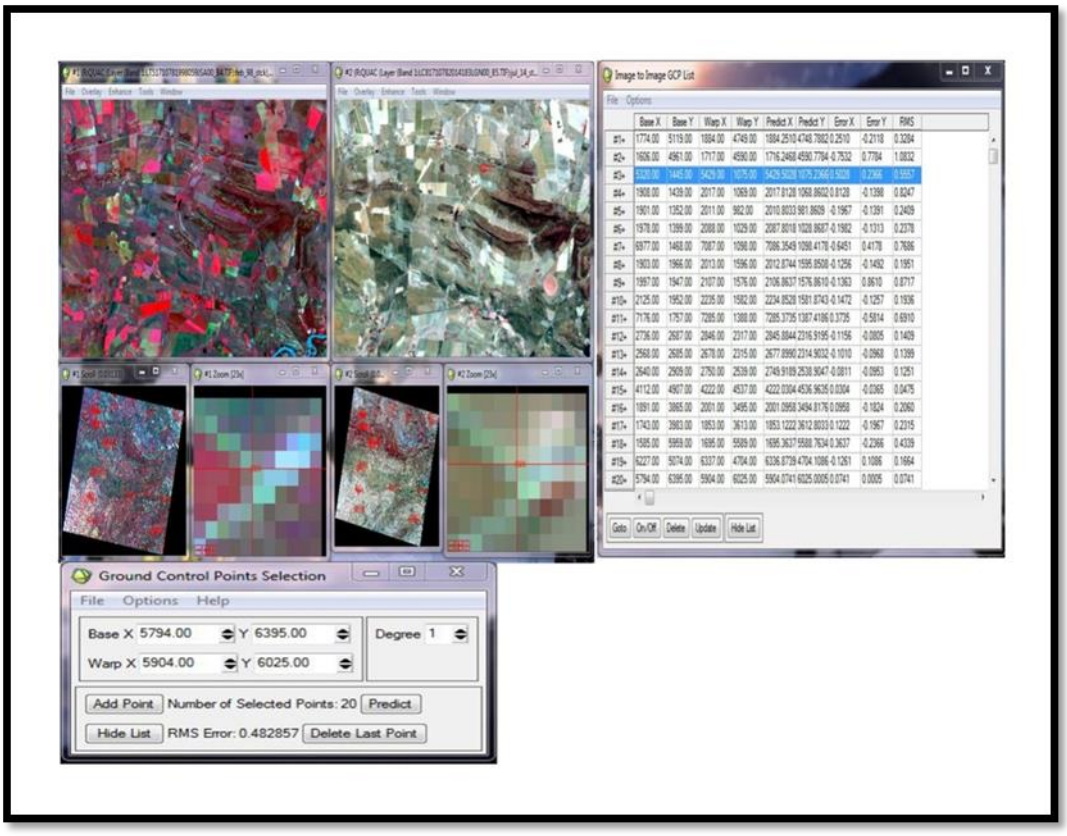

Figure 3.7: A demonstration of Image-to-Image registration for the Landsat Images for the study.

Table 3.4: RMSE values after Image-to-Image registration for Landsat images

Date	Path/ row	RMSE value
February 1998	171/078	0.482857
July 1998	171/078	0.477649
January 2007	171/078	0.453350
July 2007	171/078	0.400825
January 2014	170/078	0.493009

The average of the RMSE for all the images for this study was 0.461538. A higher RMSE value shows that the seed points of the imagery do not tie in together, which leaves room for geometric distortion, which could affect image classification and post-classification results in multi-temporal land cover change analysis.

3.3.3.3 Image classification

Image classification entails, collecting information on the satellite imagery through spectral and spatial aspects to determine the research interest. It involves a couple of methods such as ratioing and the use of classification algorithms. Before image classification takes place, sub-setting the satellite imagery is necessary to the spatial size of the area desired for study. This reduces the time for processing the satellite data and only works with the necessary input. Image subsets are either land boundaries developed from shapefiles or one can generate a shapefile to create their boundary of desire. The area of interest selected for the land cover change analysis of HartRAO, comprised selecting geographical coordinate points from Google Earth PRO and it is illustrated in Table 3.5. The points were saved in an excel workbook, the uploaded into ArcMap 10.1, and then digitized to create a polygon. The polygon was saved as a vector file in the format of an ESRI shapefile. The subset had a radius of two kilometres, from the middle point HartRAO location. The shapefile was used to subset the satellite imagery, for image classification.

Table 3.5: Coordinate points selected from Google Earth used to create a shapefile for the study area

Point	Latitude	Longitude
A	-25.8823	27.66042
B	-25.8668	27.6979
C	-25.878	27.70631
D	-25.8834	27.70407
E	-25.8864	27.70084
F	-25.8926	27.70294
G	-27.9027	27.70414
H	-25.9059	27.68605
I	-25.9051	27.66653
J	-25.8955	27.65936
K	-25.8836	27.65979

3.3.3.3.1 Image ratioing

The process of image classification, involves determining the amount of land cover depicted in an area. Image ratioing is a method that is used to assist in determining the amount of land cover on a satellite image (Coppin *et al.*, 2004; Lu *et al.*, 2004; Hussain *et al.*, 2013). It includes the division of bands, which depict the absorption and reflectance bandwidth of a land cover type in specific pixels at the time the image was captured (Lu *et al.*, 2004). Image ratioing methods formulate spectral indices that provide the simple ratio to complex ratios that can extract information of the land cover type, such as the biophysical attributes. Spectral indices range from -1 to 1, where -1 depicts the other land cover and 1 strongly agrees that a specific pixel contains the land cover studied in Lu *et al.*, (2004).

To determine the spectral indices used, it encompassed the analysis of aerial photographs, Google Earth imagery and field validation. Therefore the result led to four spectral indices selected for image ratioing, and they include Enhanced Vegetation Index (EVI) (Matsushita *et al.*, 2007; Jiang *et al.*, 2008; Stroppiana *et al.*, 2012). The Normalized Difference Vegetation Index (NDVI) (Wedderburn-bisshop *et al.*, 2001; Li, Jiang and Feng, 2013), Normalized Difference Built-up Index (NDBI) (As-syakur *et al.*, 2012) and Normalized Difference Bareness Index (NDBaI) (As-syakur *et al.*, 2012). The NDVI and EVI indices

were selected due to the presence of tree cover, grass and scattered vegetation. Use of NDBaI was due to the occurrence of rocks and bare-soil amongst the vegetation land cover. Analysis of the NDBI was to provide information of the presence of the built-up in the area this includes HartRAO and facilities enclosed in area, roads, terrain, and demolished households. The water index was not used in the area, due to the streams being covered by the trees in the area, and some stream channels were currently dry. This also is a factor to consider, the fact that Landsat is an optical sensor and digital elevation models were used to extract the river profile (Hoffmann and Sander, 2006). Since the area is dominantly mixed bushveld and rocky Highveld vegetation, the EVI and NDVI spectral indices were best suited for the area.

Vegetation indices

The Normalized Difference Vegetation Index (NDVI) is calculated by the ratio of the difference of the NIR and Red and addition of the NIR and Red bands in the visible light of the electromagnetic spectrum Liu *et al.,* (2015). The range of values are from the -1 to 1 where extreme negative values depict a different land cover, while a higher positive values show the presence of vegetation in a study area, NDVI is depicted in Equation (3) .

$$\mathrm{NDVI} = \frac{\mathrm{nir} - \mathrm{red}}{\mathrm{nir} + \mathrm{red}}. \tag{3}$$

Enhanced Vegetation Index (EVI) was primarily developed from MODIS products to which picks up quantities of vegetation canopy structure as supported in Huete *et al.,* (2002) making it more advantageous over NDVI which is profound in detecting the level of greenness, through its sensitivity to chlorophyll in the type of vegetation as published in Gao *et al.,* (2000). Advantage of EVI over NDVI is the inclusion of the blue band to remove atmospheric and moisture interference on the satellite imagery as documented in Miura *et al.,* (2001). This is useful when looking at forest and canopy type vegetation, where presence of rainfall is dominant in the area. The EVI value ranges are the same as NDVI where negative values depict other land cover and the more positive the value the higher the vegetation occurrence is on an area. Equation (4) illustrates the calculation of EVI.

$$\mathrm{EVI} = \mathrm{G} \times \frac{\left(\mathrm{nir} - \mathrm{red}\right)}{\left(\mathrm{nir} + \mathrm{C1} \times \mathrm{red} - \mathrm{C2} \times \mathrm{blue} + \mathrm{L}\right)}. \tag{4}$$

Built-up area index

The Normalized Difference Built-up Index (NDBI) was formulated by Zha *et al.*, (2003) and advanced by He *et al.*, (2010) and Waqar *et al.*, (2012) due to an increase of urbanization within developed countries. With the same calculation principal as NDVI, the NDBI is the ratio of the difference between MIR and NIR and the addition of the MIR and NIR. Built-up areas absorb NIR and reflect MIR, the range of NDBI values are -1 to 1, where positive values depict high occurrence of built-up and the opposite for the negative values. The NDBI is formulated in Equation (5).

$$\text{NDBI} = \frac{\text{mir} - \text{nir}}{\text{mir} - \text{nir}}. \tag{5}$$

Bare-land index

The built-up index was used to calculate the area that was not occupied by neither vegetation nor water. This index showed a generalization of land cover information because researchers realised that land cover types representing bare-land were selected as built-up. This resulted in an error within land cover classification, as bare-land is a different land cover type that emits its own spectral values according to (Li *et al.*, (2014). The bare-land cover is represented by areas such as: open fallow lands, uncultivated lands, and desert area. This led to the concise effort to develop the Normalized Difference Bareness Index (NDBaI), in order to differentiate between the bare-land from the built-up illustrated in Zhao *et al.*, (2005). The NDBaI was modified for the Landsat sensor Zhou *et al.*, (2014). It is crucial to note that bare-land and built-up reflectance is within the middle infrared. However, soils and rocks have a higher thermal capacity and depth that leads to absorption in the TIR band, which differentiates it from built-up land cover type. Negative values of NDBaI represent index values of other land cover types while positive NDBaI values indicate bare-land type. Equation (6) can be used for calculating NDBaI.

$$\text{NDBaI} = \frac{\text{mir} - \text{tir}}{\text{mir} - \text{tir}}. \tag{6}$$

As discussed, spectral indices used in the study provided a general overview of the land cover type studied in the area and it was also used as a precursor study for field analysis and image classification.

3.3.3.3.2 Supervised classification

After image ratioing, the training data for supervised classification were selected on the satellite images. This process involved carefully selecting satellite image pixels according to land cover type as perceived from the field assessment conducted for LCC analysis. Due to the spatial pixel size of the Landsat imagery, there were pure and mixed pixels. Selection of training data on a satellite image is a manual process, which involves, looking at the different colour composites and spectral information of the area from the satellite data. The heterogeneity of the terrain allows us to interchange different colour composites to carefully selected land cover types. Due to the complexity of the terrain, land cover changes every 10 meters, we had to categorise the data according to the most prevalent land cover types. Through comparison of Google Earth images, photographs taken during the field work to verify complex areas that cannot be carefully identified from the satellite images, Google Earth images and aerial photographs in some geographical locations. These images also contributed well to the selection of the training data.

3.3.3.3.3 Training sites selection and region of interest statistics

The training sites were selected by using the region of interest (ROI) tool in ENVI 5.1 classic. The study area is small; which resulted in less pixels being selected for some land cover types. The regions of interest ranged between 10-15 ROIs per land cover class. Selection of these training data was through pixel-based selection method. Likewise, we selected the purest pixel to be used as ground truth data. This was done for determining the accuracy for the classification algorithms selected for this study.

3.3.3.4 Pixel-based classification

3.3.3.4.1 Parametric and non-parametric classification

After carefully selecting the training data, two classification algorithms were used; the maximum likelihood (ML) and support vector machine (SVM) which are in-built algorithms in ENVI 5.1. These are parametric and non-parametric classification algorithms respectively as documented by (Erbek, Özkan and Taberner, 2004; Otukei and Blaschke, 2010). Parametric classification methods uses the Gaussian method, which takes into account that the data has a normal distribution, whereas non-parametric classification methods do not imply the use of a normal distribution, and the advantage is using other parameters which learns the algorithm. The training data and the ground truth data were run in the ENVI 5.1 software to determine which one of the algorithms selected produces the best accuracy data,

through the Chi-square test has the best accuracy illustrated in Equation (7) The results were used to determine the rate of change.

$$\chi_c^2 = \frac{\left(O_i - E_i\right)^2}{E_i} \tag{7}$$

Maximum likelihood Algorithm

The maximum likelihood (ML) classification algorithm uses the Gaussian method for its statistical analysis, that assumes that the training data have a normal distribution (Sun *et al.*, 2013). This classification algorithm has been used by several researchers and is carefully explained by Kavzoglu and Colkesen, (2009); Otukei *et al.*, (2010) and the formula in Equation (8).

$$D = \ln\left(a_C\right) - \left[0.5\ln\left(\left|cov_C\right|\right)\right] - \left[0.5\left(X - M_C\right)T\left(cov_C^{-1}\right)\left(X - M_C\right)\right]. \tag{8}$$

Support vector machines

The support vector machine (SVM) algorithm is a statistical based learning algorithm originally formulated by Vapnik and Kotz in 1982, as published by Mountrakis *et al.*, (2011). This classification algorithm's main advantage is the use of parameters to determine the best accuracy value to classify an image through influence of the type of hyper plane that will be used (Huang *et al.*, 2002; Foody and Mathur, 2004; Mountrakis *et al.*, 2011). Playing around with different parameters assists the researcher to determine the level at which the SVM learning algorithm can perform best when classifying an satellite image Huang *et al.*, (2002). Selecting parameters involves choosing a kernel type that is best for different type of LCC studies as illustrated in Kavzoglu *et al.*, (2009), and choosing the type for multi-class change detection through multi-class LCC analysis Hsu and Lin, (2002); Foody *et al.*, (2004). Support vector machine provides a platform where the hyper-plane selects and groups of classes. Unlike most classification algorithms, the SVM has little application in remote sensing (Mountrakis *et al.*, 2011) and studies are still being done. Even if there are fewer studies conducted using SVM classification algorithm, this has only been focused on large data sets, and it is usually stated that the advantage of SVM against ML algorithm is that it performs better with large data sets Foody *et al.*, (2006). There are some studies that have

shown that SVM can perform as better as the ML algorithm with smaller datasets with an example from Mantero et al., (2005).

In this analysis, the radial basis kernel was selected as the best kernel for LCC analysis. This was done by from trying out different parameters and it is well documented by Kavzoglu and Colkesen, (2009), Otukei and Blaschke, (2010) in their literature. This is also demonstrated in Dixon and Candade, (2008) as the performances of accuracies of other kernel basis were determined from the other kernels to observe their accuracies. Within the ENVI 5.1 software, the radial basis kernel illustrates the inverse of the number of bands used in the analysis, and this automatically set when the imagery is selected for input. To get the best results for SVM classification algorithm, input values were interchanged between the penalty parameter, pyramid levels and pyramid reclassification to determine the best accuracy assessment for LCC analysis as illustrated in Pal *et al.*, (2005); Gidudu *et al.*, (2007); Mountrakis *et al.*, (2011). The penalty parameter ranged from 100-2000, the pyramid level did not matter during the analysis because there was no change within the accuracy therefore level 2 was used. The pyramid reclassification parameter, which is the probability factor was selected between the 0.01 and 0.5 confidence class to determine the best accuracy for satellite image analysis. Through classifying using the pyramid level of 0.01 and 0.5, the best pyramid parameter was selected at the penalty parameter of 1000. At the end of it all, it was noted that the most suitable pyramid reclassification level, was 0.01 confidence which gave the best result. Table 3.6 indicates the best parameters selected for Landsat 5 (TM) and Landsat 8 (OLI-TIRS) analysis.

Table 3.6: The best selected parameters for SVM

Imagery	**Bands**	**Gamma kernel calculation**	**Penalty parameter**	**Pyramid level**	**Pyramid reclassification**
Landsat 5	6	0.165	1000	2	0.01
Landsat 8	7	0.143	1000	2	0.01

3.3.4 Post classification

3.3.4.1 Change detection

The classified images generated, provided the delineation of the land cover type according to the season and the algorithm. This is demonstrated by the areal changes of the land cover over the seasons, time, and change detection was used. The change detection images were generated from the image-differencing tool from the change detection tab in ENVI 5.1. This file generates the areal changes and percentage changes of every land cover class selected in the study. The importance of image differencing is to determine changes within classes and between classes especially with optical satellite images used for various change detection methods Tewkesbury *et al.*, (2015). To carry out change detection analysis, this method encompasses the comparison of percentage LCC values within seasons across the years of the study. The comparison results from seasonal and year analysis, were then used separately for the classification algorithms, to illustrate changes across the season and years. After this, the same results generated were compared to determine the performance of the algorithms on the individual LC class and across the years. This is discussed in detail in using the change detection tables generated from image differencing, which provides support for the best classification algorithm suitable for LCC analysis.

3.3.4.2 Accuracy assessment

After the change detection was completed, the accuracy assessment for the performance of the algorithms on the land cover using ground truth data was determined. Ground truth data in this study was describes as purest pixel to that determined the LC type of the area. With the help of Google Earth images, aerial photographs and field assessment conducted for the validation for the LC type the purest pixels were selected. The accuracy assessment was determined using a covariance matrix, which provided the omission, commission errors and producer and user accuracy.

3.3.5 Basic hydrology

The purpose of using a DEM was to determine the river flow and direction of the Doringspruit river which would be used in determining the land cover type dominant around the section of the river. Using the Hydrology classification tool in ArcMap, the river profile was generated from the DEM file.

3.3.6 Meteorological data analysis

Data from Kroningspark station were imported into Excel 2013; data were analyzed according to the mean annual maximum temperature (MATmax), mean annual minimum

temperature (MATmin) and total annual rainfall (TAR). The information was on was split into the early 25 years from the time HartRAO started and to the recent 25 years of the study. This is demonstrated by using the first (1^{st}) and second (2^{nd}) normal in the study. The 1^{st} Normal ranged from 1960 to 1989 and the 2^{nd} Normal was from 1985 to 2014. The data received from the study was organized and sorted using EXCEL and saved as comma delimited files. The CSV files were then used in the TREND software to carry out statistical analysis. The statistical test conducted for the climate data was Mann-Kendall test and the results of this test provided the various trends.

4 RESULTS AND DISCUSSIONS

The four objectives are reported on and discussed. They include the delineation of the land cover type, which means that the land cover types are identified using field based assessments, image ratioing, basic hydrology, aerial photographs and satellite image analysis. These methods were used for visual and statistical interpretation to determine the dominant land cover type. Climate information is included in the analysis when comparing the land cover types as the trends help in telling why there has been a change within and between land cover types. The second and third objective looks at comparison of classification algorithms and best classification algorithm in with regards to hilly landscapes with the use of parametric and non-parametric classification algorithms. The discussion brings all the first three objectives together and analyses these data sets by identifying trends and changes in land cover types.

4.1 Delineation of Land Cover Types

This section describes the various land cover types noted from the field assessment conducted. The images varying differences in the land cover, which is used to determine the title of the land cover types for this study.

4.1.1 Land cover delineation through field based assessment

4.1.1.1 The forest-land cover type

The forest-land cover type is described as having both deciduous trees, evergreen trees and tall grass. The occurrence of this land cover type is generally located along the Doringspruit stream and the slopes of the Witswatersberg hills. In the midst of the trees, there is the presence of grass as demonstrated from the images in Figure 4.1. As noted in Figure 4.1a, a section of the study area depicts a valley that contains a mixture of trees and some tall grass. According to Figure 4.1b, this section of the study area includes trees growing on the slopes, in general the trees grow on the hilltops as well as the change in elevation is relatively small. In between the trees there is the appearance of some patches of long grass. As presented in Figure 4.1c, this is an overview of the distribution of the forest-land cover across the slopes of the study area.

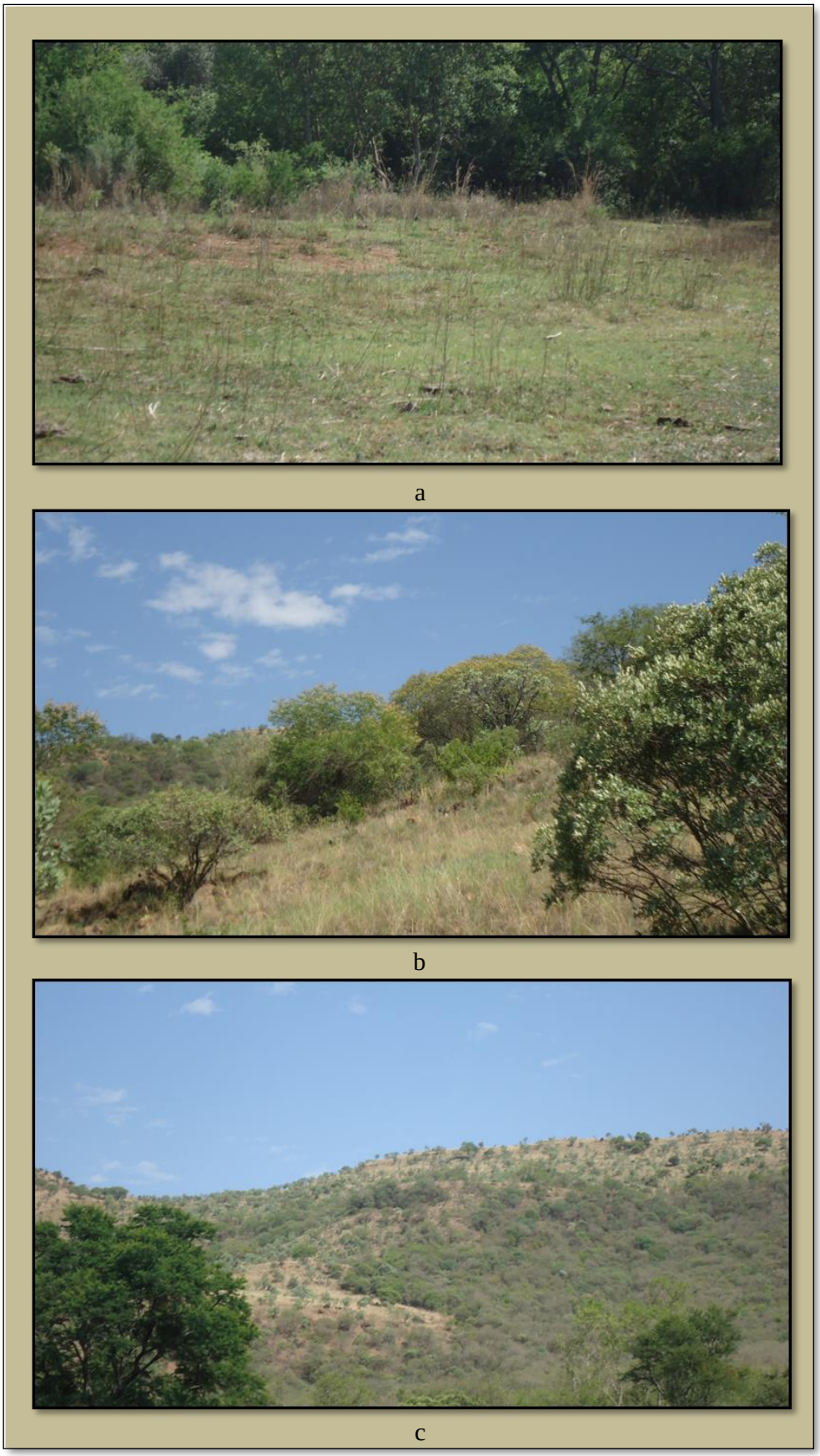

a

b

c

Figure 4.1(a,b,c): Photographs of the various forest-land cover in the study area.

4.1.1.2 The grassland cover type

Figure 4.2 illustrates that the grassland cover type comprises tall grass and pasture grass and a few shrubs. The pasture grass indicates that this area is suitable farmland for cattle farming. Figure 4.2a illustrates pasture grass, indicating that within some areas of the HartRAO surroundings there is potential for cattle farming as a land use activity. Figure 4.2b illustrates tall grass which indicates deeper soils, presence of underground water and trees in the distance indicate a river channel. Typically, on site, trees cluster stream banks, this is clearly visible in the aerial photographs of the area. According Figure 4.2c, this pictures grassland cover type, which is predominantly on level ground and the slopes indicate random distribution of trees.

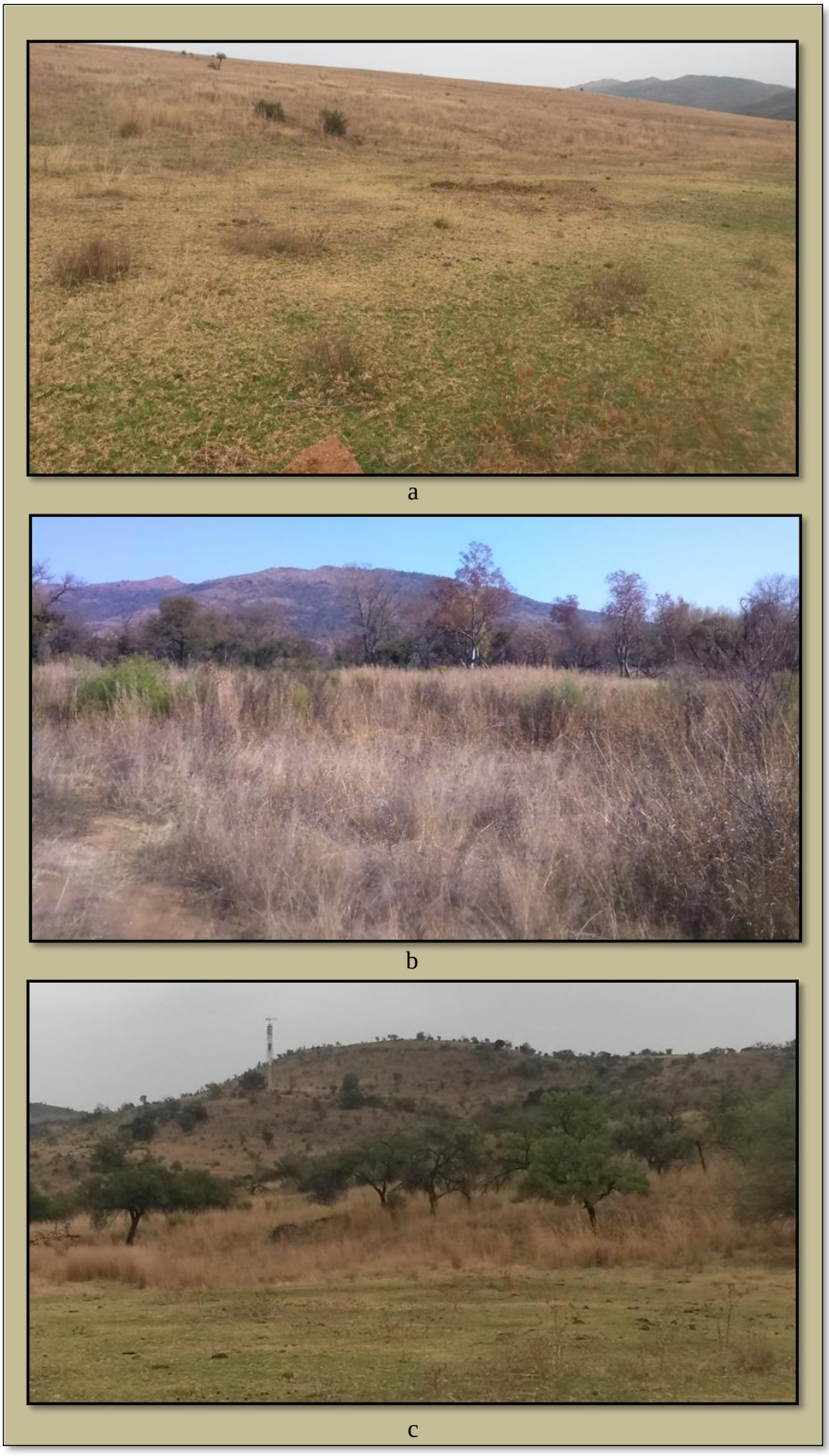

a

b

c

Figure 4.2 (a,b,c): Photographs of the various grassland cover in the study area.

4.1.1.3 The scattered vegetation land cover type

According to the images contained in Figure 4.3, these images provide the description of scattered vegetation land cover selected for the study. This land cover type composed of, a mixture of shrubs, grass and rocks out crop. There was a notable variety of acacia tree species was dominant as shrubs. According to Figure 4.3a, the scattered vegetation land cover type is illustrated as dry grass, and some shrubs (mainly acacia trees), some patches bare-soils and a few shale rocks. The description in Figure 4.3b, provides a different grass type, mainly herbaceous and tall grass that can be found in flooded areas. There are some shrubs located in the area and smooth shale rocks, usually located on river profiles or flood zones. Overall, the shale rocks in these areas seem to be smooth in shape.

Figure 4.3(a,b,c): Photographs of various scattered vegetation land cover in the study area.

4.1.1.4 The shale rock with scattered vegetation land cover type

This land cover type falls within bare-soil and bare-rock land cover. This describes some sections of the HartRAO environment and its environment depicted more of the shale rock type. This land cover type is usually located on the top parts of the Witswatersberg hills. Growing in between the shale rock, are grass, shrubs, interspersed with patches of bare-soils as shown in Figure 4.4. According to Figure 4.4a, the shale rock is sharp with presence of bare-soils and short grass. In Figure 4.4b this land cover type is illustrated with the presence of shale rock, thorny shrubs, short grass and patches of bare-soils.

a

b

Figure 4.4 (a, b, c): Photographs of the various shale rocks with scattered vegetation and land cover types in the study area.

4.1.1.5 Milky quartz rocks with scattered vegetation land cover type

This land cover type is described by the occurrence of herbaceous species, which was appears to be slightly different from the shale rock with scattered vegetation land cover type. The various types are represented in Figure 4.5 images. Figure 4.5a, depicts presence of milky quartz rocks with green herbaceous plants. Bordering this land cover are some trees species, this land cover type is located towards the top of the hills in this study area. According to Figure 4.5b and Figure 4.5c, these images were enlarged to provide a detailed background of this land cover type. The last two images illustrate that there are some short thorny shrubs growing amongst the milky quartz rocks. There is a huge presence of bare-soil exposed on this land cover type.

a

b

c

Figure 4.5(a,b,c): Photographs of the various milky quartz rock with scattered vegetation land cover in the study area.

4.1.1.6 The built-up land cover type

The built-up land cover description entails any form of construction and demolition. This land cover is dominated by the presence of buildings, roads, impervious surfaces as illustrated in some images of

Figure 4.6. This is seen near HartRAO and its facilities. Since much of the land use activities, rotate around the radio observatory.

Figure 4.6a depicts a picture of a water tank on scattered vegetation.

Figure 4.6b illustrates the 26m dish within HartRAO and buildings within the Observatory. The land cover is also predominantly grassland and a few trees. There are a few roads leading to HartRAO and some local roads to give way to vehicles used in HartRAO. The image in

Figure 4.6c depicts an abandoned house structure, this illustrates that apart from HartRAO there were people living in the area at least a hundred years ago. The house structure is made from a mixture of mud and shale rock. These could be abandoned pastoralists houses.

Figure 4.6d illustrates a demolished area, with run down cement remains illustrating there used to be a shelter that was demolished.

Figure 4.6 (a,b,c,d):Photographs of the various built-up land cover type within the study area

To complete the delineation of the land cover change section, short summary of the land cover types and locations are tabulated in Table 4.1.

Table 4.1: Land cover type and description selected for the analysis and study area

	Land Cover type for the study area	**Group**	**Description**	**Occurrence on the landscape**
1	Forest (F)	Mixed Forest	Broadleaf and narrow leaf, with thorn tree.	Middle of the hills near stream, and 500 m from the valley
2	Grassland (G)	Herbaceous	Grass and pasture	Near stream profile, Valley
3	Sparse Vegetation (SV)	Herbaceous	Shrubs and dry grass	Near stream profile, Valley
4	Shale rock and scattered vegetation (SSV)	Bare-land	Low vegetation cover, high occurrence of shale rocks with brown and red soils	Top part of the hills
5	Milk quartz rocks and scattered vegetation(MSV)	Bare-land	Low vegetation cover, high occurrence of milky quartz rocks, brown and red soils	Top parts of the hills
6	Built-up (BU)	Built-up	Demolished houses, and HartRAO, road and paths	Within 200m to 500m radius of HartRAO

4.1.2 Image ratioing

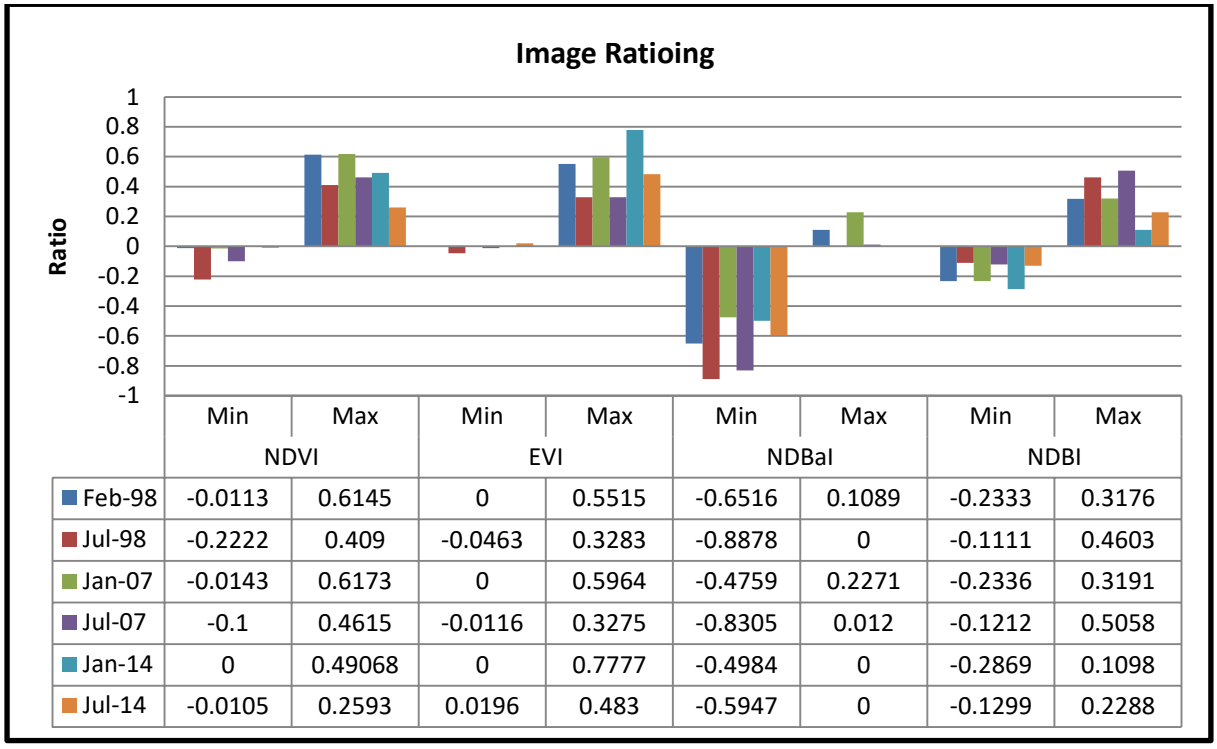

	Min	Max	Min	Max	Min	Max	Min	Max
	NDVI		EVI		NDBaI		NDBI	
Feb-98	-0.0113	0.6145	0	0.5515	-0.6516	0.1089	-0.2333	0.3176
Jul-98	-0.2222	0.409	-0.0463	0.3283	-0.8878	0	-0.1111	0.4603
Jan-07	-0.0143	0.6173	0	0.5964	-0.4759	0.2271	-0.2336	0.3191
Jul-07	-0.1	0.4615	-0.0116	0.3275	-0.8305	0.012	-0.1212	0.5058
Jan-14	0	0.49068	0	0.7777	-0.4984	0	-0.2869	0.1098
Jul-14	-0.0105	0.2593	0.0196	0.483	-0.5947	0	-0.1299	0.2288

Figure 4.7: Graph of maximum and minimum values of the spectral indices used in image ratioing.

The results for the spectral indices used in this analysis are demonstrated in Figure 4.7. The NDVI and EVI values are greater than 0.25 for all the years as illustrated in Figure 4.7, which shows there is presence of high vegetation cover. It is also noted that the NDVI values are higher than EVI values for both summer and winter seasons of the years 1998 and 2007. As much as the NDVI and EVI values are higher in summer and winter, it is only selected that the EVI values are higher than the NDVI values especially in January 2014, which indicates highest EVI values recorded on the Landsat images used in the study. Contrary, NDBaI values are lower. This is the opposite of EVI and NDVI values as it is also demonstrated from the results that the NDBaI. As stated the uses in the literature review, NDVI and EVI spectral indices are used to measure the presence of vegetation cover in a landscape, while NDBaI measures the exposure of bare-land. In confirming the result, the indices demonstrate that vegetation is the dominant land cover type in the study.

An interesting result was the values of NDBI calculations were higher for this study. The built-up infrastructure of HartRAO and its surroundings is lower as this area is prevalently free from any atmospheric and built-up interference. As we did the field analysis, since this

was the most dominant issue within the land cover change analysis using Landsat data, the study area contains rock out crops of shale and milky quartz rocks. This influenced the values of the NDBI, as NDBI can pick up rock formation and interpret it as built-up structures. The influence of the thermal band and the reflective properties of the rocks had an influence of the NDBI results. Thus, the importance of incorporating the NDBaI spectral index, as it is an index that picks up the thermal properties of the bare-soil unlike the NDBI spectral index. This section of the results is expanded in the discussion, as to why these indices were selected and to demonstrate the rate of change in the area over the period of study.

4.1.3 Basic hydrology

It was necessary to extract the river profile to complete the land cover type. It was also important to determine the flow of the river, which also plays a part on the land cover types. Extraction of the river profile is illustrated in Figure 4.8 and this was done by analyzing SRTM data (DEM file). In studies, river flow towards lower altitude. Presence of vegetation and tree cover are dominant in on river profile. Higher altitudes indicate presence of exposed bare-rock and lower vegetation due to temperature variability and rainfall.

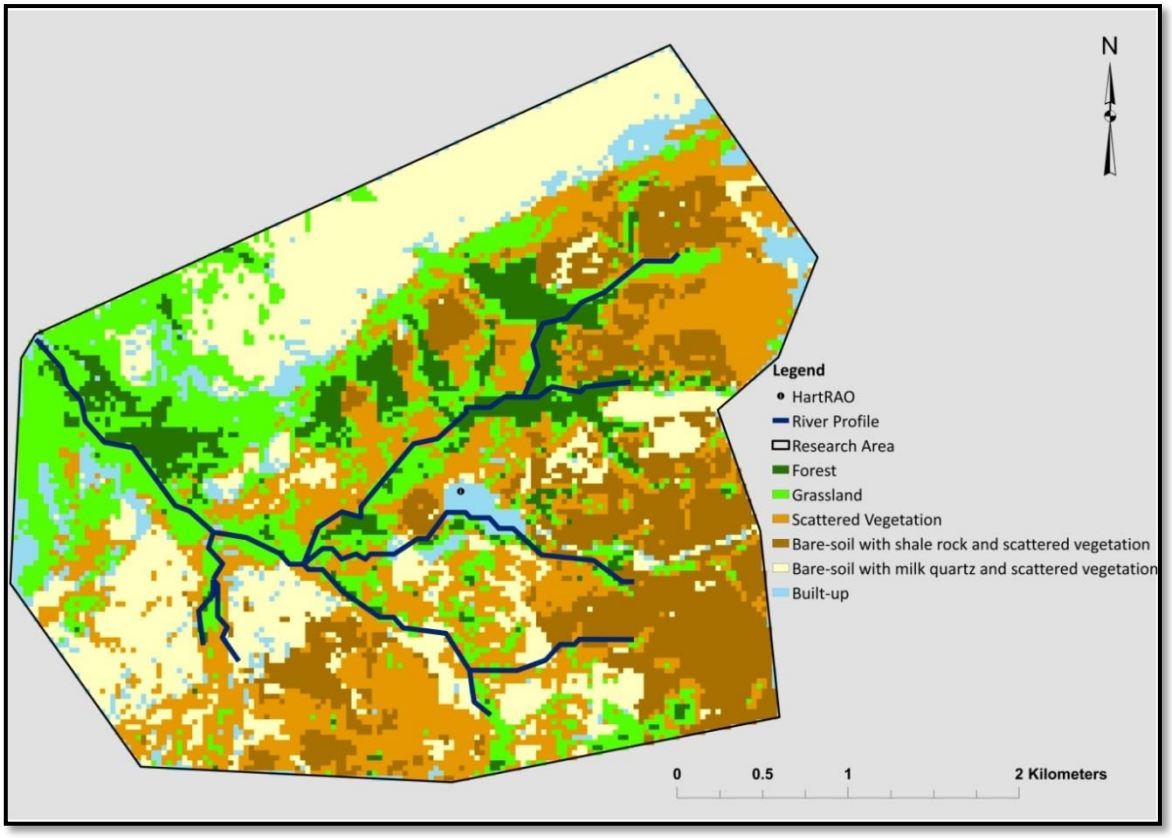

Figure 4.8: River flow direction and land cover types.

The main channel of the river flows from the north-west parts of the study area, and tributaries emerge towards the east and south-east areas. Trees growth is closer to the river profile. Tall grass and some trees are slightly further away from the river profile. Towards the top of the hills is the presence of milky quartz rocks and some herbaceous plants with short grass. Towards the south east and east part of the river profile, there is a heavy presence of shale rocks, closer to the tributaries, the shale rocks were round and smooth while further away from the river profile they were sharp with defined edges.

4.1.4 Aerial image interpretation and climate data analysis for the first normal

a


Land Cover around HartRAO Location-1963
N
475
21/4/63
LENS 152.55mm.
1/36.000

b


Land Cover around HartRAO Location-1963
N
475
21/4/63
LENS 152.55mm.
1/36.000

c

d

Figure 4.9 (a,b,c): Aerial photographs depicting land and cover type within the HartRAO location in 1963.

The overview of the position of HartRAO and its surrounding is illustrated from the 1963 aerial photograph in Figure 4.9a. This demonstrates the demarcation of the farmlands the rock pattern of the Witswatersberg. In Figure 4.9b and Figure 4.9c are the zoomed images of HartRAO and its surroundings. The light and bright tones indicate that there is presence of exposed bare-land. Tree cover is minimal due to an increase in agricultural activity; this is demonstrated with bright and dark parcels. Figure 4.9d is zoomed to HartRAO and it depicts that there is some tree cover between the slopes of the Witswatersberg hills. Along the Doringspruit River flows from northwest to south-east and east, vegetation is dominant as illustrated by the dark grains in the picture. This can be noted from Figure 4.9d as there is alignment of trees along the rivers course. The cliffs of the Witswatersberg hills indicate sharp rock outcrops. There is a presence of defined roads heading as towards HartRAO illustrated in Figure 4.9d, north and north east of HartRAO as illustrated in Figure 4.9c and north to south of HartRAO as indicated in Figure 4.9c.

a

b

Figure 4.10(a,b,c): Aerial photographs depicting land and cover type within the HartRAO location in 1984.

Figure 4.10a provides an overview of HartRAO and its surroundings in the year 1984. The image seems brighter and the farmlands appear to be fewer than in the year 1963. This could be an indication of an increased in exposed bare-land due to the brighter tones appearing on the aerial photographs. The aerial photographs show lighter tones. According to the zoomed in aerial photograph of the year 1984 from Figure 4.10b, the image gives an indication of darker tones, demonstrating a presence of vegetation increase in the area as compared to the 1963 images. There is an increase of vegetation cover on the slopes of the Witswatersberg and along the Doringspruit River profile. There is a significant increase in the brighter tones on the parcels of land. This indicates exposure of bare-land in these areas because of agricultural activities. This is an indication that there is low presence of crop cover in the area. According to Figure 4.10b and Figure 4.10c, there are fewer agricultural land demarcations. The other evident change is the decrease of the roads as noted in 1963 aerial

photographs, that means there was reduction of movement and an alternative route was created for people to pass through.

a

b

c

Figure 4.11(a, b, c): Aerial photographs depicting land cover type within the HartRAO location in 2004.

The overview of the aerial photograph 2004 in Figure 4.11a indicated an increase in larger agricultural farms when one compares the size of the parcels of land from the years 1963 and 1984 of the same area. Another interesting aspect is the increase of roads and visible demarcations of the parcels of land this means there was access to areas that were to accessible by vehicles. It is also an indication of increase agricultural activity within the surrounding areas of HartRAO. There is an increase in vegetation along the slopes of the Witswatersberg hills as illustrated in Figure 4.11b and Figure 4.11c. The darker pixels in the aerial photograph, illustrate vegetation cover and this indicated on the image by the increase of the number of trees along the slopes. On the left side of the images in Figure 4.11b and Figure 4.11c it is noted that there is a bright undertone indicating presence of a mining activity. Bare-soil land has increased within the HartRAO facility because this is a built-up area as demonstrated in Figure 4.11b and Figure 4.11c. So far, the only noticeable road that heads towards HartRAO, all the roads as described from the 1963 and 1984 aerial photographs have disappeared and covered with a different land cover type. Figure 4.11b and Figure 4.11c indicate there is an increase in the density of the trees along the Doringspruit River. Concentration of tree cover illustrates a mixture of tree types and explained during the process of delineation of the land cover types using the field study as what type of forest is within HartRAO and its environment.


Aerial Photograph 2013
N

a

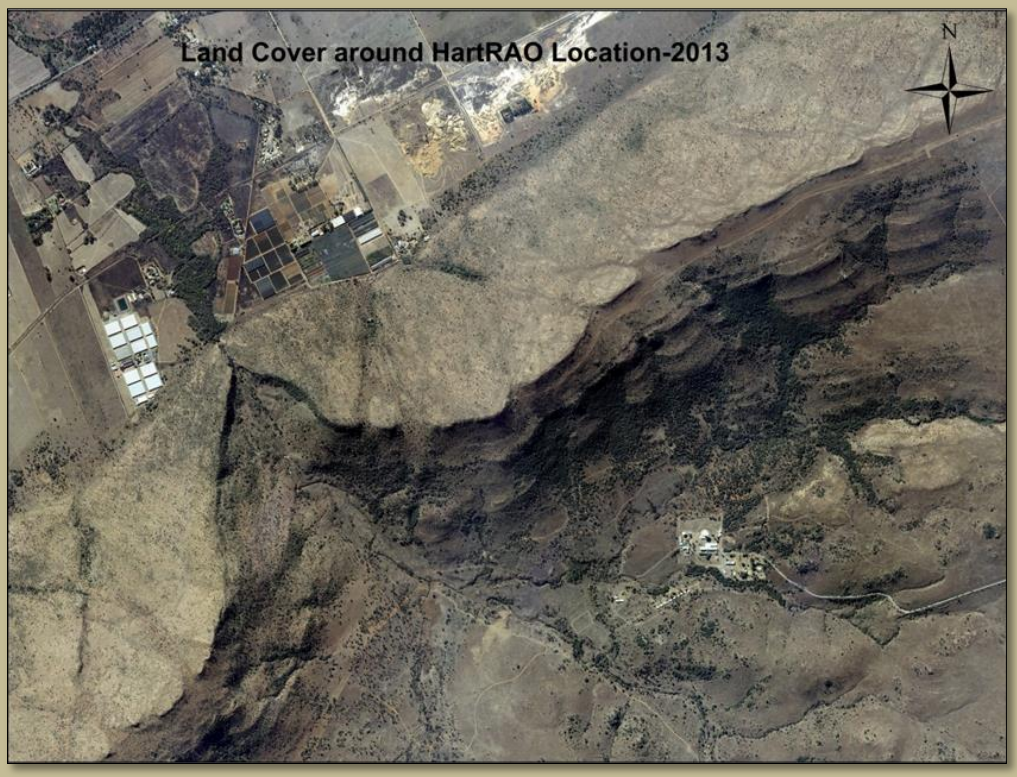
Land Cover around HartRAO Location-2013
N

b

c

Figure 4.12(a,b,c): Aerial photographs depicting land cover type within HartRAO location in 2013.

The coloured aerial photograph of the year 2013 in Figure 4.12a, provides a recent image of the area of study. According to Figure 4.12a, the agricultural parcels are larger compared to the preceding years. On the top part of Figure 4.12a there is an increase in abandoned areas and some have been converted into a mining environment and a notable increase of the roads in general. On the top right of Figure 4.12a there is an increase of residential areas compared to the farmlands noted in 1963 to 2004. Figure 4.12b and Figure 4.12c, are zoomed in image, which illustrates an increase in vegetation cover and distribution on the slopes of the Witswatersberg hills. There are more trees towards the north, while the river profile is not visible. The HartRAO facility has expanded and, there road that heads towards HartRAO is defined.

The importance of using these aerial photographs it to demonstrate the reason why the facility was built within this area, the impact of land use and to determine land cover changes over

the years within HartRAO and its environment. The other important thing was to have a feel of the general land cover type that has been within HartRAO and its environment. The aerial photographs play a role in delineating the land cover type and confirming what would have been the general situation over the years that would affect the land cover within HartRAO. This also gave some guidance when conducting image classification.

1ST Normal Climate Data Analysis 1960-1989

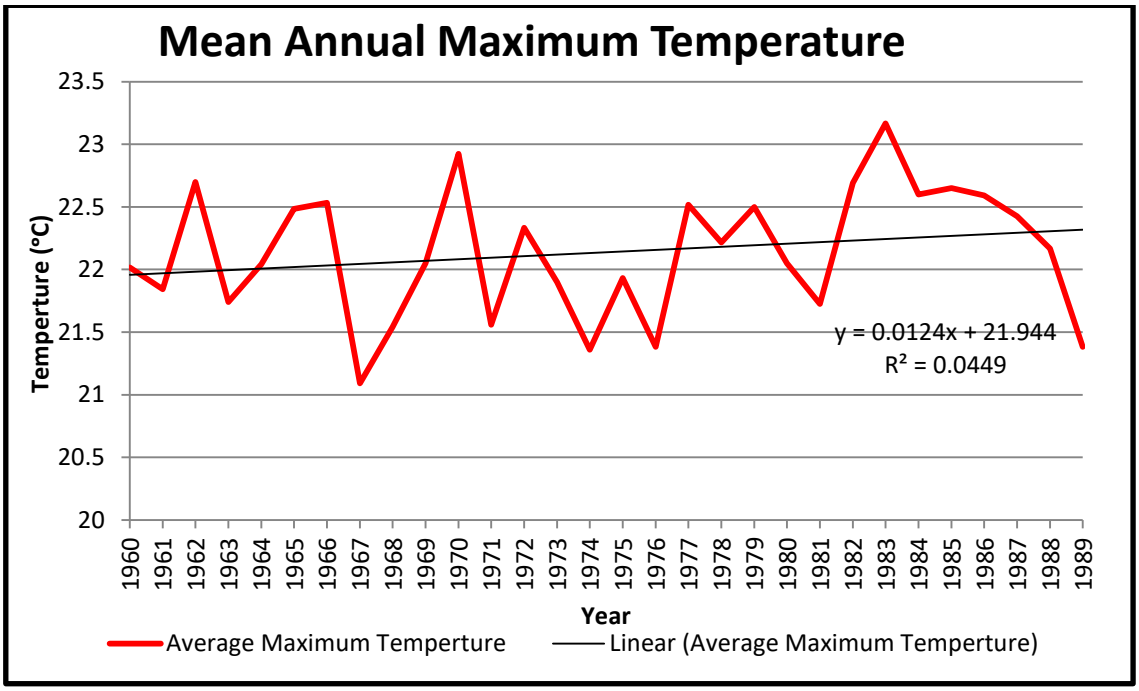

Figure 4.13: Mean annual maximum temperature from 1960 to 1989

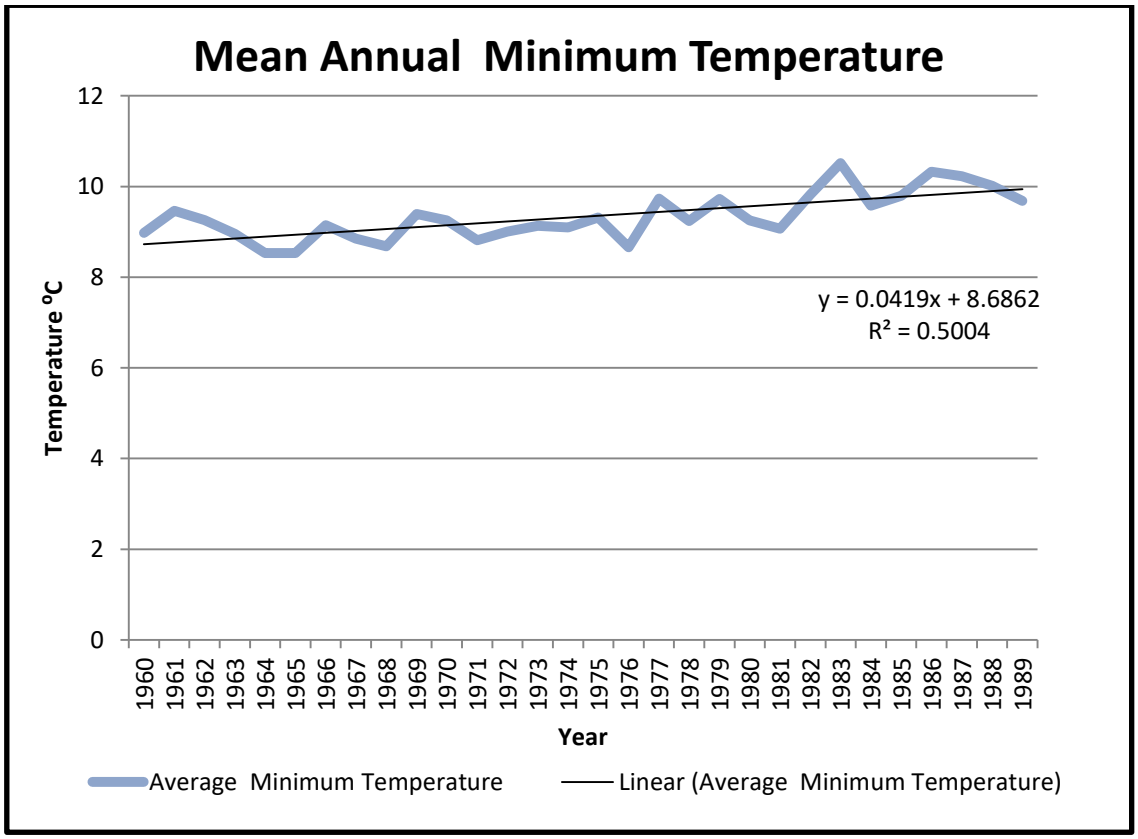

Figure 4.14: Mean annual minimum temperature from 1960 to 1989

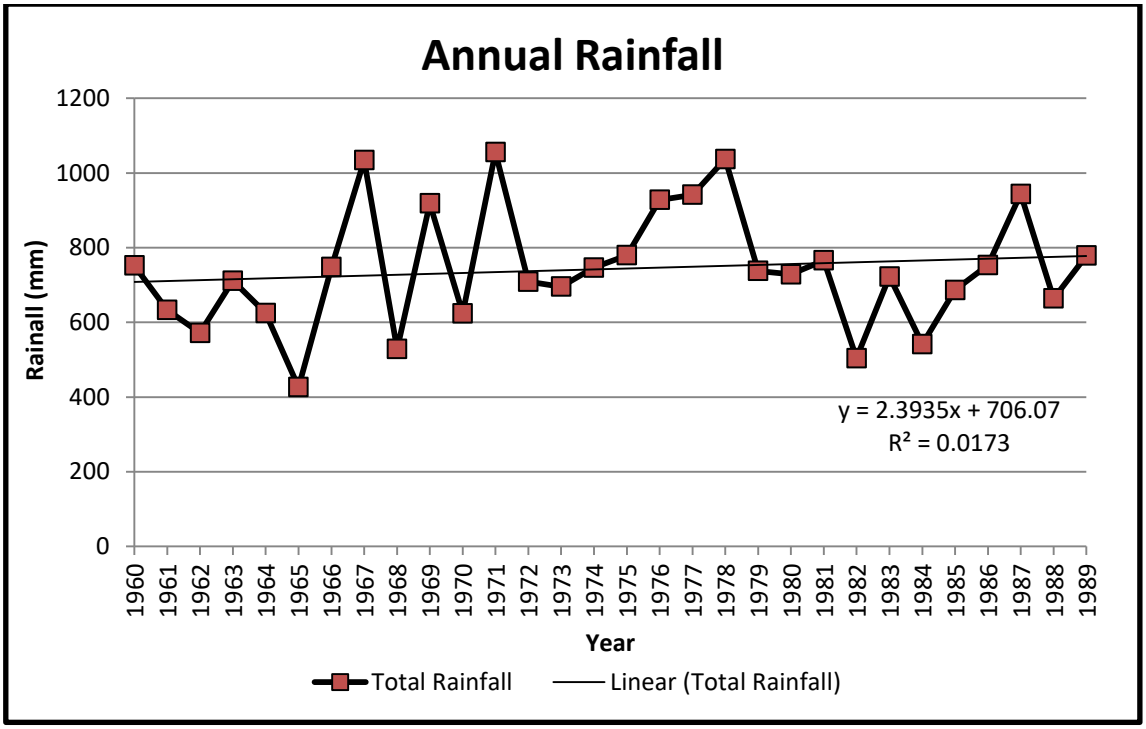

Figure 4.15: Total annual precipitation from 1960 to 1989.

Table 4.2: Mann-Kendall test for the 1st Normal of the years 1960 to 1985.

	Mean	Total Score	Standard Deviation	z-statistic	Result
MATmax	22.13°C	64	56.051	1.124	Increasing/no stat significance a= 0.10
MATmin	9.33°C	205	56.051	3.64	Increasing, stat significance a<0.10
AR	743mm	49	56.051	0.856	Increasing/no stat significance a=0.10

Analysis of the first normal is composed of temperature and rainfall data from 1960 to 1989 from Figure 4.13 to Figure 4.15. According to Figure 4.13, MATmax has an increasing trend, but using the linear trend analysis from the Mann-Kendall test illustrates no significance at the 90% confidence level from Table 4.2. For the year 1967, MATmax has the lowest recorded value. Towards the end of the first normal, from the years 1985 to 1989, MATmax indicates a declining trend. The highest MATmax recorded was in year 1983 with the mean MATmax is for the year was 22.13°C. The MATmin values are illustrated in Figure 4.14 and points towards an increasing trend. The minimum temperature values recorded keep increasing with a new MATmin recorded. At the same time, the highest MATmin recorded was in 1983 as the same as MATmax. According to Table 3.1, the Mann-Kendall test results

indicate an increasing trend, with statistical significance at the 90% confidence level and the average MATmin is 9.33^{o}C. The annual rainfall (AR) values in Figure 4.15, indicate an increasing trend with the highest rainfall values in 1971, while the lowest AR was recorded in 1965. However, from the Mann-Kendall test results in Table 4.2 give the average value of 743 ml with an increasing trend, but with no statistical significance at 90%.

4.1.5 Satellite image analysis and climate data analysis for the second normal

Landsat satellite imagery was used to determine the changes in the land cover and the rate of change. Two classification algorithms: maximum likelihood (ML) and support vector machine (SVM) were used to determine the land cover types. The techniques are: classification of land cover types, change detection to determine area changes of the land cover types in the study, determining the accuracy of the classification algorithms and comparison of these change detection and accuracy of these classification algorithms. The importance of the using these methods was to determine the rate of changes and the level of classification on a hilly terrain on Landsat TM and Landsat OLI of the area.

4.1.5.1 Change detection

The importance of land cover changes is useful to delineate the land cover type of the area and determine the percentage and areal changes that have occurred over a period. Land cover changes can be categorized as: changes between land cover classes and within land cover classes. The overall classification results and the change detection results were used to determine the various land cover changes. This was used to pin point the land cover conversions and shifts. Illustrations from Figure 4.16 to Figure 4.21 depict specific land cover changes from the outputs of the image classification. The analysis was dependent on the type of classification algorithm, seasonal and yearly climatic changes.

Summer images

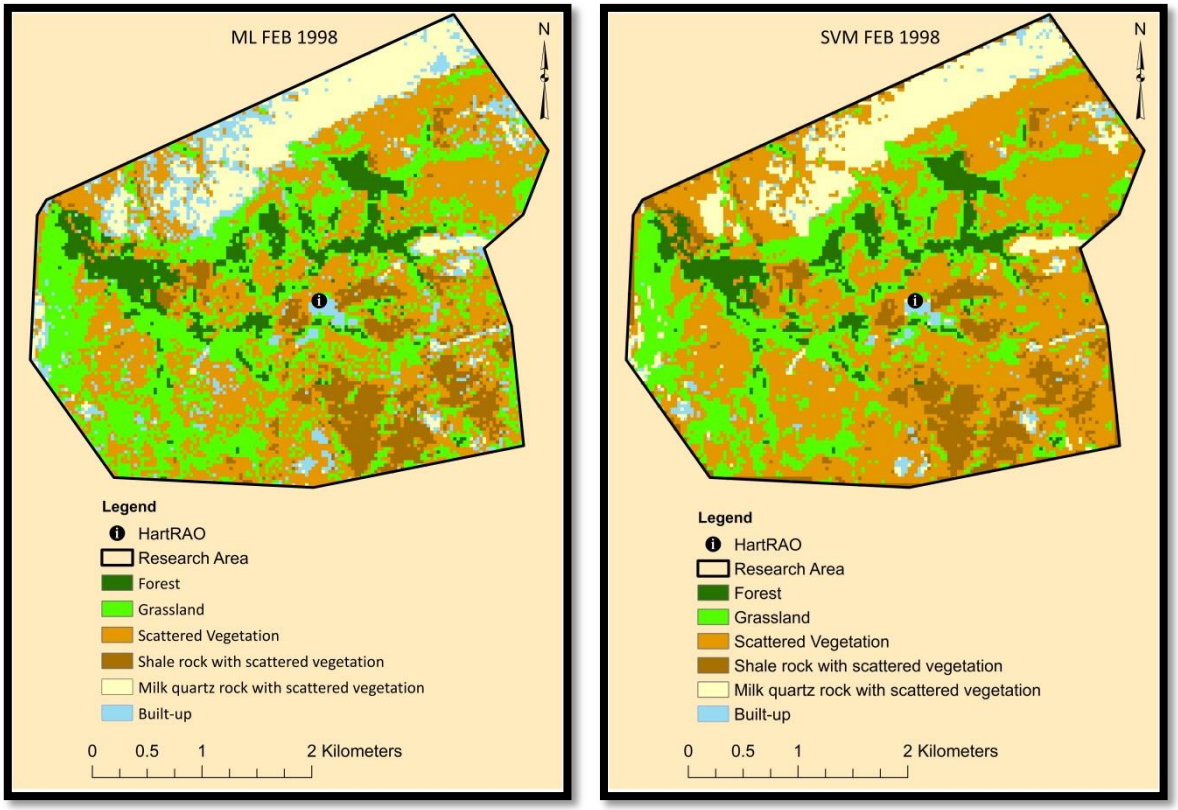

Figure 4.16: ML and SVM classification for February 1998 Landsat imagery.

In this analysis of the Landsat images for the summer images of the year 1998, the ML and SVM image classification depicted in Figure 4.16, illustrated there is an increase of built-up areas within the ML classification analysis compared to SVM classification images. This is demonstrated by the increase of built-up from the north-west side of the images of the ML classification images. Whereas, with the SVM classification image, there are more areas that contain scattered vegetation. The grassland cover was dominant from the ML classification compared to the SVM classification image. While areas covered with grassland from ML classification images are covered by scattered vegetation in SVM classification images.

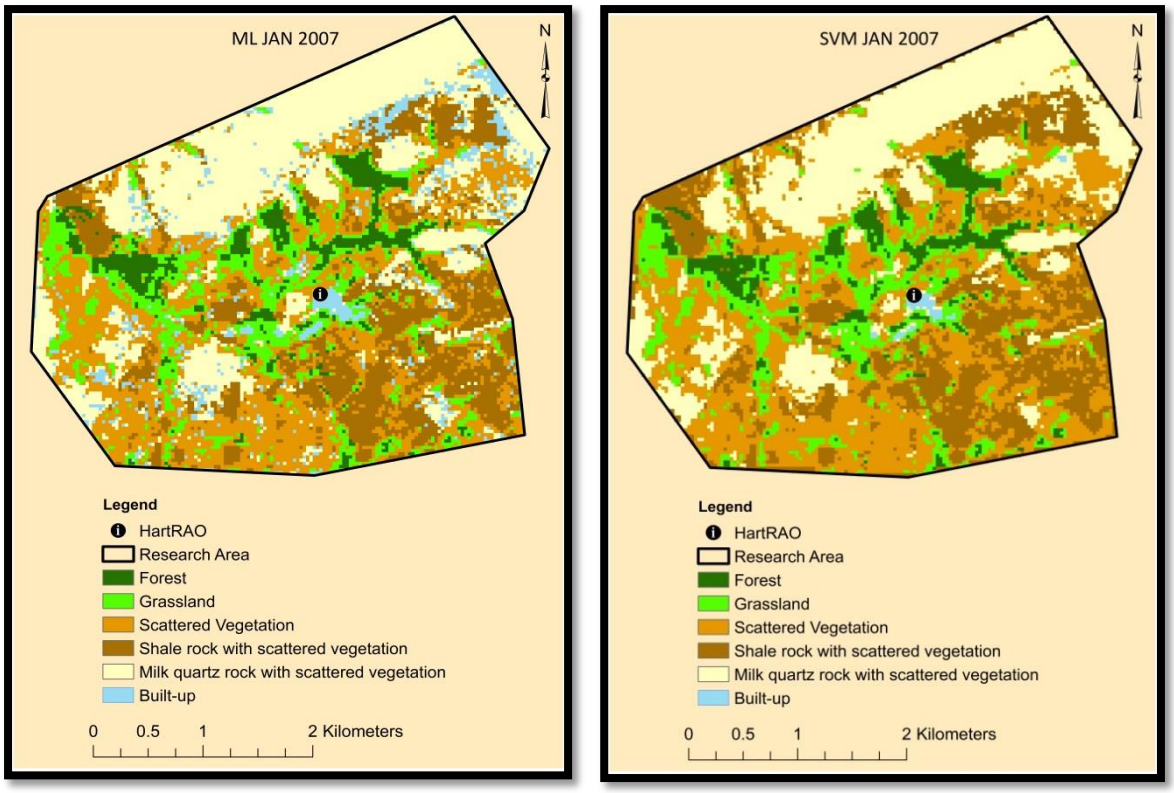

Figure 4.17: ML and SVM classification for January 2007 Landsat imagery.

According to ML and SVM image classification of the Landsat images of the 2007 in Figure 4.17, both images indicate there is an increase all the other land covers except for grassland and forest land cover. There is a significant built-up land cover is dominant on the ML classification compared to the SVM classification image. Areas covered in milky quartz rock with scattered vegetation land cover are much more visible from the ML classification compared to SVM classification.

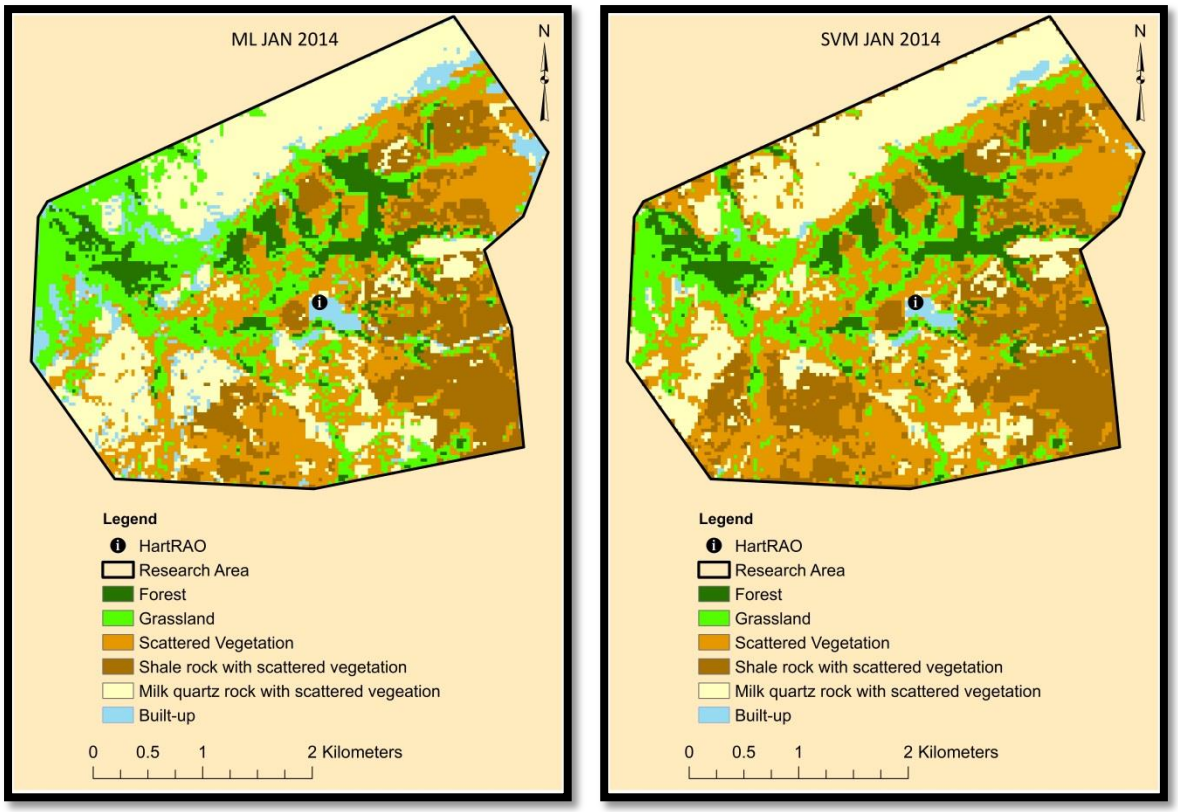

Figure 4.18: ML and SVM classification for January 2014 Landsat imagery.

The classification for the January 2014 images in Figure 4.18, depicts there is an increase in the grassland, forest and milky quartz rock with scattered vegetation land cover for both images. According to the ML classification image, the grassland land cover is much more dominant compared to SVM classification. The built-up land cover is also dominant in the ML classification image compared to SVM classification image. Milk-quartz rock land cover is very dominant on the west side of the ML classification image, while shale-rock with scattered vegetation is dominant on the west part side of the SVM classification image. The grassland land cover is dominant on the north part of the ML classification image whilst scattered vegetation is dominant on the north part of SVM classification image.

Winter images

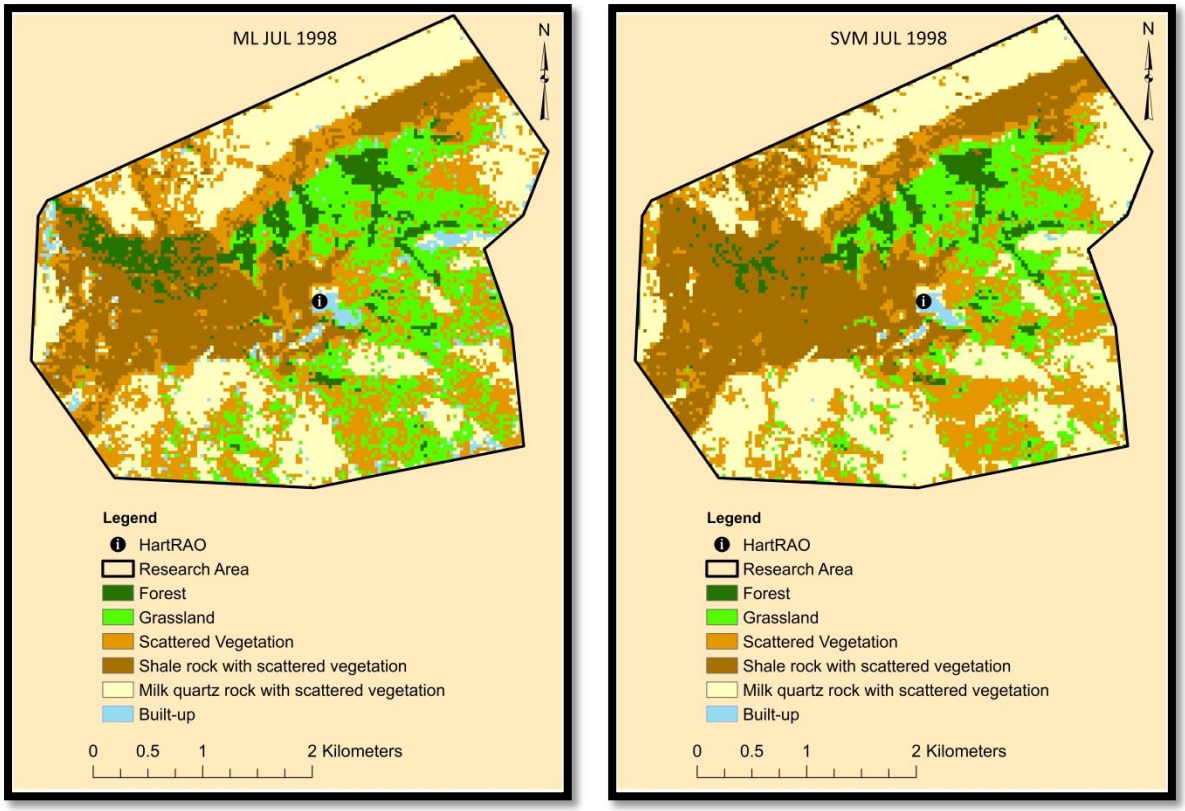

Figure 4.19: ML and SVM classification for July 1998 Landsat imagery.

Both ML and SVM classification images of July 1998 in Figure 4.19, depict that there is a decrease in forest and grassland cover. The shale rocks with scattered vegetation cover type appear dominant on the west parts of both ML and SVM classification images. According to the ML classification image, the grassland land cover is dominant on the east part of the images. Agreeing with the SVM classification image there is a mixture of the scattered vegetation and grassland cover type from the north part of both images. Forest, grassland and built-up land cover occupies a bigger percentage of the area in the ML classification image in proportion to the SVM classification image.

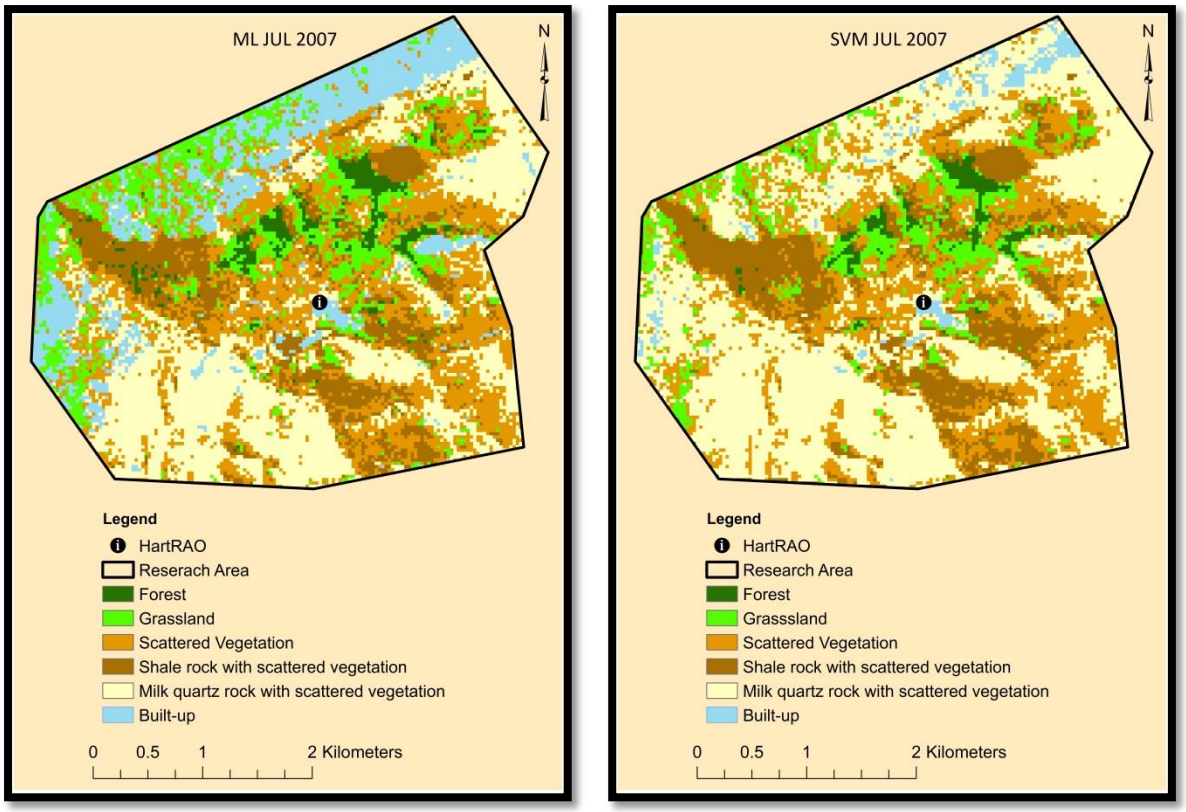

Figure 4.20: ML and SVM classification for July 2007 Landsat imagery.

Figure 4.20, classification of the Landsat imagery of the year 2007, illustrates there is an increase of built-up land cover in ML classification compared to SVM classification imagery. Both satellite image classifications demonstrate and increase in compared to the shale rock with scattered vegetation land cover in Figure 4.19. The grassland cover occupies the north part of the classification images in Figure 4.20. The areas covered by built-up in ML classification is represented as milky quartz rocks with scattered vegetation in SVM image classification.

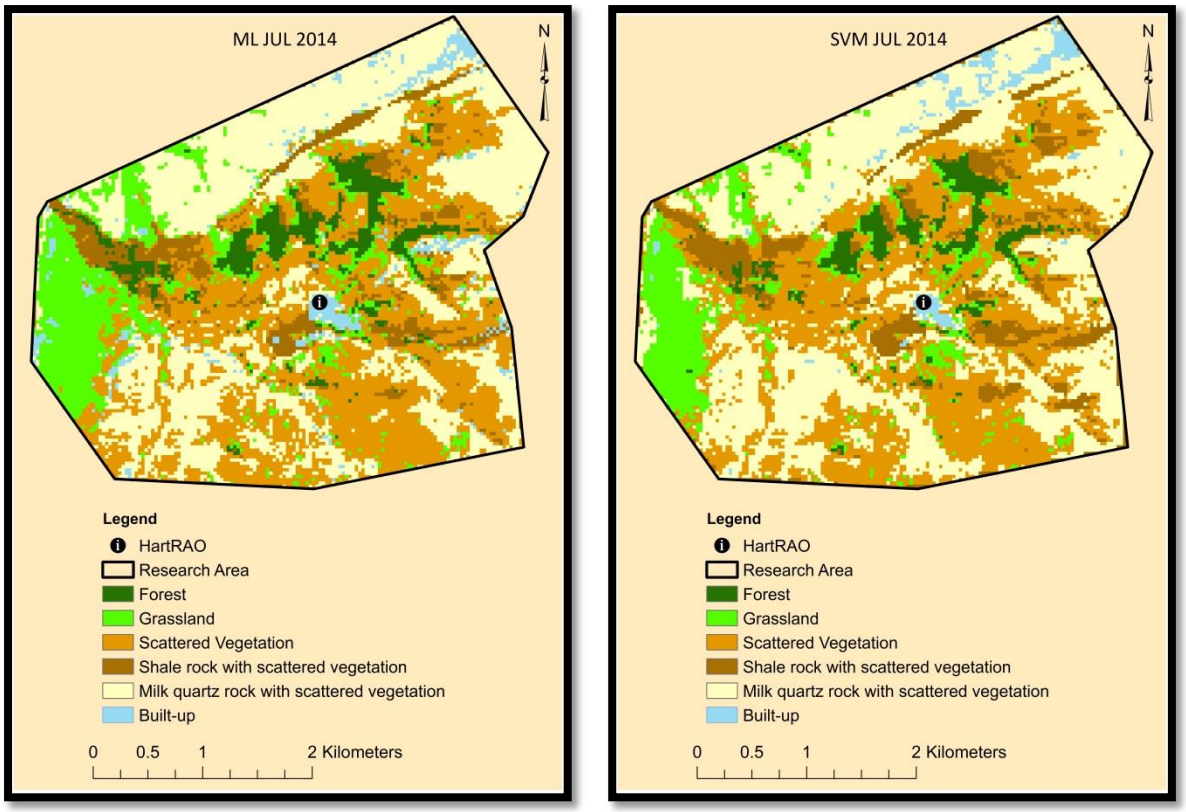

Figure 4.21: ML and SVM classification for July 2014 Landsat imagery.

According to the ML and SVM classification, analysis of from Figure 4.21 illustrates that grassland cover type covers the west part of the images respectively. In both classification images, there is an increase in scattered vegetation. Both images depict less built-up area compared to Figure 4.20. In this analysis the forest land cover has increased for both ML and SVM classification compared to the images in Figure 4.20.

4.1.5.2 2nd Normal climate data analysis

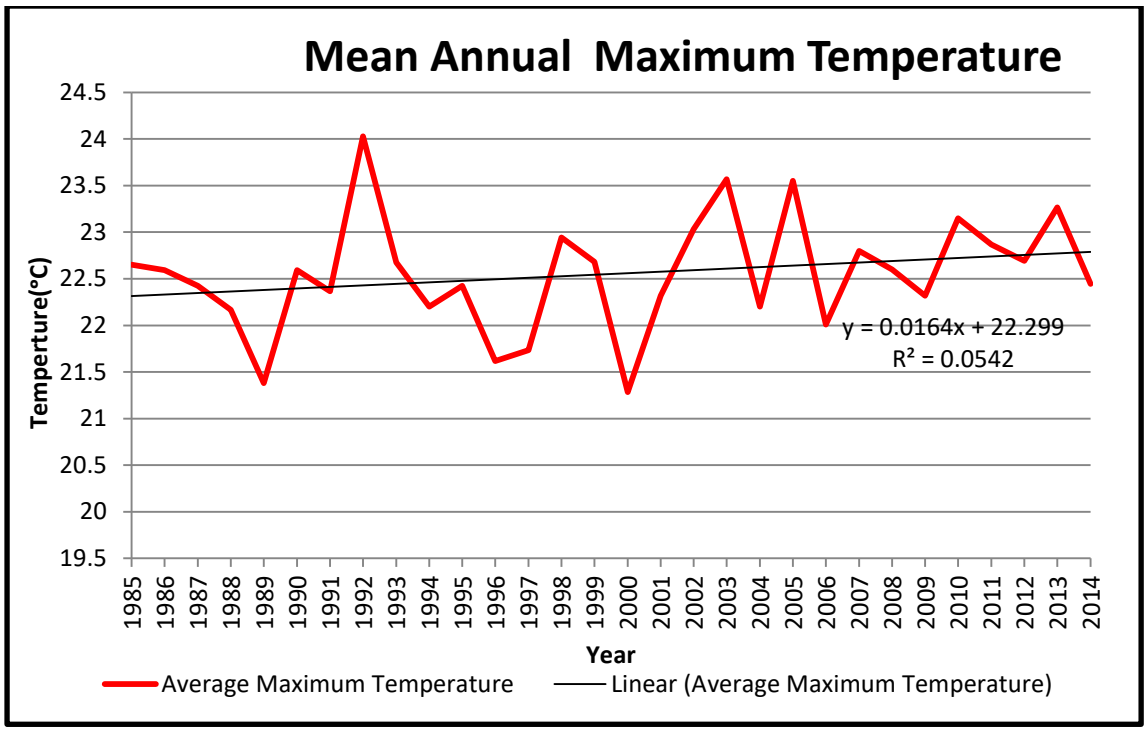

Figure 4.22: Mean annual maximum temperature from 1985-2014

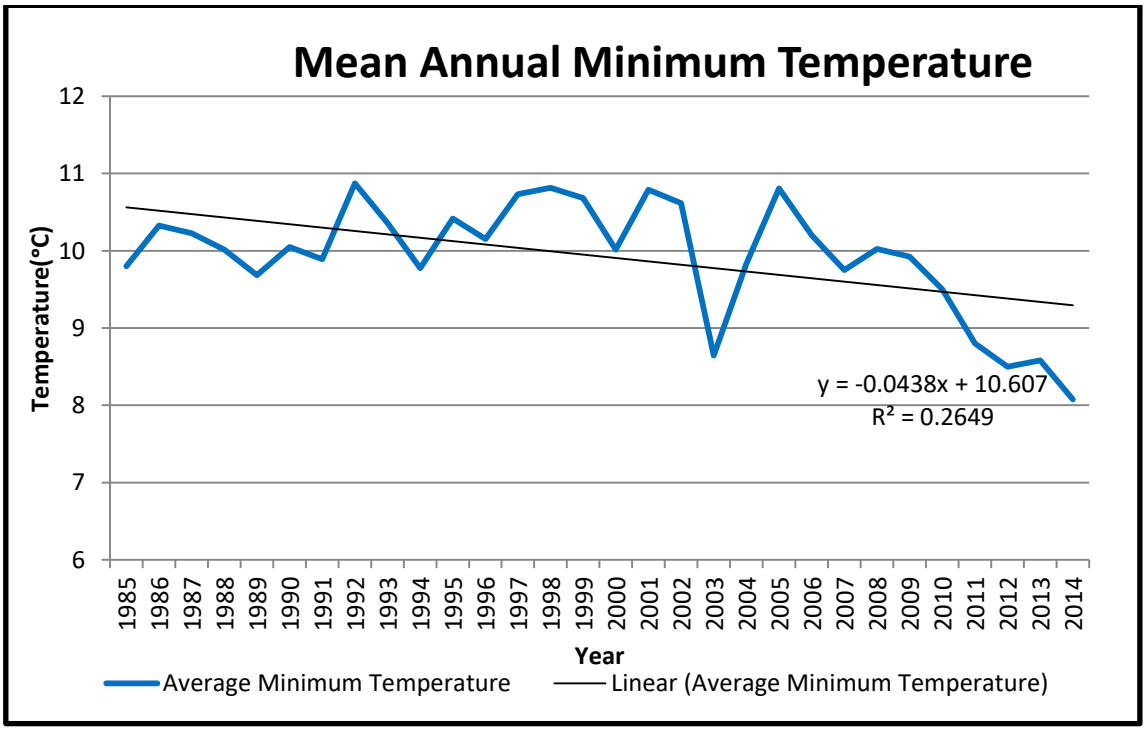

Figure 4.23: Mean annual minimum temperature from 1985 to 2014

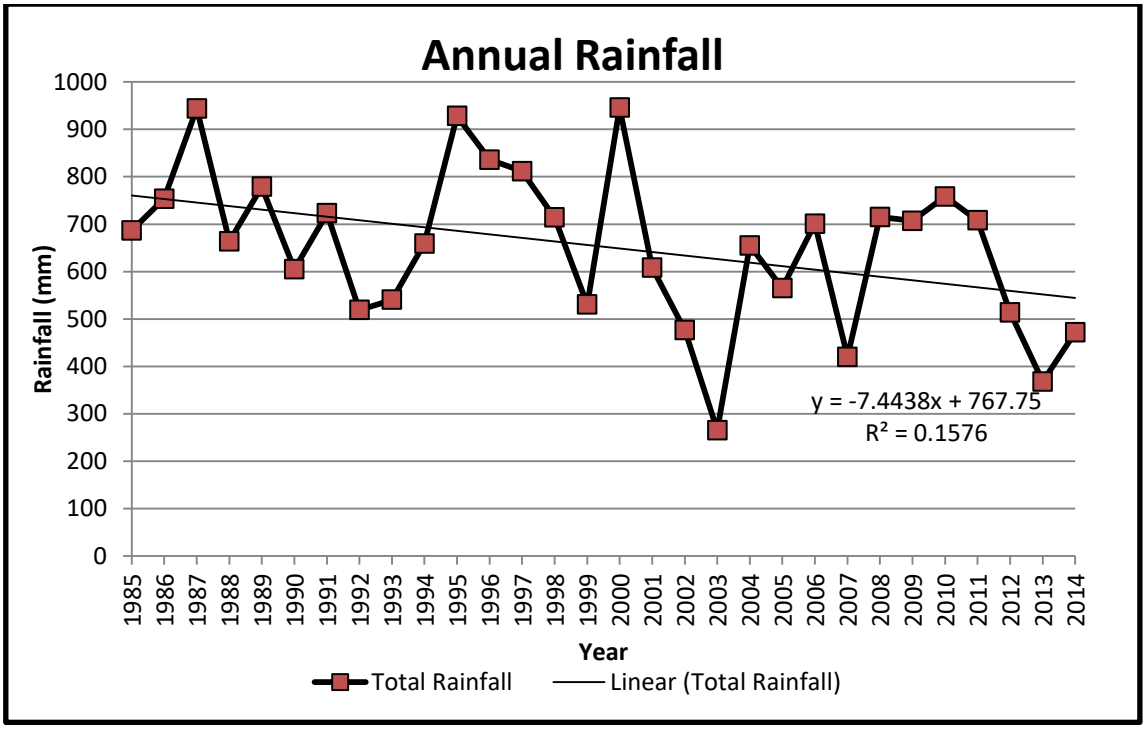

Figure 4.24: Total annual precipitation from 1985 to 2014

Table 4.3: Mann-Kendall test for the 2nd normal of the years 1985 to 2014

	Mean	Total Score	Standard Deviation	z-statistic	Result
MATmax	22.55°C	81	56.051	1.47	Increasing/no stat significance a=0.10
MATmin	9.93°C	-124	56.051	-2.194	Decreasing/significance a<0.05
AR	625mm	-113	56.051	-1.998	Decreasing/significance a<0.05

In the analysis for the 2nd normal climate data analysis in Figure 4.22 indicates that, the MATmax values illustrate an increasing trend. According to the year 1992 and the year 2000, the highest and lowest MATmax values were recorded respectively. According to the Mann-Kendall test results in Table 4.3, states an increasing trend for the MATmax, but with no statistical significance at 90% confidence level and an average of 22.52˚C. The MATmin chart illustrated in Figure 4.23, suggest that there is a decreasing trend in MATmin values, with every year recording lower temperatures. The highest MATmin recorded was in 1992 and 2005 and the lowest recorded MATmin was in 2003. Another significant note illustrates that there is a further decrease in MATmin values from 2005 to 2014. According to the Mann-Kendall test results in Table 4.3, the MATmin reported a decreasing trend and it is significant at 95% confidence level with a mean is 9.93˚C. The AR for the period of 1985 to

2014 indicates a decreasing trend according to Figure 4.24 and Table 4.3 respectively. From Figure 4.24, dictates that 1987, 1996 and 2001 had the highest rainfall. The years 2003 recorded the lowest annual rainfall. The Mann- Kendall test results in Table 4.3 indicate a decreasing trend in AR with statistical significance at the 95% confidence level and an average of 625 mm.

4.2 Performance of Maximum likelihood and support vector machine on Landsat

After describing the land cover using aerial photographs and delineating the land cover using ML and SVM classification algorithms, the following method, change detection was analysed to determine percentage area changes. From change detection techniques, the accuracy assessment was used to the categorization of pixels according to spectral data. This study also carried out a comparison of ML and SVM algorithm to determine the best pixel-based classification algorithm performs better on the Landsat satellite imagery that represents a hilly terrain. This was conducted using the Chi-square test.

4.2.1 Maximum likelihood and support vector machine change detection for summer images

Table 4.4: Change detection analysis for ML for the summer images of 1998 and 2007

	F	**G**	**SV**	**SSV**	**MSV**	**BU**	**Row Total**	**Class Total**
Unclassified	0.000	0.000	0.000	0.000	0.000	0.000	0.000	0.000
F	**55.842**	4.356	0.875	1.018	0.000	0.052	100.000	100.000
G	25.687	**24.023**	7.099	6.327	0.116	0.338	100.000	100.000
SV	10.137	41.491	**35.496**	21.091	0.930	2.187	100.000	100.000
SSV	7.646	10.485	23.526	**63.418**	0.814	1.562	100.000	100.000
MSV	0.258	13.224	24.319	6.545	**96.686**	10.923	100.000	100.000
BU	0.430	6.421	8.684	1.600	1.453	**84.937**	100.000	100.000
Class Total	100.000	100.000	100.000	100.000	100.000	100.000		
Class changes	**44.158**	**75.977**	**64.504**	**36.582**	**3.314**	**15.063**		
Image difference	-21.392	-57.027	-24.220	117.236	170.756	-3.815		

The change detection for the summer images of the year 1998 to 2007 are illustrated in Table 4.4. The bold data illustrates no changes in the area belonging to the land cover class. As tabulated in Table 4.4, 55.84% of the forest area had no change, while 25.69% was converted to grassland and 10.14% to scattered vegetation. The result of the grassland areas indicates

that 24.02% remained the same, a major conversion of 41.94% to scattered vegetation, 13.22% and 10.49% of the area exposed milk quartz and scattered vegetation and to shale rock with scattered vegetation respectively. Areas that were previously scattered vegetation, were exposed as the milk-quartz with scattered vegetation by 23.53% and 24.32% as shale rock with scattered vegetation, while 35.50% remained the same. Shale rocks with scattered vegetation areas remained as 63.49%, with an increase of scattered vegetation by 21.09%. Milky quartz rocks with scattered vegetation showed less significant changes because the original occurrences of the land cover as the area remained by 96.69%. Just as the milk quartz with scattered vegetation areas, the built-up land cover largely also had low change of its portion, as the area occupied by the land cover remained at 84.94%.

Table 4.5: Change detection analysis for SVM for the summer images of 1998 and 2007

	F	G	SV	SSV	MSV	BU	Row Total	Class Total
Unclassified	0.000	0.000	0.000	0.000	0.000	0.000	0.000	0.000
F	**59.502**	5.467	1.031	0.216	0.054	0.275	100.000	100.000
G	26.661	**28.161**	6.828	0.977	0.702	3.581	100.000	100.000
SV	7.749	45.957	**43.494**	4.049	3.510	16.529	100.000	100.000
SSV	5.996	6.805	26.926	**93.806**	1.458	11.570	100.000	100.000
MSV	0.092	13.297	21.579	0.901	**94.222**	56.749	100.000	100.000
BU	0.000	0.313	0.142	0.051	0.054	**11.295**	100.000	100.000
Class Total	100.000	100.000	100.000	100.000	100.000	100.000		
Class changes	**40.498**	**71.839**	**56.506**	**6.194**	**5.778**	**88.705**		
Image difference	-13.653	-45.587	-28.910	25.070	124.892	-81.267		

Table 4.5 illustrates support vector machine change detection analysis for the year 1998 and 2007. According to Table 4.5, the forest land cover remained the same by 59.50% and 26.66% of the original area was converted into grassland. The grassland area mostly changed to scattered vegetation by 45.96% and an exposure of milky quartz rocks with scattered vegetation by 13.30%, while the 28.16% of previous grassland area unaffected. Approximately, 43.49% of the previous area in 1998, remained as scattered vegetation while, 26.93% and 21.58% of the original area exposed shale rocks with scattered vegetation and milk quartz rocks respectively. The shale with scattered vegetation, and milky quartz rocks with scattered vegetation show the areas were not largely converted to the other land covers in the study because the original areas as these areas remained intact by 93.81% and 94.22% respectively. Built-up land cover indicates that only 11.30% of the area remained as it was, while there was coverage of 56.75% of milky quartz rocks with scattered vegetation.

.

Table 4.6: Change detection analysis for ML for the summer images of 2007 and 2014

	F	G	SV	SSV	MSV	BU	Row Total	Class Total
Unclassified	0.000	0.000	0.000	0.000	0.000	0.000	0.000	0.000
F	**63.060**	15.517	3.355	2.913	0.666	0.217	100.000	100.000
G	25.246	**41.797**	21.046	12.420	12.218	2.707	100.000	100.000
SV	9.290	28.997	**41.765**	24.774	11.875	4.101	100.000	100.000
SSV	1.639	4.075	15.120	**43.622**	10.436	2.044	100.000	100.000
MSV	0.219	5.329	14.793	14.697	**54.907**	2.558	100.000	100.000
BU	0.546	4.284	3.922	1.573	9.899	**88.373**	100.000	100.000
Class Total	100.000	100.000	100.000	100.000	100.000	100.000		
Class changes	**36.940**	**58.203**	**58.235**	**56.378**	**45.093**	**11.627**		
Image difference	26.995	63.898	-9.521	-8.704	-14.795	-1.137		

Referring to Table 4.6, this table illustrates change detection values for the maximum likelihood classification algorithms for the years 2007 to 2014. The forest land cover remained by 63.06% and decreased to grassland by 25.25% and scattered vegetation by 9.29%. According to the changes of the Grassland cover, 41.80% unaffected, while there was a shift into the scattered vegetation by 29.00% and 15.52% changed to forest land cover. For the scattered vegetation 41.77% remained as the original area, but 21.05% of original area changed to grassland, 15.12% and 14.79% exposed the shale rocks with scattered vegetation and milky quartz rocks with scattered vegetation land cover correspondingly. The shale rocks with scattered vegetation land cover result indicated that 43.62% remained the same, while there was an increase in the scattered vegetation, milky quartz rock with scattered vegetation and grassland respectively. The milky quartz rocks with scattered vegetation designated areas were unaffected as 54.91% with an increase of grassland by 12.22%, scattered vegetation by 11.86% and exposure of 10.44% to shale rocks with scattered vegetation. Built-up land cover had 88.37% of the area unchanged.

Table 4.7: Change detection analysis for SVM for the summer images of 2007 and 2014

	F	G	SV	SSV	MSV	BU	Row Total	Class Total
Unclassified	0.000	0.000	0.000	0.000	0.000	0.000	0.000	0.000
F	**65.812**	17.111	2.791	1.106	0.816	0.000	100.000	100.000
G	21.047	**36.944**	15.984	2.091	8.283	11.765	100.000	100.000
SV	9.829	35.426	**46.049**	10.890	18.271	5.882	100.000	100.000
SSV	2.885	4.134	23.487	**81.468**	11.525	0.000	100.000	100.000
MSV	0.427	4.814	11.345	4.455	**58.343**	8.824	100.000	100.000
BU	0.000	1.570	0.344	0.020	2.761	**73.529**	100.000	100.000
Class Total	100.000	100.000	100.000	100.000	100.000	100.000		
Class changes	**34.188**	**63.065**	**53.951**	**18.532**	**41.657**	**26.471**		
Image difference	32.479	22.658	-6.760	0.568	-13.637	217.647		

From the SVM change detection analysis of the summer satellite images for the years 2007 and 2014, Table 4.7 illustrates there is was 65.83% forest class area that was unchanged, while 21.05% was converted into the grassland. For the grassland area had 36.94% remains unaffected, while 35.43% of it shifted to scattered vegetation and 17.11% into forest land cover. Scattered vegetation land cover had 46.05% of the area as it was, while 23.49% was exposure to into shale rock with scattered vegetation, another 15.98% into grassland and exposure of 11.35% into milky quartz rocks with scattered vegetation. The shale rocks with scattered vegetation areas remained by 81.47%, and mostly covered by scattered vegetation. For the milky quartz rocks with scattered vegetation areal remained as 58.34% with 18.27% of the area was covered in scattered vegetation, 11.53% of the previous area was exposed as shale rocks with scattered vegetation and 8.28% covered in grassland. Built-up remained by 73.53% with the previous area covered by 11.77% grassland, an exposure of milky quartz rocks with scattered vegetation by 8.82%.

4.2.2 Maximum likelihood and support vector machine change detection for winter images.

Table 4.8: Change detection analysis for ML for the winter images of 1998 and 2007

	F	G	SV	SSV	MSV	BU	Row Total	Class Total
Unclassified	0.000	0.000	0.000	0.000	0.000	0.000	0.000	0.000
F	**30.531**	4.312	0.213	0.984	0.000	0.000	100.000	100.000
G	14.915	**19.089**	5.783	10.823	8.463	15.914	100.000	100.000
SV	9.109	39.638	**74.436**	33.716	9.873	17.204	100.000	100.000
SSV	44.645	22.531	4.543	**18.104**	0.776	7.527	100.000	100.000
MSV	0.400	13.108	12.084	27.156	**46.921**	28.387	100.000	100.000
BU	0.400	1.321	2.942	9.216	33.968	**30.968**	100.000	100.000
Class Total	100.000	100.000	100.000	100.000	100.000	100.000		
Class changes	**69.469**	**80.911**	**25.564**	**81.896**	**53.079**	**69.032**		
Image difference	-51.752	-27.434	-0.037	-27.681	9.144	379.570		

The change detection results for the ML of the winter satellite images of the years 1998 to 2007 are illustrated in Table 4.8. Table 4.8 indicates that the forest land cover area was unaffected by 30.53% while there was exposure to shale rock with scattered vegetation by 44.65% and 14.92% was converted to grassland. Within the grassland class 19.09% of the area was unchanged, 39.64% was converted to scattered vegetation. About 22.51% of shale rocks with scattered vegetation and 13.11% of milky quartz rocks with scattered vegetation was exposed from the original grassland area. For the scattered vegetation 74.44% in its previous state, while 12.08% and 5.78% of the area uncovered milky quartz rocks with scattered vegetation and shale rocks with scattered vegetation. The remaining 5.78% land cover increased as grassland cover. The 18.10% of the shale rocks with scattered vegetation remained unchanged, while 33.75% increased to scattered vegetation, Approximately, 27.16% exposed the milky quartz rock with scattered vegetation, and the rest was converted into grassland by 10.82% and 9.22% to built-up. The milky quartz rocks with scattered vegetation land cover an unaffected area of about 46.92%, and most of it being converted to

33.97% built-up area. Within the built-up land cover class, 30.97% of the area was unchanged while, 28.39% of original area exposed the milky quartz rocks with scattered vegetation. About 17.20% was converted to scattered vegetation and 15.91% to grassland class.

Table 4.9: Change detection analysis for SVM for the winter images of 1998 and 2007

	F	**G**	**SV**	**SSV**	**MSV**	**BU**	**Row Total**	**Class Total**
Unclassified	0.000	0.000	0.000	0.000	0.000	0.000	0.000	0.000
F	**3.060**	4.104	0.132	0.255	0.00	0.000	100.000	100.000
G	1.665	**25.125**	8.366	7.849	2.051	2.247	100.000	100.000
SV	0.527	31.932	**43.041**	29.197	12.380	2.247	100.000	100.000
SSV	94.677	25.976	18.101	**22.019**	1.706	5.618	100.000	100.000
MSV	0.071	12.763	30.124	40.079	**77.597**	35.955	100.000	100.000
BU	0.000	0.100	0.237	0.602	6.267	**53.933**	100.000	100.000
Class Total	100.000	100.000	100.000	100.000	100.000	100.000		
Class changes	**96.940**	**74.875**	**56.959**	**77.81**	**22.403**	**46.067**		
Image difference	-95.545	-30.681	11.023	106.159	38.310	362.921		

Table 4.9 provides results for the SVM change detection analysis of the winter satellite images of the years 1998 and 2007. According to the forest land cover class, approximately 3.06% of the area was unaffected, while 94.68% was mostly converted into shale rock with scattered vegetation. About 25.13% of grassland area was unchanged. Approximately 31.93% was converted to scattered vegetation, while 25.98% and 12.76% of the area exposed the shale rocks with scattered vegetation and milky quartz rock with scattered vegetation respectively. Within the scattered vegetation class, 43.04% of the area was unaffected, but 30.12% and 18.11% exposed the milk quartz with scattered vegetation and shale rocks with scattered vegetation correspondingly. Shale rocks with scattered vegetation area remained unaffected by 22.02% as a larger percentage of the area exposed 40.08% as milky quartz rock with scattered vegetation and was converted into 29.20% of scattered vegetation. Whereas 77.60% remained as milky quartz rocks with scattered vegetation and 12.38% was converted into scattered vegetation and 6.27% into the built-up land cover class. For the built-up land cover class 53.93% remained unchanged, while 35.96% exposed the milky quartz rocks with scattered vegetation land cover class.

Table 4.10: Change detection analysis of ML for the winter images of 2007 and 2014

	F	G	SV	SSV	MSV	BU	Row Total	Class Total
Unclassified	0.000	0.000	0.000	0.000	0.000	0.000	0.000	0.000
F	**73.859**	13.321	0.602	9.977	0.000	0.090	100.000	100.000
G	7.054	**36.080**	4.970	5.986	6.052	17.758	100.000	100.000
SV	6.639	22.760	**23.010**	50.295	28.236	5.471	100.000	100.000
SSV	12.448	1.629	61.986	**29.977**	1.680	2.377	100.000	100.000
MSV	0.000	24.916	8.904	3.084	**60.930**	58.879	100.000	100.000
BU	0.000	1.294	0.528	0.680	3.101	**15.426**	100.000	100.000
Class Total	100.000	100.000	100.000	100.000	100.000	100.000		
Class changes	**26.141**	**63.920**	**76.990**	**70.023**	**39.070**	**84.574**		
Image difference	91.079	2.204	-48.769	243.900	22.593	-73.677		

Table 4.10 illustrates change detection results for the ML classification of the winter satellite images for the years 2007 and 2014. In Table 4.10, 73.86% of the forest land area was unaltered, while 12.45% of the original area exposed the shale rocks with scattered vegetation. Approximately, 36.08% of the area remained unaffected, although 24.92% of the original area exposed milky quartz rocks with scattered vegetation. In the same token, 22.76% and 13.32% of the area was converted to scattered vegetation and forest land cover respectively. While 23.01% of scattered vegetation area remained unaffected, 61.99% of the original area exposed the shale rocks with scattered vegetation land cover type. For the shale rocks with scattered vegetation class, 29.98% remained as it was originally, 50.30% and 9.98% was converted into scattered vegetation and forest land cover respectively. Milk quartz with scattered vegetation shows that 60.93% remained the same, while 28.24% was converted into scattered vegetation. Built-up land cover class illustrates that 15.43% of the area was unaffected, while 58.58% exposed the milky quartz rocks with scattered vegetation and 17.76% was covered in grassland.

Table 4.11: Change detection analysis of SVM for the winter images of 2007 and 2014

	F	G	SV	SSV	MSV	BU	Row Total	Class Total
Unclassified	0.000	0.000	0.000	0.000	0.000	0.000	0.000	0.000
F	**80.831**	20.866	0.735	1.831	0.014	0.000	100.000	100.000
G	3.195	**32.708**	9.005	1.280	9.436	7.524	100.000	100.000
SV	5.112	31.986	**53.223**	15.341	18.678	1.456	100.000	100.000
SSV	10.863	2.671	8.934	**80.649**	3.118	1.456	100.000	100.000
MSV	0.000	11.697	28.033	0.898	**66.690**	38.350	100.000	100.000
BU	0.000	0.072	0.071	0.000	2.065	**51.214**	100.000	100.000
Class Total	100.000	100.000	100.000	100.000	100.000	100.000		
Class changes	**19.169**	**67.292**	**46.777**	**19.351**	**33.310**	**48.786**		
Image difference	135.463	20.505	28.555	-11.725	-11.376	-11.650		

The details in Table 4.11 illustrated the change detection for the SVM classification for the winter satellite images of the year 2007 to 2014. According to this analysis, 80.83% of the forest area remained as the original area while, 10.86% was exposed shale rock with scattered vegetation. Grassland area was unaffected by 32.71% as 31.99% changed to scattered vegetation, 20.87% to forest land cover and exposed 11.70% of the area as shale rocks with scattered vegetation. According to the results, 53.23% of scattered vegetation area was unaffected, while 28.03% of the area exposed the milky quartz rocks with scattered vegetation. Shale rocks with scattered vegetation results indicate that 80.65% of the area was unchanged, while 15.34% changed to scattered vegetation. About 66.69% of milky quartz rocks with scattered vegetation remained as it was while 18.68% and 9.44% was covered in scattered vegetation and grassland respectively. Built-up land cover indicates that 51.21% of the area was originally the same, while 38.35% was exposure of milky quartz rocks with scattered vegetation.

4.2.3 Annual rate of change for satellite image change detection

The change detection results obtained in ENVI classic provide the percentage changes. The annual rate of change outcome calculated using the percentage changes and the difference in years. Annual rate of change is important when determining a positive or negative land cover change in the area. The Equation (9) used in this study to determine the annual rate of change and the results are listed in Table 4.12 to Table 4.15 .

$$\text{rate} = \left({}^{1}\!/_{t_2 - t_1} \right) \times \ln\left(A_2 - A_1 \right). \tag{9}$$

Table 4.12: Annual rate of LCC overall percentage areal remain and changes of the summer images 1998-2007

	Maximum likelihood			**Support vector machines**		
Land Cover Type	***Remain***	***Change***	***Δchange***	***Remain***	***Change***	***Δchange***
F	55.842	44.158	-0.065	40.498	59.502	-0.100
G	24.023	75.977	-0.158	28.161	71.839	-0.141
SV	35.496	64.504	-0.115	43.494	56.506	-0.093
SSV	63.418	36.582	-0.051	93.806	6.194	-0.007
MSV	96.686	3.314	-0.004	94.22	5.778	-0.007
BU	84.937	15.063	-0.018	11.295	88.705	-0.242

Table 4.12 illustrates the annual rate of changes for the ML and SVM classifications for the summer satellite images for the years 1998 and 2007. Both classification algorithms demonstrate that there is a negative change in the areas. The grassland and the scattered vegetation land cover have the largest change in ML classification. In SVM classification, it is depicted that built-up and grassland had the largest land cover changes in the area. Milky quartz rock with scattered vegetation and built-up land cover had the lowest change and the lowest annual rate of change in ML classification. While SVM classification results illustrate, that shale with scattered vegetation and milk quartz had the lowest percentage areal change and lowest annual rate of change.

Table 4.13: Annual rate of LCC overall percentage areal remain and changes of the summer images 2007-2014

	Maximum Likelihood			**Support vector machines**		
Land Cover Type	***Remain***	***Change***	***Δchange***	***Remain***	***Change***	***Δchange***
F	63.06	36.94	-0.066	65.812	34.188	-0.060
G	41.797	58.203	-0.125	36.944	63.056	-0.142
SV	41.765	58.235	-0.125	46.049	53.951	-0.111
SSV	43.622	56.378	-0.119	81.468	18.532	-0.029
MSV	54.907	45.093	-0.086	58.343	41.657	-0.077
BU	88.373	11.627	-0.018	73.529	26.471	-0.044

The annual rate of change analysis for ML and SVM summer satellite images of years 2007 and 2014 are in Table 4.13. It illustrates, that both ML and SVM analysis depict negative changes. The annual rate of change of the land covers was lower, than the change detection results of the years 1998 to 2007. For both ML and SVM classification, the grassland and scattered vegetation had the highest percentage areal change. For the shale with scattered vegetation, the ML classification had a higher rate of change compared to SVM analysis.

Table 4.14: Annual rate of LCC, overall percentage areal remain and changes of the winter images 1998-2007

	Maximum likelihood			**Support vector machines**		
Land Cover Type	***Remain***	***Change***	***Δchange***	***Remain***	***Change***	***Δchange***
F	30.531	69.469	-0.132	3.06	96.94	-0.387
G	19.089	80.911	-0.184	25.125	74.875	-0.153
SV	74.436	25.564	-0.033	43.041	56.959	-0.094
SSV	18.104	81.896	-0.190	22.019	77.981	-0.168
MSV	46.921	53.079	-0.084	77.597	22.403	-0.029
BU	30.968	69.032	-0.130	53.933	46.067	-0.069

Annual rate of change for the winter satellite images of the years 1998 to 2007 are illustrated in Table 4.14.The overall annual changes higher compared to the classifications conducted on the summer images. Grassland and shale with scattered vegetation had the highest areal and annual rate of change in ML classification. For the SVM classification it is illustrated that forest, grassland and shale with scattered vegetation had the highest areal change.

Table 4.15: Annual rate of LCC overall percentage areal remain and changes of the winter images 2007-2014

	Maximum likelihood			Support vector machines		
Land Cover Type	***Remain***	***Change***	***Δchange***	***Remain***	***Change***	***Δchange***
F	73.859	26.141	-0.043	80.831	19.169	-0.030
G	36.08	63.92	-0.146	32.708	67.292	-0.160
SV	23.01	76.99	-0.230	53.223	46.77	-0.090
SSV	29.977	70.023	-0.172	80.649	19.351	-0.030
MSV	60.93	39.07	-0.071	66.69	33.31	-0.058
BU	15.426	84.574	-0.267	51.214	48.786	-0.096

Table 4.15 depicts the results of the annual rate of change analysis for ML and SVM classification of the winter satellite images of the years 2007 to 2014. Quite distinguishingly, the maximum likelihood shows that most of the land covers had a higher annual rate of change per annum compared to SVM classification. Illustrated in this table, built-up and scattered vegetation have the highest annual rate of change, while grassland and built-up had the highest annual rate of change in SVM classification.

4.2.4 Post classification results and chi-square test for the best classification algorithm

4.2.4.1 Post classification results

In post classification analysis, the analysis is dependent on the ground truth pixels. This has been used to determine how accurate a pixel is at classifying as the land cover class, a result known as the producer accuracy. At the same time, determining the probability a land cover class is represented by the pixel in the study at the time of classification at a given time period and this is known as the user accuracy. The producer accuracy is calculated as the exact pixels representing a land cover class over the total pixels selected for the land cover class. The user accuracy is represented as the exact pixels representing the land cover divided by the total pixels that are said to represent the land cover class. Examples of Producer and User accuracy calculations are represented in Equation (10) and Equation (11) for the land cover classes in the error matrix table for both ML and SVM classification algorithms.

$$\text{producer accuracy}_a = \frac{a}{Total(a_c)} \times 100. \tag{10}$$

$$\text{user accuracy}_a = \frac{a}{\text{Total a}_r} \times 100. \tag{11}$$

Table 4.16: Error matrix for February 1998 ML

Classes	**F**	**G**	**SV**	**SSV**	**MSV**	**BU**	**Totals**	**User Accuracy**
F	**165**	4	0	0	0	0	169	**97.63**
G	1	**145**	5	0	0	0	151	**96.03**
SV	0	0	**77**	21	0	0	98	**78.57**
SSV	0	0	0	**120**	0	0	120	**100.00**
MSV	0	0	0	0	**229**	11	240	**95.42**
BU	0	0	0	0	19	**59**	80	**73.75**
Total	166	149	82	143	248	70	858	
Producer accuracy	**99.40**	**97.32**	**93.90**	**83.92**	**92.34**	**84.29**		
Percentage Accuracy	**92.6573**							
Kappa Coefficient	**0.9092**							

Table 4.16 indicates that shale rocks with scattered vegetation and built-up had lower producer accuracies, while scattered vegetation and built-up point out low user accuracy percentages. Most of the pixels selected to classify shale rocks with scattered vegetation land cover had 21 pixels left out and were classified as scattered vegetation in the producer accuracy analysis, and for the built-up land cover it said to represent milky quartz rocks with scattered vegetation. According to the user accuracy, scattered vegetation had additional pixels included to the selected pixels, which represented shale rocks with scattered vegetation, and for the built-up class was milky quartz rocks with scattered vegetation.

Table 4.17: Error matrix for February 1998 SVM

Classes	**F**	**G**	**SV**	**SSV**	**MSV**	**BU**	**Totals**	**User Accuracy**
F	**166**	4	0	0	0	0	170	**97.65**
G	0	**145**	2	0	0	0	149	**97.32**
SV	0	0	**80**	24	1	0	105	**76.19**
SSV	0	0	0	**119**	0	0	119	**100.00**
MSV	0	0	0	0	**242**	12	254	**95.28**
BU	0	0	0	0	5	**56**	61	**91.80**
Total	166	149	82	143	248	70	858	
Producer accuracy	**100.00**	**97.32**	**97.56**	**83.22**	**97.58**	**80.00**		
Percentage Accuracy	**94.1725**							
Kappa Coefficient	**0.9276**							

The error matrix for the SVM classification for the year 1998 in Table 4.17 illustrates that shale rock with scattered vegetation and built-up land cover class had the lowest producer accuracy. While scattered vegetation had a lower user accuracy for SVM classification. Excluded pixels within the shale rocks with scattered vegetation classification for the producer accuracy, were misplaced in the scattered vegetation class. For the built-up land cover class, the excluded pixels are misplaced in milky quartz rocks with scattered vegetation categories. In the user accuracy, some of the scattered vegetation category pixels that were incorrectly classified to shale rocks with scattered vegetation and milky quartz rock with scattered vegetation categories.

Table 4.18: Error matrix for July 1998 ML

Classes	**F**	**G**	**SV**	**SSV**	**MSV**	**BU**	**Totals**	**User Accuracy**
F	**72**	24	1	3	0	0	100	**72.00**
G	0	**60**	4	0	0	0	64	**93.75**
SV	0	1	**51**	9	0	0	61	**83.61**
SSV	0	0	0	**162**	0	0	162	**100.00**
MSV	0	0	6	0	**150**	14	170	**88.24**
BU	0	0	1	0	1	**59**	61	**96.72**
Total	72	85	63	174	151	73	618	
Producer accuracy	**100.00**	**70.59**	**80.95**	**93.10**	**99.34**	**80.82**		
Percentage Accuracy	**89.6440**							
Kappa Coefficient	**0.8712**							

For the ML classification of the July 1998 satellite imagery, the error matrix in the categories of Table 4.18 indicate that grassland, scattered vegetation and built-up land cover class had lower producer accuracies. The forest and scattered vegetation had lower user accuracies. Most of the pixels left out in the producer accuracy for the grassland were placed in forest land cover category. For the scattered vegetation it was mostly distributed to grassland and milky quartz rock with scattered vegetation category. In the built-up producer accuracy, it is noted that the pixels left out were placed in the milky quartz rock with scattered vegetation category. In the user accuracy, it is noted that the forest land cover class had incorrectly classified pixels to grassland and shale rock with scattered vegetation. As for the scattered vegetation category it is noted that the incorrectly placed pixels were found in the shale-rock with scattered vegetation category.

Table 4.19: Error matrix for July 1998 SVM

Classes	**F**	**G**	**SV**	**SSV**	**MSV**	**BU**	**Totals**	**User Accuracy**
F	**70**	24	0	1	0	0	95	**73.68**
G	2	**59**	1	0	0	0	62	**95.16**
SV	0	0	**41**	2	0	0	45	**91.11**
SSV	0	0	0	**171**	0	0	171	**100.00**
MSV	0	0	21	0	**150**	17	188	**79.79**
BU	0	0	0	0	1	**56**	57	**98.25**
Total	72	85	63	174	151	73	618	
Producer accuracy	**97.22**	**69.41**	**65.08**	**98.28**	**99.34**	**76.71**		
Percentage Accuracy	**88.5113**							
Kappa Coefficient	**0.8560**							

In the SVM classification accuracy assessment analysis listed in Table 4.19, it is noted that grassland, scattered vegetation and built-up land cover class had very low producer accuracies, while forest and milky quartz rock and scattered vegetation category had lower user accuracies. Producer accuracy for the grassland category suggests that the pixels left out in this category were placed in forest category, for the scattered vegetation and built-up category the pixels that were left out were grouped into the milky quartz rocks with scattered vegetation category. In the user accuracy, pixels which were misclassified for the forest category were placed into grassland category, and the milky quartz rocks with scattered vegetation category had pixels incorrectly classified as scattered vegetation and built-up land cover class.

.Table 4.20: Error matrix for January 2007 ML

Classes	**F**	**G**	**SV**	**SSV**	**MSV**	**BU**	**Totals**	**User Accuracy**
F	**156**	2	0	0	0	0	158	**98.73**
G	6	**119**	0	0	0	0	125	**95.20**
SV	0	0	**54**	15	0	0	69	**78.26**
SSV	0	0	4	**164**	0	0	168	**97.62**
MSV	0	0	0	1	**118**	5	124	**95.16**
BU	0	7	1	0	1	**56**	65	**86.15**
Total	162	128	59	180	119	61	709	
Producer accuracy	**96.30**	**92.97**	**91.53**	**91.11**	**99.16**	**91.80**		
Percentage Accuracy	**94.0762**							
Kappa Coefficient	**0.9270**							

Maximum likelihood classification accuracy assessment for the January 2007 in Table 4.20, displays that all the producer accuracies were above 90% which indicates better accuracy assessment compared to the preceding year. The user accuracy however shows that the scattered vegetation and built-up up category had lower accuracies. Analysis of the user accuracy for scattered vegetation, dictates that most inappropriately classified pixels were laced in shale-rock with scattered vegetation group. While for built-up it was grassland category.

Table 4.21: Error matrix for January 2007 SVM

Classes	**F**	**G**	**SV**	**SSV**	**MSV**	**BU**	**Totals**	**User Accuracy**
F	**157**	2	0	0	0	0	**159**	**98.74**
G	5	**124**	1	0	0	0	**130**	**95.38**
SV	0	0	**51**	**17**	0	0	**68**	**75.00**
SSV	0	0	7	**163**	0	0	**170**	**95.88**
MSV	0	0	0	0	**119**	13	134	**88.81**
BU	0	0	0	0	0	**48**	48	**100.00**
Total	162	128	59	180	119	61	709	
Producer accuracy	**96.91**	**96.88**	**86.44**	**90.56**	**100.00**	**78.69**		
Percentage Accuracy	**93.3709**							
Kappa Coefficient	**0.9181**							

The SVM accuracy assessment analysis for the satellite images for January 2007 indicates that scattered vegetation and built-up had lower user accuracies while the user accuracies for the scattered vegetation and milky quartz rocks with scattered vegetation are lower as per Table 4.21. Most of the scattered vegetation pixels placed some pixels into the shale rocks with scattered vegetation category in the producer accuracy. The built-up pixels were categorised in the milky quartz rock with scattered vegetation category for the producer accuracy. For the user accuracy assessment, the misclassified pixels of the scattered vegetation were in shale rocks with scattered vegetation category, as for the milky quartz rocks with scattered vegetation category, added pixels were for the built-up category.

Table 4.22: Error matrix for July 2007 ML

Classes	**F**	**G**	**SV**	**SSV**	**MSV**	**BU**	**Totals**	**User Accuracy**
F	**94**	37	3	3	0	0	137	**68.61**
G	5	**40**	4	5	4	0	58	**68.97**
SV	0	0	**53**	26	4	0	83	**63.86**
SSV	0	0	2	**145**	12	0	159	**91.19**
MSV	0	0	0	2	**155**	5	162	**95.68**
BU	0	0	0	0	3	**41**	44	**93.18**
Total	99	77	62	181	178	46	643	
Producer accuracy	**94.95**	**51.95**	**85.48**	**80.11**	**87.08**	**89.13**		
Percentage Accuracy	**82.1151**							
Kappa Coefficient	**0.7764**							

The ML accuracy assessment for July 2007 imagery in Table 4.22 displays that grassland had the lowest accuracy followed by the shale rocks with scattered vegetation. The land cover classes with the lowest user accuracies were forest, grassland and scattered vegetation. Pixels left out in the producer accuracy for the grassland category were placed into forest land cover, for shale rocks with scattered vegetation were categorized in scattered vegetation and for the scattered vegetation class it was the pixels were in grassland and shale rocks with scattered vegetation land cover class. The user accuracies for forest shows additional pixels into this category were mostly from grassland, in grassland land cover class it was across all the land cover classes except for built-up, and for the scattered vegetation class most of them were misclassified as shale rocks with scattered vegetation.

Table 4.23: Error matrix for July 2007 SVM

Classes	**F**	**G**	**SV**	**SSV**	**MSV**	**BU**	**Totals**	**User Accuracy**
F	**97**	29	0	0	0	0	126	**76.98**
G	2	**48**	3	2	5	0	60	**80.00**
SV	0	0	**45**	24	7	0	76	**59.21**
SSV	0	0	6	**152**	8	0	166	**91.57**
MSV	0	0	8	3	**158**	5	174	**90.80**
BU	0	0	0	0	0	**41**	41	**100.00**
Total	99	77	62	181	178	0	643	
Producer accuracy	**97.98**	**62.34**	**72.58**	**83.98**	**88.76**	**89.13**		
Percentage Accuracy	**84.14%**							
Kappa Coefficient	**0.8005**							

The error matrix in Table 4.23 for the SVM July 2007 image notes that the lowest producer accuracies were distinguished in the following classes: grassland, scatted vegetation and the shale rocks with scattered vegetation class. The lowest user accuracies are from the forest, grassland and scattered vegetation, where scattered vegetation provides the lowest of the three. Pixels within the producer accuracy for the grassland class were placed added to the forest category. In scattered vegetation class the pixels were distributed across all the land cover classes, while in the shale rocks with scattered vegetation category, most of them are present in the scattered vegetation category. For the forest land cover class in the user accuracy analysis, the misrepresented pixels were seen in the grassland land cover class. In the grassland category it is across all the land cover types, and in the scattered vegetation category it is mostly represented in the shale rocks with scattered vegetation followed by the milky quartz with scattered vegetation category.

Table 4.24: Error matrix for January 2014 ML

Classes	**F**	**G**	**SV**	**SSV**	**MSV**	**BU**	**Totals**	**User Accuracy**
F	**297**	10	0	0	0	0	307	**96.74**
G	11	**174**	17	0	0	0	202	**86.14**
SV	0	0	**57**	4	0	0	61	**93.44**
SSV	0	0	0	**221**	0	0	221	**100.00**
MSV	0	0	0	1	**225**	0	226	**99.56**
BU	0	0	0	0	27	**53**	80	**66.25**
Total	308	184	74	226	252	53	1097	
Producer accuracy	**96.43**	**94.57**	**77.03**	**97.79**	**89.29**	**100.00**		
Percentage Accuracy	**93.6190**							
Kappa Coefficient	**0.9197**							

Maximum likelihood accuracy assessment analysis for January 2014 in Table 4.24 indicates that the lowest producer accuracy recorded in for the scattered vegetation category, while built-up had the lowest user accuracy. Most of the pixels belonging to the scattered vegetation class were placed in the grassland category. For the user accuracy, the misrepresented pixels in the built-up category were from the milky quartz rocks with scattered vegetation.

Table 4.25: Error matrix for January 2014 SVM

Classes	**F**	**G**	**SV**	**SSV**	**MSV**	**BU**	**Totals**	**User Accuracy**
F	**303**	33	0	0	0	0	336	**90.18**
G	5	**151**	3	0	0	0	159	**94.97**
SV	0	0	**70**	3	0	0	73	**95.89**
SSV	0	0	1	**223**	0	0	224	**99.55**
MSV	0	0	0	0	**228**	0	228	**100.00**
BU	0	0	0	0	24	**53**	77	**68.83**
Total	308	184	74	226	252	53	1097	
Producer accuracy	**98.38**	**82.07**	**94.59**	**98.67**	**90.48**	**100.00**		
Percentage Accuracy	**93.7101**							
Kappa Coefficient	**0.9206**							

For the SVM machine accuracy assessment for the January 2014 images in Table 4.25, indicates that the grassland class had the lower producer accuracy, but it remains the same for the built-up class which also represents lower user accuracy as in maximum likelihood classification. Grassland had a lower producer accuracy due to pixels from this group were removed and put into the forest category. Built-up had a lower accuracy, because misclassified pixels were in the milky quartz rocks with scattered vegetation category.

Table 4.26: Error matrix for July 2014 ML

Classes	**F**	**G**	**SV**	**SSV**	**MSV**	**BU**	**Totals**	**User Accuracy**
F	**133**	2	0	1	0	0	136	**97.79**
G	0	**11**	2	1	0	0	114	**97.37**
SV	0	0	**61**	79	0	0	140	**43.57**
SSV	0	0	0	**68**	0	0	68	**100.00**
MSV	0	0	17	0	**162**	0	179	**90.50**
BU	0	0	0	0	2	**50**	52	**96.15**
Total	133	113	80	149	164	50	689	
Producer accuracy	**100.00**	**98.23**	**76.25**	**45.64**	**98.78**	**100.00**		
Percentage Accuracy	**84.9057**							
Kappa Coefficient	**0.8165**							

Table 4.26, represents the ML accuracy assessment for July 2014, indicates that shale rocks with scattered vegetation category had lower producer accuracy, and scattered vegetation had lower producer and user accuracy. Shale rocks with scattered vegetation producer accuracy points out that the remaining pixels were distributed into the scattered vegetation category. For the scattered vegetation producer accuracy, they were mostly placed in the milky quartz rock with scattered vegetation category. In the user accuracy, most misplaced pixels for the scattered vegetation belonged to shale rock with scattered vegetation category.

Table 4.27: Error matrix for July 2014 SVM

Classes	**F**	**G**	**SV**	**SSV**	**MSV**	**BU**	**Totals**	**User Accuracy**
F	**133**	5	0	0	0	0	138	**96.38**
G	0	**107**	1	0	0	0	108	**99.07**
SV	0	1	**51**	46	0	0	98	**52.04**
SSV	0	0	0	**102**	0	0	102	**100.00**
MSV	**0**	**0**	**28**	**1**	**159**	1	189	**84.13**
BU	0	0	0	0	5	**49**	54	**90.74**
Total	133	113	80	149	164	50	689	
Producer accuracy	**100.00**	**94.69**	**63.75**	**68.46**	**96.95**	**98.00**		
Percentage Accuracy	**87.2279**							
Kappa Coefficient	**0.8435**							

The SVM accuracy assessment for July 2014 in Table 4.27, indicates that scattered vegetation and shale rocks with scattered vegetation classes had the lowest producer accuracies. As for the lowest user accuracies, the scattered vegetation and milky quartz rocks with scattered vegetation displayed low results. Scattered vegetation producer accuracy indicates most removed pixels were placed in the milky quartz rock with scattered vegetation category. Shale rocks with scattered vegetation class, displays that the removed pixels were paced in the scattered vegetation category. Scattered vegetation user accuracy shows misplaced pixels that represented this class belonged to the shale rocks with scattered vegetation class. For the milky quartz rock with scattered vegetation category it is noted that the erroneous pixels represented scattered vegetation.

The overall accuracy percentages and the kappa coefficient are represented in Figure 4.25 where the summer images display higher overall accuracy percentages than winter images. Maximum likelihood classification overall accuracy is higher for the years July 1998, January 2007, while the other years indicate that support vector machine had a higher overall accuracy.

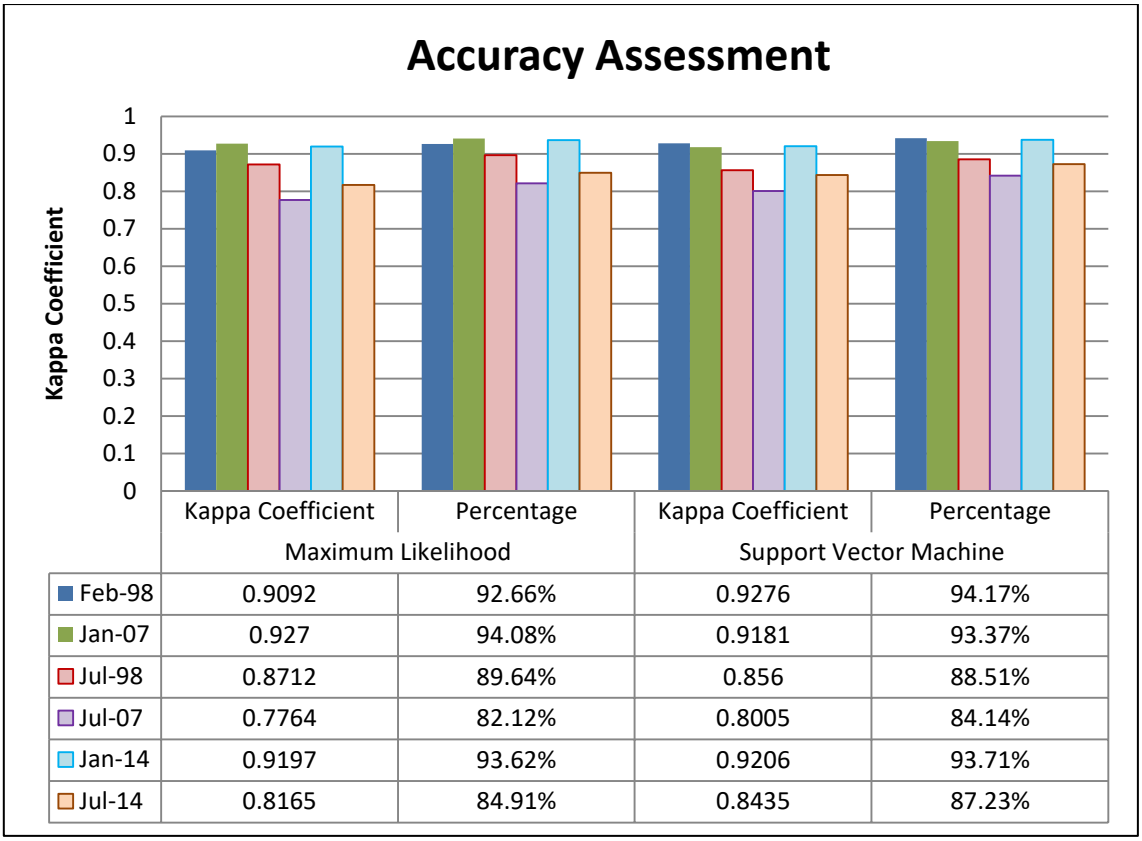

	Maximum Likelihood		Support Vector Machine	
	Kappa Coefficient	Percentage	Kappa Coefficient	Percentage
Feb-98	0.9092	92.66%	0.9276	94.17%
Jan-07	0.927	94.08%	0.9181	93.37%
Jul-98	0.8712	89.64%	0.856	88.51%
Jul-07	0.7764	82.12%	0.8005	84.14%
Jan-14	0.9197	93.62%	0.9206	93.71%
Jul-14	0.8165	84.91%	0.8435	87.23%

Figure 4.25: Graph of overall accuracy percentages and Kappa coefficients

4.2.4.2 Chi-square test for the best classification algorithm

To determine the best classification algorithm for this study area, the Chi-square test was used. This was conducted using the producer and user accuracy assessment values of the ML (parametric) and SVM (non-parametric) classification algorithms for the satellite images studied. Calculation was done in Microsoft excel and the Chi-square distribution table was used to determine the p-value. This is illustrated in:

H_o= Non-parametric classification algorithms perform better than parametric classification on a hilly landscape.

H_a= Parametric and non-parametric classification algorithms perform the same on a hill terrain.

Table 4.28: Chi-square test results for the producer accuracy for ML and SVM classification

Producer Accuracy			
		α =0.05	**Degree of freedom=5**
Season	Year	Chi-square test	p-value
	Feb 1998	0.312928	0.995
Summer	Jan 2007	1.080317	0.975
	Jan 2014	2.639143	0.20
Winter	July 1998	1.680409	0.20
	July 2007	2.1149	0.20
	July 2014	5.774025	0.20

Table 4.29: Chi-square test results for the user accuracy for ML and SVM classification

User Accuracy			
		α =0.05	**Degree of freedom=5**
Season	*Year*	*Chi-square test*	*p-value*
	Feb 1998	1.755836	0.20
Summer	Jan 2007	4.085316	0.20
	Jan 2014	0.695041	0.975
	July 1998	0.776236	0.975
Winter	July 2007	7.762326	0.975
	July 2014	1.15557	0.975

Table 4.29 show there is no statistical significance in the performance of both ML and SVM classification algorithms within HartRAO. That means the overall accuracy illustrates that both perform well on the landscape.

4.3 Discussion

Figure 4.6 indicates the NDVI results were slightly higher for the 1998 and 2007 summer and winter images, while in calculation of the 2014 satellite images suggest EVI values are higher for both summer and winter as demonstrated in Figure 4.7. The high NDVI and EVI values can be attributed to the increase in above-ground biomass amount of annual rainfall received in the area for whole year and the lower MATmax and MATmin. For the vegetation analysis, the NDVI and EVI values of winter images are lower than summer values. This is influenced by cold dry winters contributes to reduction of above ground biomass.

Analysis of NDBaI indicates the presence of bare-land across the study area; this provides the opposite information to vegetation indices. If NDBaI has lower maximum values vegetation indices have higher maximum values. In Figure 4.7, NDBaI values range from 0 to 0.3 demonstrating presence of scattered vegetation in the area. For the January and July 2014 imagery NDBaI values of zero, demonstrating the area has presence of vegetation. The opposite says for the NDBI value as suggested that there is less built-up then the NDBI values will be low. In this study, the NDBI values are greater than to NDBaI and almost as close to the values in vegetation indices. After conducting field analysis and assessment, some areas were dominated by scattered vegetation, shale and milky quartz rocks. These rocks contribute to impervious surfaces in some land cover change studies. The presences of these rocks have contributed to the higher NDBI values especially during winter due to their reflective properties. In 2007 it is noted that NDBI was highest, this could result to more exposed bare-ground due to slow vegetation growth because of a drop in total annual rainfalls experienced years prior to the period of study according to Figure 4.24.

The results of the field assessments, aerial photograph interpretation and image ratioing were used to assist in delineating land cover classes in the study and to conduct LCC analysis through image classification. The use of supervised image classification was necessary to assist in determining the changes of the land cover in the area. The use of two classification algorithms and performance within the land cover classes were important for change detection. Change detection conducted for both ML and SVM image classification depict that most areas were converted to forest, grassland and scattered vegetation. Some change detection exposed areas as milky quartz and shale rocks with scattered vegetation land covers. While some areas exposed areas as built-up. For the summer images ML classification mostly picked up built-up land cover in areas that were represented as scattered vegetation, while support vector machine classified most areas with grassland cover as

scattered vegetation as illustrated from Figure 4.16 to Figure 4.18. Winter image analysis illustrates the ML picked up more forest, grassland cover types. While SVM analysis replaces the built-up land cover picked in maximum likelihood with milky quartz rocks with scattered vegetation land cover. Shale rocks with scattered vegetation land cover remained consistent as illustrated in Figure 4.19 to Figure 4.21.

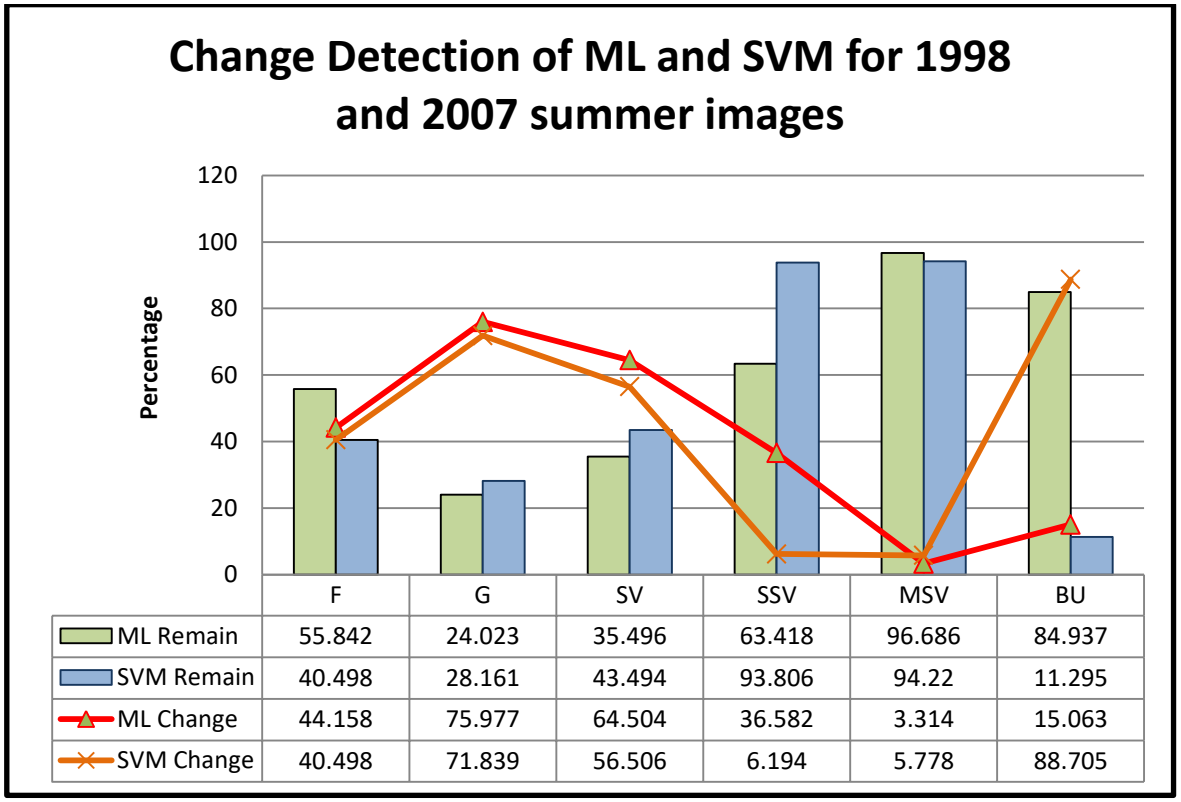

	F	G	SV	SSV	MSV	BU
ML Remain	55.842	24.023	35.496	63.418	96.686	84.937
SVM Remain	40.498	28.161	43.494	93.806	94.22	11.295
ML Change	44.158	75.977	64.504	36.582	3.314	15.063
SVM Change	40.498	71.839	56.506	6.194	5.778	88.705

Figure 4.26: Class remains and changes of ML and SVM classification for 1998 to 2007 summer images

Change detection of 1998 and 2007 summer images from Table 4.4 , Table 4.5 and Figure 4.26 of the ML and SVM analysis, points out that the shale rock with scattered vegetation land cover, and built-up land cover have a slightly different change detection percentage according to the values, compared to the other land covers. It is undeniably that grassland had a large change in areal percentage followed by scattered vegetation and milky quartz rocks with scattered vegetation.

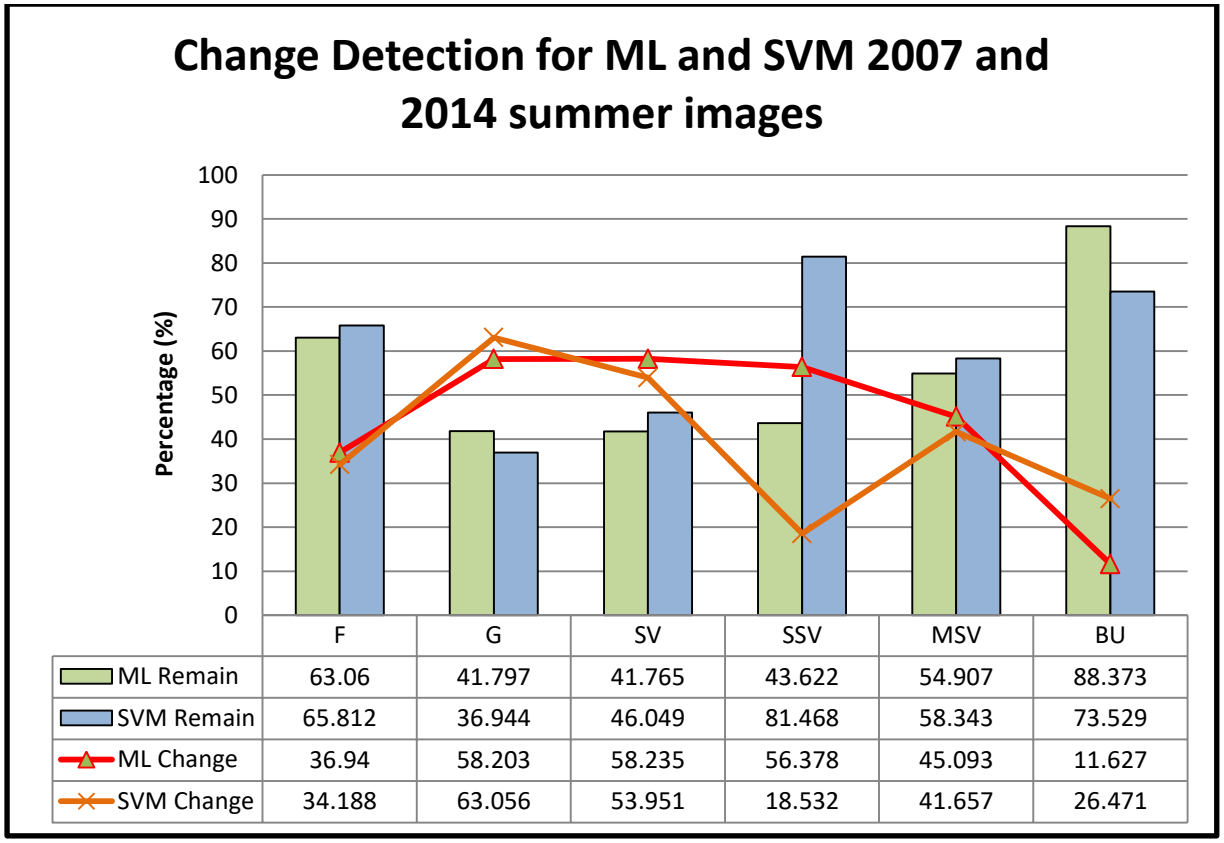

	F	G	SV	SSV	MSV	BU
ML Remain	63.06	41.797	41.765	43.622	54.907	88.373
SVM Remain	65.812	36.944	46.049	81.468	58.343	73.529
ML Change	36.94	58.203	58.235	56.378	45.093	11.627
SVM Change	34.188	63.056	53.951	18.532	41.657	26.471

Figure 4.27: Class remains and changes of ML and SVM classification for 2007 to 2014 summer images

It is eminent within ML and SVM from Table 4.6 and Table 4.7, that forest land cover and scattered vegetation land cover gave values close to each other in terms of areal remains, compared to the rest of the land covers. In terms of land cover shifts from the primarily analyzed land covers, changes were similar in terms of percentage the type of land cover except for built-up in both classification analysis according to Table 4.6, Table 4.7 and Figure 4.27. An important aspect is noted for the both classification algorithms for summer season satellite imagery used, is that the built-up and shale rocks with scattered vegetation land cover classes have a different percentage areal remains within the classification algorithms. For ML it shows that the land cover has shifted to a different land cover class for built-up and shale rocks with scattered vegetation and scattered vegetation land cover types, while in support vector machine it shows a large percentage of the area has remained.

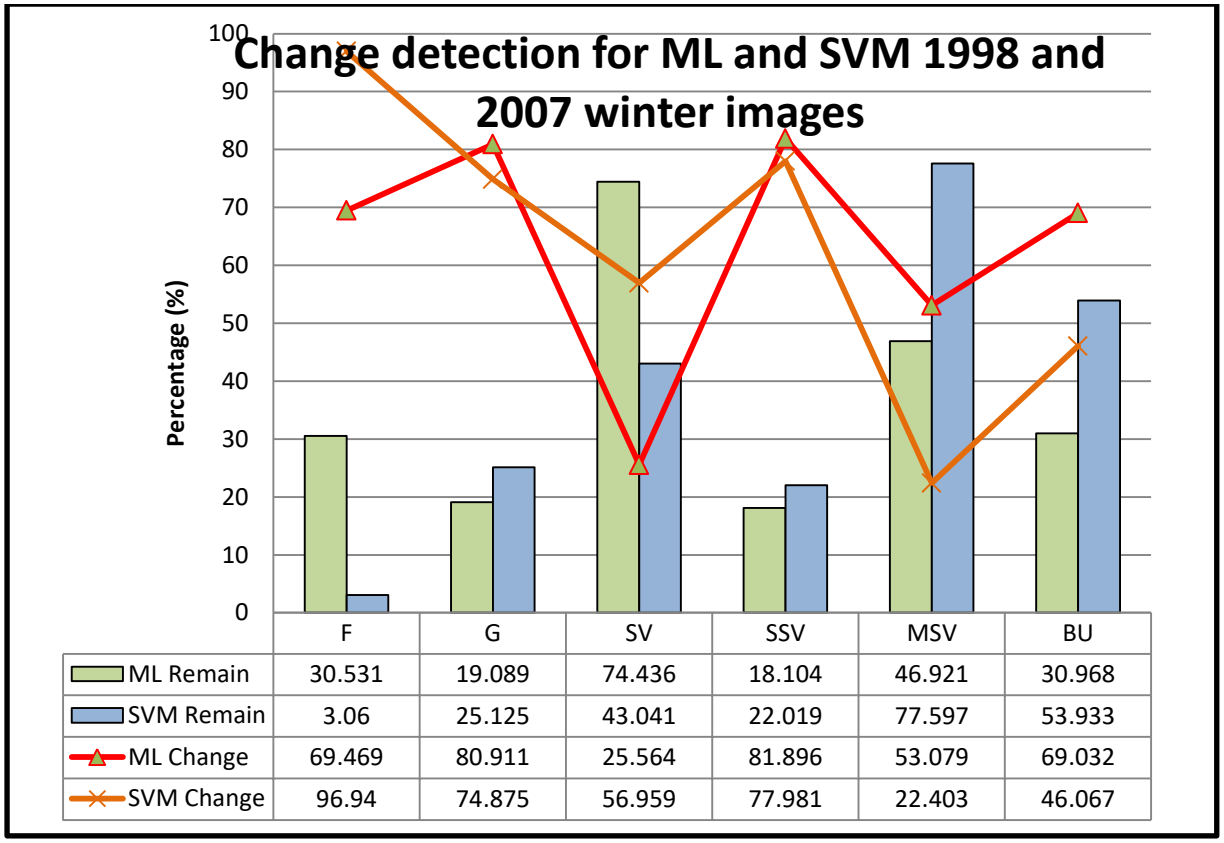

	F	G	SV	SSV	MSV	BU
ML Remain	30.531	19.089	74.436	18.104	46.921	30.968
SVM Remain	3.06	25.125	43.041	22.019	77.597	53.933
ML Change	69.469	80.911	25.564	81.896	53.079	69.032
SVM Change	96.94	74.875	56.959	77.981	22.403	46.067

Figure 4.28: Class remains and changes of ML and SVM classification for 1998 to 2007 winter images

Change detection analysis in Table 4.8 and Table 4.9 for the 1998 and 2007 winter images through ML and SVM shows a great difference with the percentage remains depicting forest, scattered vegetation, milky quartz rocks with scattered vegetation and built-up classes. The classification class changes of the land covers were the same for four land cover classes except for the milky quartz rocks with scattered vegetation and built-up land cover classes illustrated in Figure 4.28, where the percentage levels were not consistent as the other land cover class changes.

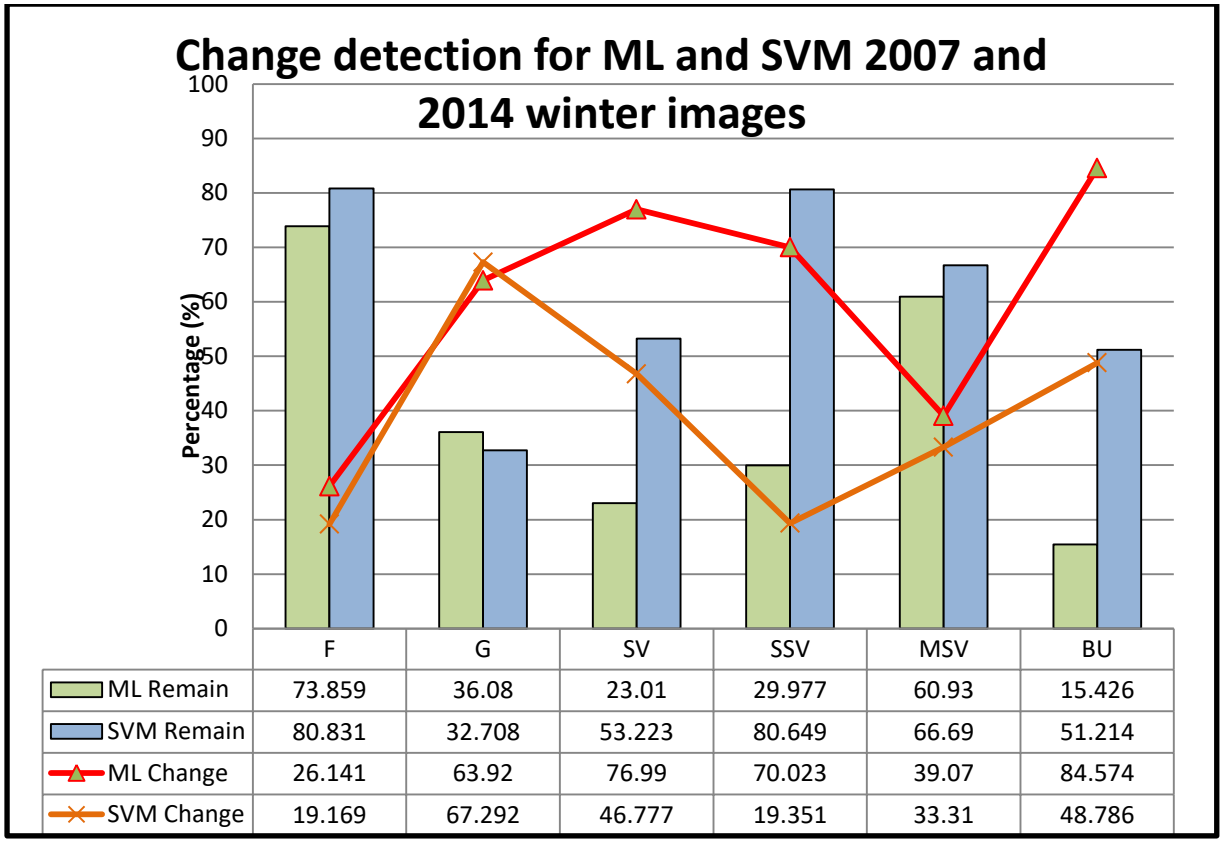

	F	G	SV	SSV	MSV	BU
ML Remain	73.859	36.08	23.01	29.977	60.93	15.426
SVM Remain	80.831	32.708	53.223	80.649	66.69	51.214
ML Change	26.141	63.92	76.99	70.023	39.07	84.574
SVM Change	19.169	67.292	46.777	19.351	33.31	48.786

Figure 4.29: Class remains and changes of ML and SVM classification for 2007 to 2014 winter images

In ML and SVM classification for 2007 and 2014 winter images as displayed in Table 4.10, Table 4.11 and Figure 4.29, demonstrates that the scattered vegetation, shale rocks with scattered vegetation and built-up land cover classes had differing class remains within the percentage scale. All the land covers had the same shift in changes within the land cover classes except for scattered vegetation. ML classification indicates that the previously scattered vegetation area was mostly converted into shale rocks with scattered vegetation and grassland while in SVM classification it was milky quartz rocks with scattered vegetation with grassland. For all the years used in change detection study, with both algorithms it shows that the scattered vegetation, shale rocks with scattered vegetation, and built-up land cover class shows inconsistency when mapping change detection statistics.

Table 4.30: Omission and Commission error for February 1998 SVM and ML classification

	Maximum likelihood		Support vector machines	
Class	***Omission Error***	***Commission Error (%)***	***Omission Error***	***Commission Error***
F	0.6	2.37	0	2.35
G	2.68	3.97	2.68	2.68
SV	6.1	21.43	2.44	23.81
SSV	16.08	0	16.78	0
MSV	7.66	4.48	2.42	4.72
BU	15.71	26.25	20	8.2

Table 4.16, and

Table 4.30 for ML and SVM classification. Scattered vegetation class had a large percentage of misplaced pixels for ML and SVM analysis, and built-up for ML classification.

Table 4.31: Omission and Commission error for January 2007 SVM and ML classification

	Maximum Likelihood		Support Vector Machine	
Class	***Omission Error (%)***	***Commission Error***	***Omission Error***	***Commission Error***
F	3.7	1.27	3.09	1.26
G	7.03	4.8	3.13	4.62
SV	8.47	21.74	13.56	25
SSV	8.89	2.38	9.44	4.12
MSV	0.84	4.84	0	11.19
BU	8.2	13.85	21.31	0

For the January 2007 post classification analysis, scattered vegetation and built-up pixels misclassified as they had a lower user accuracy and higher commission error from .Table 4.20, Table 4.21 and Table 4.31. Support vector machine analysis demonstrates that scattered vegetation had a higher percentage of omitted pixels leading to a lower producer accuracy and higher commission error for the built-up, milky quartz rock with scattered vegetation and shale rock with scattered vegetation leading to lower user accuracy.

Table 4.32: Omission and Commission error for January 2014 SVM and ML classification

	Maximum likelihood		**Support vector machines**	
Class	***Omission Error (%)***	***Commission Error***	***Omission Error***	***Commission Error***
F	3.57	3.26	1.62	9.82
G	5.43	13.86	17.93	5.03
SV	22.97	6.56	5.41	4.11
SSV	2.21	0	1.33	0.45
MSV	10.71	0.44	9.52	0
BU	0	33.75	0	31.17

According to the error matrix tables for Table 4.24 and Table 4.25, and in addition to the omission and commission of the Table 4.32 for the January 2014, scattered vegetation and built-up illustrates lower producer accuracy and higher omission error in ML classification. For the SVM analysis, the grassland had a lower user accuracy and lower producer accuracy. Built-up had a lower user accuracy and higher commission error for ML and SVM classification. From the post classification of summer images, the classification algorithms cannot particularly classify; scattered vegetation and built-up land cover classes correctly.

Table 4.33: Omission and Commission error for July 1998 SVM and ML classification

	Maximum Likelihood		**Support Vector Machine**	
Class	***Omission Error***	***Commission Error (%)***	***Omission Error***	***Commission Error***
F	0	28	2.78	26.32
G	29.41	6.25	30.59	4.84
SV	19.05	16.39	34.92	8.89
SSV	6.9	0	1.72	0
MSV	0.66	11.76	0.66	20.21
BU	19.18	3.28	23.29	1.75

Post classification results of ML and SVM for July 1998 imagery in the categories Table 4.18 and Table 4.19 respectively suggests that grassland scattered vegetation and built-up class had lower producer accuracy for ML and SVM classification. This vetoes a higher omission error as demonstrated in Table 4.33. Forest and milky quartz rock with scattered vegetation, and had a higher commission error and lower user accuracy percentage for ML and SVM. While scattered vegetation was poorly classified in ML classification.

Table 4.34: Omission and Commission error for July 2007 SVM and ML classification

	Maximum likelihood		**Support vector machines**	
Class	***Omission Error***	***Commission Error***	***Omission Error***	***Commission Error***
F	5.05	31.39	2.02	23.02
G	48.05	31.03	37.66	20
SV	14.52	36.14	27.42	40.79
SSV	19.89	8.81	16.02	8.43
MSV	12.92	4.32	11.24	9.2
BU	10.87	6.82	10.87	0

July 2007 post classification results in Table 4.23 and Table 4.34 contains values that have a higher omission and commission error for grassland cover in ML and SVM analysis. Forest and scattered has a higher commission error suggesting misclassified pixels for ML and SVM analysis.

Table 4.35: Omission and Commission error for July 2014 SVM and ML classification

	Maximum Likelihood		**Support Vector Machine**	
Class	***Omission Error***	***Commission Error***	***Omission Error***	***Commission Error***
F	0	2.21	0	3.6
G	1.77	2.63	5.31	0.93
SV	23.75	56.43	36.25	47.96
SSV	54.36	0	31.54	0
MSV	1.22	9.5	3.05	15.87
BU	0	3.85	2	9.26

Scattered vegetation contained a lower producer and user accuracy, while resulted to higher omission and commission errors for ML and SVM analysis as demonstrated in Table 4.26 and Table 4.35. Milky quartz rock with scattered vegetation indicates a higher omission error for both ML and SVM analysis according to Table 4.35.With this said, from image classification, change detection and post classification analysis, the most misclassified land covers were scattered vegetation and built-up in summer. While in winter, the changes noted were between forest, grasslands and scattered vegetation. From Table 4.12 to Table 4.15 a negative rate of change is portrayed for all land cover types. It depicted from all the tables containing annual rate of change that grass and scattered vegetation have a higher annual rate of change. Built-up also portrays the negative high values, however this is due to the dominance of the rock types and scattered vegetation, thus contributing to a higher annual rate of change.

Climate influences changes in vegetation type in the area. From the interpretation of the aerial photographs, there has been a significant growth of tree and increase in scattered and grassland over the years. It is due to a reduction of animal and crop farming as noted from the aerial photographs. With time, the area has been able to regenerate in vegetation. However, there is a sudden change in vegetation type, where the grass appears yellow and scattered, and there are more drought resistant trees, which have thorns to reduce the impact of transpiration. Vegetation structure is influenced by the rainfall and temperature patterns. Climate data analysis illustrates that the first normal shows an increase in MAtmax, MATmin and AR according to Mann-Kendall test results from Table 4.2. This led to an increase in vegetation, crop farming and plant growth. In Table 4.3, MATmax values are increasing in the area, while MATmin and AR values are decreasing. Vegetation is rejuvenating but the agriculture has reduced in the areas, this has resulted in the growth of drought resistant plants and trees, and an increase in grassland and scattered vegetation. There is an increase in rainfall as towards the end of a 10-year cycle while lower rainfall values are experienced at the beginning of a new cycle as demonstrated in Figure 4.15 and Figure 4.24. Analysis of this climate data also led to the reason why some areas had milky-quartz and shale-rock land cover exposed while some areas changed into scattered vegetation and grassland.

5 CONCLUSIONS AND RECOMMENDATIONS

5.1 Conclusions

The aim of this study was to focus on the change in land cover of HartRAO and its surroundings. The study conducted was to look at the impact of HartRAO within the area over five decades and its surrounding land cover. The position of HartRAO facility is important in the international research community with its primary focus on radio and optical astronomy, geodetic studies and other research studies. This study was to look at the impact of human interaction from the time of the construction to the area, as this also affects some of the facilities input and data collection over the years. Natural phenomenon such a veld fires, agricultural activities and climate data provide information on the land cover of the area. At the same time, the importance of this to provide a chronological aspect of the climate and the various stages of a countries development from the year 1960 to 2014.

Going through the first objective, delineation of land cover types encompassed the field based assessments, where six land cover types were identified. Likewise the use of archived information such as climate data, aerial photographs and Google Earth images tell a story of the changes in the area. The importance of Landsat satellite images for analysis and field assessments provides information of the nature of the landscape and the changes that happen within and between land cover types. Thus the results of this objective were to specifically delineate the land cover of the area, and to also provide information why HartRAO is specifically located in this area. Satellite image analysis provides image classification results that look at land cover conversions and exposures at different points in the time line, which provides information of the rock structure, the location of tree and vegetation cover and the shifts due to climate information.

The second and third objectives are usually used in land cover change studies to find a suitable method to analyse satellite data. This is comparison as some of the areas in the world are different and it also depends on the analyst and needs thereof. The study focused on parametric and non-parametric analysis in pixel-based classification. This was done with the knowledge of the spectral data provided from the satellite images, and the clustering of the pixels to different land cover. It also highlighted the advantages and disadvantages of change detection and accuracy assessment of the Landsat data. Mapping land cover such as grasslands and scattered vegetation were problematic as the values crossed each other. Mapping milky-quartz with scattered vegetation and built-up provided problems to the

classification algorithms as the data was interchanged. Comparison of the classification algorithms was necessary to look at the advantage of one algorithm over the other in a hilly area. The performance was similar with SVM being slightly higher. The similarity came about the classification of the land cover; ML classified grassland and Forest-land cover well, while SVM classified built-up and scattered vegetation well.

Climate data was combined with delineation of land cover types and analysing the land cover changes. Climate variables are useful in identifying the course of changes in land cover within an area. This aspect was necessary as an impact factor in the research as this can be explored further when looking at the vegetation type in the area, evapotranspiration rates, nitrogen level and chlorophyll within various vegetation types. The climate information was useful as this indicated that there was a decrease in rainfall. Analysing the data over a ten-year cycle, the trend showed that there was sharp increase rainfall information at the end of the decade and lower rainfalls experienced in the middle of the decade. Maximum temperatures were rising over the years, but not significantly. This signified the vegetation growth patterns, as there was an increase in grassland and drought resistant tree-species. Increase in temperatures are attributed to the increase in large farmlands, residential and mining environment as noted in the 2004 to 2013 aerial photographs. The basic overview and the use of climate data can be utilised for further studies in geodesy, remote sensing or both fields as they are affected by seasonal variability with regards to climate of an area.

The analysis and rates of changes vary with he complexity of the terrain makes the mapping difficult as most of the land cover varies over time. In a good rainy season, the area is mostly covered in grassland cover, therefore mapping can prove to be cumbersome. The importance of determining the rate of change in the area would be to identify which land cover types are affected why is there a change between and within the land cover types. It is noted that during the dry season one can collect information of the nature of the area concerning the bedrock, rock type and the above-ground biomass of the area. Thus, the generation of the land cover classes came about the seasons and time of the year. During the heavy rainy seasons, it is best to analyse vegetation type in the area as the bedrock is covered by the grassland type and woody vegetation.

Limitations in this study were:

- The use of Synthetic Aperture Radar (SAR) data and optical data can be used to give a better description of the area. The SAR data are not freely available to conduct studies.
- A lower production of aerial photographs and satellite imagery for the previous years, poses a challenge when conducting multi-temporal and seasonal land cover changes. Likewise, cloud cover on some satellite imagery pose a problem when conducting the study.
- Variation of terrain, places a difficult problem when carefully labelling the land cover types.
- The use of hyperspectral imagery especially from UAVs would be helpful; however, the influence of Radio waves from UAVs would influence collection of satellite data. Cost of Hyperspectral satellite imagery and cost of UAVs also limits the study to freely available satellite data.

5.2 Recommendations

- More land cover change research is needed for hilly landscapes to monitor land cover and climate influence in South Africa, through training and the use of SAR data and optical data.
- Interferometry studies using SAR data to determine elevation, rock structure and vegetation heights and cover.
- There needs to be an increase in LC data for HartRAO and its environment, so that monitoring the land cover can provide for conservation purposes due to the position of HartRAO in the international research community.
- Consider further classification of the vegetation type, why there has been an increase of drought resistant vegetation especially within HartRAO and it environment and a shift within the land cover.
- Further studies may include using freely available European Space Agency (ESA) satellite data Sentinel 1 and 2 data for monitoring land cover and for specifically LC studies. The freely available SNAP tool from ESA can be used especially monitoring land cover.

REFERENCES

Abbas, I. I. (2012) 'An Assessment of Land Use/Land Cover Changes in a Section of Niger Delta, Nigeria', *Frontiers in Science*, 2(6), pp. 137–143. doi: 10.5923/j.fs.20120206.02.

Abd El-Kawy, O. R., Rød, J. K., Ismail, H. A. and Suliman, A. S. (2011) 'Land use and land cover change detection in the western Nile delta of Egypt using remote sensing data', *Applied Geography*. Elsevier Ltd, 31(2), pp. 483–494. doi: 10.1016/j.apgeog.2010.10.012.

Abdulaziz, A. M., Hurtado, J., J. M. and Al-Douri, R. (2009) 'Application of multitemporal Landsat data to monitor land cover changes in the Eastern Nile Delta region, Egypt', *International Journal of Remote Sensing*, 30(11), pp. 2977–2996. doi: 10.1080/01431160802558675.

Adam, E., Mutanga, O. and Rugege, D. (2010) 'Multispectral and hyperspectral remote sensing for identification and mapping of wetland vegetation: A review', *Wetlands Ecology and Management*, 18(3), pp. 281–296. doi: 10.1007/s11273-009-9169-z.

Agrawal, A., Kumar, N. and Radhakrishna, M. (2007) 'Multispectral image classification: a supervised neural computation approach based on rough–fuzzy membership function and weak fuzzy similarity relation', *International Journal of Remote Sensing*, 28(20), pp. 4597–4608. doi: 10.1080/01431160701244898.

Aguirre-Gutiérrez, J., Seijmonsbergen, A. C. and Duivenvoorden, J. F. (2012) 'Optimizing land cover classification accuracy for change detection, a combined pixel-based and object-based approach in a mountainous area in Mexico', *Applied Geography*. Elsevier Ltd, 34, pp. 29–37. doi: 10.1016/j.apgeog.2011.10.010.

Ahmed, B., Kamruzzaman, M., Zhu, X., Rahman, M. and Choi, K. (2013) 'Simulating Land Cover Changes and Their Impacts on Land Surface Temperature in Dhaka, Bangladesh', *Remote Sensing*, 5(11), pp. 5969–5998. doi: 10.3390/rs5115969.

Akar, Ö. and Güngör, O. (2015) 'Integrating multiple texture methods and NDVI to the Random Forest classification algorithm to detect tea and hazelnut plantation areas in northeast Turkey', *International Journal of Remote Sensing*, 36(2), pp. 442–464. doi: 10.1080/01431161.2014.995276.

Almeida-Filho, R. and Shimabukuro, Y. E. (2002) 'Digital processing of a Landsat-TM time series for mapping and monitoring degraded areas caused by independent gold miners, Roraima State, Brazilian Amazon', *Remote Sensing of Environment*, 79(1), pp. 42–50. doi: 10.1016/S0034-4257(01)00237-1.

Alphan, H. (2003) 'Land-use change and urbanization of Adana, Turkey', *Land Degradation and Development*, 14(6), pp. 575–586. doi: 10.1002/ldr.581.

Aly, Z., Bonn, F. J. and Magagi, R. (2007) 'Analysis of the backscattering coefficient of salt-affected soils using modeling and RADARSAT-1 SAR data', *IEEE Transactions on Geoscience and Remote Sensing*, 45(2), pp. 332–341. doi: 10.1109/TGRS.2006.887163.

As-syakur, A. R., Adnyana, I. W. S., Arthana, I. W. and Nuarsa, I. W. (2012) 'Enhanced built-UP and bareness index (EBBI) for mapping built-UP and bare land in an urban area', *Remote Sensing*, 4(10), pp. 2957–2970. doi: 10.3390/rs4102957.

Atkinson, P. M. and Tatnall, A. R. L. (1997) 'Introduction Neural networks in remote sensing', *International Journal of Remote Sensing*, 18(4), pp. 699–709. doi: 10.1080/014311697218700.

Atzberger, C. (2013) 'Advances in remote sensing of agriculture: Context description, existing operational monitoring systems and major information needs', *Remote Sensing*, 5(2), pp. 949–981. doi: 10.3390/rs5020949.

Badreldin, N., Frankl, A. and Goossens, R. (2013) 'Assessing the spatiotemporal dynamics of vegetation cover as an indicator of desertification in Egypt using multi-temporal MODIS satellite images', *Arabian Journal of Geosciences*, 7(11), pp. 4461–4475. doi: 10.1007/s12517-013-1142-8.

Bahari, N. I. S., Ahmad, A. and Aboobaider, B. M. (2014) 'Application of support vector machine for classification of multispectral data', *IOP Conference Series: Earth and Environmental Science*, 20, p. 012038. doi: 10.1088/1755-1315/20/1/012038.

Baldyga, T. J., Miller, S. N., Driese, K. L., Gichaba, C. M. and Valle, L. (2007) 'Assessing land cover change in Kenya ' s Mau Forest region using remotely sensed data', *African Journal of Ecology*, pp. 46–54. doi: 10.1111/j.1365-2028.2007.00806.x.

Baltsavias, E. P. (2002) 'Object Extraction and Revision By Image Analysis Using Existing Geospatial Data and Knowledge: State-of-the-Art and Steps Towards Operational Systems ', *Integrated System for Spatial Data Production, Custodian and Decision Support* , XXXIV, par. Available at: http://www.isprs.org/commission2/proceedings02/paper/003_066.pdf.

Baraldi, A. and Parmiggiani, F. (1990) 'Urban Area Classification by Multispectral SPOT Images', *IEEE Transactions on Geoscience and Remote Sensing*, pp. 674–680. doi: 10.1109/TGRS.1990.572979.

Barbero, M., Bonin, G., Loisel, R. and Qu, P. (2016) 'Changes and Disturbances of Forest Ecosystems Caused by Human Activities in the Western Part of the Mediterranean Basin Author (s): M . Barbero , G . Bonin , R . Loisel and P . Quézel Published by : Springer Stable URL : http://www.jstor.org/stable/2003', 87(2), pp. 151–173.

Beck, P. S. A., Atzberger, C., Høgda, K. A., Johansen, B. and Skidmore, A. K. (2006) 'Improved monitoring of vegetation dynamics at very high latitudes: A new method using MODIS NDVI', *Remote Sensing of Environment*, 100(3), pp. 321–334. doi: 10.1016/j.rse.2005.10.021.

Below, T. B., Mutabazi, K. D., Kirschke, D., Franke, C., Sieber, S., Siebert, R. and Tscherning, K. (2012) 'Can farmers' adaptation to climate change be explained by socio-economic household-level variables?', *Global Environmental Change*. Elsevier Ltd, 22(1), pp. 223–235. doi: 10.1016/j.gloenvcha.2011.11.012.

Benediktsson, J. A., Swain, P. H. and Ersoy, O. K. (1990) 'Neural Network Approaches Versus Statistical Methods in Classification of Multisource Remote Sensing Data', *12th Canadian Symposium on Remote Sensing Geoscience and Remote Sensing Symposium*, 28(4), pp. 540–552. doi: 10.1109/IGARSS.1989.578748.

Benz, U. C., Hofmann, P., Willhauck, G., Lingenfelder, I. and Heynen, M. (2004) 'Multi-resolution, object-oriented fuzzy analysis of remote sensing data for GIS-ready information', *ISPRS Journal of Photogrammetry and Remote Sensing*, 58(3–4), pp. 239–258. doi:

10.1016/j.isprsjprs.2003.10.002.

Berberoglu, S. and Akin, A. (2009) 'Assessing different remote sensing techniques to detect land use/cover changes in the eastern Mediterranean', *International Journal of Applied Earth Observation and Geoinformation*, 11(1), pp. 46–53. doi: 10.1016/j.jag.2008.06.002.

Berni, J. A. J., Zarco-Tejada, P. J., Suárez, L., Fereres, E., Suarez, L. and Fereres, E. (2009) 'Thermal and narrowband multispectral remote sensing for vegetation monitoring from an unmanned aerial vehicle', *IEEE Transactions on Geoscience and Remote Sensing*, 47(3), pp. 722–738. doi: 10.1109/TGRS.2008.2010457.

Bhatti, S. S. and Tripathi, N. K. (2014) 'Built-up area extraction using Landsat 8 OLI imagery', *GIScience & Remote Sensing*, 51(4), pp. 445–467. doi: 10.1080/15481603.2014.939539.

Bian, Z., Inyang, H. I., Daniels, J. L., Otto, F. and Struthers, S. (2010) 'Environmental issues from coal mining and their solutions', *Mining Science and Technology*. China University of Mining and Technology, 20(2), pp. 215–223. doi: 10.1016/S1674-5264(09)60187-3.

Bindschadler, R. A., Scambos, T. A., Choi, H. and Haran, T. M. (2010) 'Ice sheet change detection by satellite image differencing', *Remote Sensing of Environment*. Elsevier Inc., 114(7), pp. 1353–1362. doi: 10.1016/j.rse.2010.01.014.

Blaschke, T. (2010) 'Object based image analysis for remote sensing', *ISPRS Journal of Photogrammetry and Remote Sensing*. Elsevier B.V., 65(1), pp. 2–16. doi: 10.1016/j.isprsjprs.2009.06.004.

Blaschke, T., Lang, S., Lorup, E., Strobl, J. and Zeil, P. (2000) 'Object-Oriented Image Processing in an Integrated GIS / Remote Sensing Environment and Perspectives for Environmental Applications', *Environmental Information for Planning, Politics and the Public*, (1995), pp. 555–570.

Blignaut, J. and Van Heerden, J. (2009) 'The impact of water scarcity on economic development initiatives', *Water SA*, 35(4), pp. 415–420. doi: 10.4314/wsa.v35i4.76800.

Bocco, G., Mendoza, M. and Velázquez, A. (2001) 'Remote sensing and GIS-based regional geomorphological mapping—a tool for land use planning in developing countries', *Geomorphology*, 39(3–4), pp. 211–219. doi: 10.1016/S0169-555X(01)00027-7.

Bonan, G. B. (2008) 'Forests and climate change: forcings, feedbacks, and the climate benefits of forests.', *Science*, 320(5882), pp. 1444–1449. doi: 10.1126/science.1155121.

Botai, O. J., Combrinck, W. L. and Sivakumar, V. (2009) 'Assessing the degree of synchronization between geophysical records using the method of instantaneous phase differences', *Advances*, (September), pp. 588–593.

Breiman, L. (1996) 'Bagging Predictors', *Machine Learning*, 24(421), pp. 123–140. doi: 10.1007/BF00058655.

Breiman, L. (2001a) 'Random forests', *Machine Learning*, 45(1), pp. 5–32. doi: 10.1023/A:1010933404324.

Breiman, L. (2001b) 'Random Forests', *Machine Learning*, 45(1), pp. 5–32.

Brink, A. B. and Eva, H. D. (2009) ‘Monitoring 25 years of land cover change dynamics in Africa: A sample based remote sensing approach’, *Applied Geography*. Elsevier Ltd, 29(4), pp. 501–512. doi: 10.1016/j.apgeog.2008.10.004.

Bruzzone, L., Cossu, R. and Vernazza, G. (2002) ‘Combining parametric and non-parametric algorithms for a partially unsupervised classification of multitemporal remote-sensing images’, *Information Fusion*, 3(4), pp. 289–297. doi: 10.1016/S1566-2535(02)00091-X.

Bucini, G. and Lambin, E. F. (2002) ‘Fire impacts on vegetation in Central Africa: a remote-sensing- based statistical analysis’, *Applied Geography*, 22(1), pp. 27–48.

Butt, A., Shabbir, R., Ahmad, S. S. and Aziz, N. (2015) ‘Land use change mapping and analysis using Remote Sensing and GIS: A case study of Simly watershed, Islamabad, Pakistan’, *The Egyptian Journal of Remote Sensing and Space Science*. Authority for Remote Sensing and Space Sciences, 18(2), pp. 251–259. doi: 10.1016/j.ejrs.2015.07.003.

Buyantuyev, A. and Wu, J. (2010) ‘Urban heat islands and landscape heterogeneity: Linking spatiotemporal variations in surface temperatures to land-cover and socioeconomic patterns’, *Landscape Ecology*, 25(1), pp. 17–33. doi: 10.1007/s10980-009-9402-4.

Calvo, S., Ciraolo, G. and Loggia, G. La (2003) ‘Monitoring Posidonia oceanica meadows in a Mediterranean coastal lagoon (Stagnone, Italy) by means of neural network and ISODATA classification methods’, *International Journal of Remote Sensing*, 24(13), pp. 2703–2716. doi: 10.1080/0143116031000066882.

Canadell, J. G., Le Quéré, C., Raupach, M. R., Field, C. B., Buitenhuis, E. T., Ciais, P., Conway, T. J., Gillett, N. P., Houghton, R. A. and Marland, G. (2007) ‘Contributions to accelerating atmospheric CO2 growth from economic activity, carbon intensity, and efficiency of natural sinks.’, *Proceedings of the National Academy of Sciences of the United States of America*, 104(47), pp. 18866–70. doi: 10.1073/pnas.0702737104.

Canty, M. J. and Nielsen, A. a. (2006) ‘Visualization and unsupervised classification of changes in multispectral satellite imagery’, *International Journal of Remote Sensing*, 27(18), pp. 3961–3975. doi: 10.1080/01431160500222608.

Carrão, H., Gonçalves, P. and Caetano, M. (2008) ‘Contribution of multispectral and multitemporal information from MODIS images to land cover classification’, *Remote Sensing of Environment*, 112(3), pp. 986–997. doi: 10.1016/j.rse.2007.07.002.

Chander, G., Markham, B. L. and Helder, D. L. (2009) ‘Summary of current radiometric calibration coefficients for Landsat MSS, TM, ETM+, and EO-1 ALI sensors’, *Remote Sensing of Environment*. Elsevier Inc., 113(5), pp. 893–903. doi: 10.1016/j.rse.2009.01.007.

Chander, G., Micijevic, E., Applications, S., Corporation, I., Usgs, U. S. G. S., Resources, E., Eros, S. and Falls, S. (2006) ‘Absolute calibration accuracy of L4 TM and L5 TM sensor image pairs’, *Earth*, 6296, p. 62960D–62960D–12. doi: 10.1117/12.683240.

Chen, J. M., Pavlic, G., Brown, L., Cihlar, J., Leblanc, S. G., White, H. P., Hall, R. J., Peddle, D. R., King, D. J., Trofymow, J. A., Swift, E., Van Der Sanden, J. and Pellikka, P. K. E. (2002) ‘Derivation and validation of Canada-wide coarse-resolution leaf area index maps using high-resolution satellite imagery and ground measurements’, *Remote Sensing of Environment*, 80(1), pp. 165–184. doi: 10.1016/S0034-4257(01)00300-5.

Chen, Q., Vaglio Laurin, G., Battles, J. J. and Saah, D. (2012) 'Integration of airborne lidar and vegetation types derived from aerial photography for mapping aboveground live biomass', *Remote Sensing of Environment*. Elsevier Inc., 121, pp. 108–117. doi: 10.1016/j.rse.2012.01.021.

Chen, X. L., Zhao, H. M., Li, P. X. and Yin, Z. Y. (2006) 'Remote sensing image-based analysis of the relationship between urban heat island and land use/cover changes', *Remote Sensing of Environment*, 104(2), pp. 133–146. doi: 10.1016/j.rse.2005.11.016.

Cingolani, A. M., Renison, D., Zak, M. R. and Cabido, M. R. (2004) 'Mapping vegetation in a heterogeneous mountain rangeland using landsat data: An alternative method to define and classify land-cover units', *Remote Sensing of Environment*, 92(1), pp. 84–97. doi: 10.1016/j.rse.2004.05.008.

Cleasby, N., Schwarz, A. M., Phillips, M., Paul, C., Pant, J., Oeta, J., Pickering, T., Meloty, A., Laumani, M. and Kori, M. (2014) 'The socio-economic context for improving food security through land based aquaculture in Solomon Islands: A peri-urban case study', *Marine Policy*. Elsevier, 45, pp. 89–97. doi: 10.1016/j.marpol.2013.11.015.

Cleve, C., Kelly, M., Kearns, F. R. and Moritz, M. (2008) 'Classification of the wildland-urban interface: A comparison of pixel- and object-based classifications using high-resolution aerial photography', *Computers, Environment and Urban Systems*, 32(4), pp. 317–326. doi: 10.1016/j.compenvurbsys.2007.10.001.

Collado, A. D., Chuvieco, E. and Camarasa, A. (2002) 'Satellite remote sensing analysis to monitor desertification processes in the crop-rangeland boundary of Argentina', *Journal of Arid Environments*, 52(1), pp. 121–133. doi: 10.1006/jare.2001.0980.

Coppin, P., Jonckheere, I., Nackaerts, K., Muys, B. and Lambin, E. (2004) 'Review ArticleDigital change detection methods in ecosystem monitoring: a review', *International Journal of Remote Sensing*, 25(9), pp. 1565–1596. doi: 10.1080/0143116031000101675.

D. Lu and Weng, Q. (2007) 'A survey of image classification methods and techniques for improving classification performance International Journal of Remote Sensing', *International Journal of Remote Sensing*, 8(5), pp. 823–870. doi: 10.1080/01431160600746456.

Darwish, A., Leukert, K. and Reinhardt, W. (2003) 'Image segmentation for the purpose of object-based classification', *IGARSS 2003. 2003 IEEE International Geoscience and Remote Sensing Symposium. Proceedings (IEEE Cat. No.03CH37477)*, 3(C), pp. 2039–2041. doi: 10.1109/IGARSS.2003.1294332.

Department of Water and Sanitation (2009) 'Water for Growth and Development in South Africa'.

Dewan, A. M. and Yamaguchi, Y. (2009a) 'Land use and land cover change in Greater Dhaka, Bangladesh: Using remote sensing to promote sustainable urbanization', *Applied Geography*. Elsevier Ltd, 29(3), pp. 390–401. doi: 10.1016/j.apgeog.2008.12.005.

Dewan, A. M. and Yamaguchi, Y. (2009b) 'Using remote sensing and GIS to detect and monitor land use and land cover change in Dhaka Metropolitan of Bangladesh during 1960-2005', *Environmental Monitoring and Assessment*, 150(1–4), pp. 237–249. doi: 10.1007/s10661-008-0226-5.

Dingle Robertson, L. and King, D. J. (2011) 'Comparison of pixel- and object-based classification in land cover change mapping', *International Journal of Remote Sensing*, 32(6), pp. 1505–1529. doi: 10.1080/01431160903571791.

Dixon, B. and Candade, N. (2008) 'Multispectral landuse classification using neural networks and support vector machines: one or the other, or both?', *International Journal of Remote Sensing*, 29(4), pp. 1185–1206. doi: 10.1080/01431160701294661.

Domenikiotis, C., Dalezios, N. R., Loukas, a. and Karteris, M. (2002) 'Agreement assessment of NOAA/AVHRR NDVI with Landsat TM NDVI for mapping burned forested areas', *International Journal of Remote Sensing*, 23(20), pp. 4235–4246. doi: 10.1080/01431160110107707.

Duda, T. and Canty, M. (2002) 'Unsupervised classification of satellite imagery: Choosing a good algorithm', *International Journal of Remote Sensing*, 23(11), pp. 2193–2212. doi: 10.1080/01431160110078467.

Dupuy, S., Herbreteau, V., Feyfant, T., Morand, S. and Tran, a (2012) 'Land-cover dynamics in Southeast Asia: contribution of object- oriented techniques for change detection', *Geobia*, pp. 217–222.

Duro, D. C., Coops, N. C., Wulder, M. A. and Han, T. (2007) 'Development of a large area biodiversity monitoring system driven by remote sensing', *Progress in Physical Geography*, 31(310.1177/0309133307079054), pp. 235–260. doi: 10.1177/0309133307079054.

Duro, D. C., Franklin, S. E. and Dubé, M. G. (2012) 'A comparison of pixel-based and object-based image analysis with selected machine learning algorithms for the classification of agricultural landscapes using SPOT-5 HRG imagery', *Remote Sensing of Environment*. Elsevier Inc., 118, pp. 259–272. doi: 10.1016/j.rse.2011.11.020.

Dwivedi, R. S., Sreenivas, K. and Ramana, K. V. (2005) 'Cover: Land-use/land-cover change analysis in part of Ethiopia using Landsat Thematic Mapper data', *International Journal of Remote Sensing*, 26(7), pp. 1285–1287. doi: 10.1080/01431160512331337763.

Easterling, D. R. (2000) 'Climate Extremes: Observations, Modeling, and Impacts', *Science*, 289(5487), pp. 2068–2074. doi: 10.1126/science.289.5487.2068.

Eastman, J. R. (2001) 'Introduction to Remote Sensing and Image Processing', *Clark University, USA*, 1, pp. 17–34.

El-aziz, A. O. A. (2013) 'Monitoring and Change Detection along the Eastern Side of Qena Bend , Nile Valley , Egypt Using GIS and Remote Sensing', 2013(September), pp. 276–281.

Erbek, F. S., Özkan, C. and Taberner, M. (2004) 'Comparison of maximum likelihood classification method with supervised artificial neural network algorithms for land use activities', *International Journal of Remote Sensing*, 25(9), pp. 1733–1748. doi: 10.1080/0143116031000150077.

Faid, A. M. and Abdulaziz, A. M. (2012) 'Monitoring land-use change-associated land development using multitemporal Landsat data and geoinformatics in Kom Ombo area, South Egypt', *International Journal of Remote Sensing*, 33(22), pp. 7024–7046. doi: 10.1080/01431161.2012.697207.

Feddema, J. J. (2005) 'The Importance of Land-Cover Change in Simulating Future

Climates', *Science*, 310(5754), pp. 1674–1678. doi: 10.1126/science.1118160.

Feng, S., Hu, Q. and Qian, W. (2004) 'Quality control of daily meteorological data in China, 1951-2000: A new dataset', *International Journal of Climatology*, 24(7), pp. 853–870. doi: 10.1002/joc.1047.

Fingas, M. and Brown, C. (2014) 'Review of oil spill remote sensing', *Marine Pollution Bulletin*. Elsevier Ltd, 83(1), pp. 9–23. doi: 10.1016/j.marpolbul.2014.03.059.

Flanders, D., Hall-Beyer, M. and Pereverzoff, J. (2003) 'Preliminary evaluation of eCognition object-based software for cut block delineation and feature extraction', *Canadian Journal of Remote Sensing*, 29(4), pp. 441–452. doi: 10.5589/m03-006.

Foley, J. A. (2005) 'Global Consequences of Land Use', *Science*, 309(5734), pp. 570–574. doi: 10.1126/science.1111772.

Fonji, S. and Taff, G. N. (2014) 'Using satellite data to monitor land-use land-cover change in North-eastern Latvia', *SpringerPlus*, 3(1), p. 61. doi: 10.1186/2193-1801-3-61.

Foody, G. M. (2008) 'Harshness in image classification accuracy assessment', *International Journal of Remote Sensing*, 29(11), pp. 3137–3158. doi: 10.1080/01431160701442120.

Foody, G. M. (2010a) 'Assessing the accuracy of land cover change with imperfect ground reference data', *Remote Sensing of Environment*, 114(10), pp. 2271–2285. doi: 10.1016/j.rse.2010.05.003.

Foody, G. M. (2010b) 'Assessing the accuracy of land cover change with imperfect ground reference data', *Remote Sensing of Environment*. Elsevier Inc., 114(10), pp. 2271–2285. doi: 10.1016/j.rse.2010.05.003.

Foody, G. M. M. (2002) 'Status of land cover classification accuracy assessment', *Remote Sensing of Environment*, 80(1), pp. 185–201. doi: 10.1016/S0034-4257(01)00295-4.

Foody, G. M. and Mathur, A. (2004a) 'A relative evaluation of multiclass image classification by support vector machines', *IEEE Transactions on Geoscience and Remote Sensing*, 42(6), pp. 1335–1343. doi: 10.1109/TGRS.2004.827257.

Foody, G. M. and Mathur, A. (2004b) 'Toward intelligent training of supervised image classifications: Directing training data acquisition for SVM classification', *Remote Sensing of Environment*, 93(1–2), pp. 107–117. doi: 10.1016/j.rse.2004.06.017.

Foody, G. M. and Mathur, A. (2006) 'The use of small training sets containing mixed pixels for accurate hard image classification: Training on mixed spectral responses for classification by a SVM', *Remote Sensing of Environment*, 103(2), pp. 179–189. doi: 10.1016/j.rse.2006.04.001.

Foody, G. M., Mathur, A., Sanchez-Hernandez, C. and Boyd, D. S. (2006) 'Training set size requirements for the classification of a specific class', *Remote Sensing of Environment*, 104(1), pp. 1–14. doi: 10.1016/j.rse.2006.03.004.

Foulds, S. a. and Macklin, M. G. (2006) 'Holocene land-use change and its impact on river basin dynamics in Great Britain and Ireland', *Progress in Physical Geography*, 30(5), pp. 589–604. doi: 10.1177/0309133306071143.

Gao, B. C. (1996) ‘NDWI - A normalized difference water index for remote sensing of vegetation liquid water from space’, *Remote Sensing of Environment*, 58(3), pp. 257–266. doi: 10.1016/S0034-4257(96)00067-3.

Gao, X., Huete, A. R., Ni, W. and Miura, T. (2000) ‘Optical-biophysical relationships of vegetation spectra without background contamination’, *Remote Sensing of Environment*, 74(3), pp. 609–620. doi: 10.1016/S0034-4257(00)00150-4.

Gerard, F., Petit, S., Smith, G., Thomson, A., Brown, N., Manchester, S., Wadsworth, R., Bugar, G., Halada, L., Bezak, P., Boltiziar, M., De badts, E., Halabuk, A., Mojses, M., Petrovic, F., Gregor, M., Hazeu, G., Mucher, C. A., Wachowicz, M., Huitu, H., Tuominen, S., Kohler, R., Olschofsky, K., Ziese, H., Kolar, J., Sustera, J., Luque, S., Pino, J., Pons, X., Roda, F., Roscher, M. and Feranec, J. (2010) ‘Land cover change in Europe between 1950 and 2000 determined employing aerial photography’, *Progress in Physical Geography*, 34(2), pp. 183–205. doi: 10.1177/0309133309360141.

Ghorbani, A., Mossivand, A. M. and Ouri, A. E. (2012) ‘Utility of the Normalised Difference Vegetation Index (NDVI) for land / canopy cover mapping in Khalkhal County (Iran)’, *Annals of Biological Research*, 3(12), pp. 5494–5503. Available at: http://scholarsresearchlibrary.com/archive.html.

Giada, S., De Groeve, T., Ehrlich, D. and Soille, P. (2003) ‘Information extraction from very high resolution satellite imagery over Lukole refugee camp, Tanzania’, *International Journal of Remote Sensing*, 24(22), pp. 4251–4266. doi: 10.1080/0143116021000035021.

Gidudu, A., Hulley, G. and Marwala, T. (2007) ‘Classification of images using Support Vector Machines’, *Department of Electrical and Information Engineering, arXiv: 0709.3967v1, Cornell University, Library, 2007.*, pp. 1–6.

Gillespie, T. W., Chu, J., Frankenberg, E. and Thomas, D. (2007) ‘Assessment and prediction of natural hazards from satellite imagery’, *Progress in Physical Geography*, 31(5), pp. 459–470. doi: 10.1177/0309133307083296.

Gillespie, T. W., Foody, G. M., Rocchini, D., Giorgi, a. P. and Saatchi, S. (2008) ‘Measuring and modelling biodiversity from space’, *Progress in Physical Geography*, 32(2), pp. 203–221. doi: 10.1177/0309133308093606.

Giordano, A. and Filippi, N. (1993) ‘Advantages and disadvantages of land use changes for the preservation of soil resources . Review of soil conservation practices and the need for related research’, 134(2), pp. 113–134.

Gislason, P. O., Benediktsson, J. A. and Sveinsson, J. R. (2006) ‘Random forests for land cover classification’, *Pattern Recognition Letters*, 27(4), pp. 294–300. doi: 10.1016/j.patrec.2005.08.011.

Gitas, I., Mitri, G., Veraverbeke, S. and Polychronaki, A. (2012) ‘Advances in remote sensing of post-fire vegetation recovery monitoring–a review’, *Remote Sensing of Biomass–Principles and Applications*, p. 322. Available at: http://cdn.intechopen.com/pdfs/33854.pdf.

Godfray, H. C. J., Beddington, J. R., Crute, I. R., Haddad, L., Lawrence, D., Muir, J. F., Pretty, J., Robinson, S., Thomas, S. M. and Toulmin, C. (2012) ‘The Challenge of Food Security’, *Science*, 327(February), p. 812. doi: 10.4337/9780857939388.

Gong, P., Wang, J., Yu, L., Zhao, Y., Zhao, Y., Liang, L., Niu, Z., Huang, X., Fu, H., Liu, S., Li, C., Li, X., Fu, W., Liu, C., Xu, Y., Wang, X., Cheng, Q., Hu, L., Yao, W., Zhang, H., Zhu, P., Zhao, Z., Zhang, H., Zheng, Y., Ji, L., Zhang, Y., Chen, H., Yan, A., Guo, J., Yu, L., Wang, L., Liu, X., Shi, T., Zhu, M., Chen, Y., Yang, G., Tang, P., Xu, B., Giri, C., Clinton, N., Zhu, Z., Chen, J. and Chen, J. (2013) 'Finer resolution observation and monitoring of global land cover: first mapping results with Landsat TM and ETM+ data', *International Journal of Remote Sensing*, 34(7), pp. 2607–2654. doi: 10.1080/01431161.2012.748992.

Gopal, S. and Woodcock, C. (1996) 'Remote sensing of forest change using artificial neural networks', *IEEE Transactions on Geoscience and Remote Sensing*, 34(2), pp. 398–404. doi: 10.1109/36.485117.

Gorokhovich, Y. and Voustianiouk, A. (2006) 'Accuracy assessment of the processed SRTM-based elevation data by CGIAR using field data from USA and Thailand and its relation to the terrain characteristics', *Remote Sensing of Environment*, 104(4), pp. 409–415. doi: 10.1016/j.rse.2006.05.012.

Goward, S. N., Xue, Y. and Czajkowski, K. P. (2002) 'Evaluating land surface moisture conditions from the remotely sensed temperature/vegetation index measurements: An exploration with the simplified simple biosphere model', *Remote Sensing of Environment*, 79(2–3), pp. 225–242. doi: 10.1016/S0034-4257(01)00275-9.

Di Gregorio, A. (2016) *Land Cover Classification System : Classification concepts. Software version 3*. Available at: http://www.fao.org/3/a-i5232e.pdf.

Guindon, B., Zhang, Y. and Dillabaugh, C. (2004) 'Landsat urban mapping based on a combined spectral-spatial methodology', *Remote Sensing of Environment*, 92(2), pp. 218–232. doi: 10.1016/j.rse.2004.06.015.

Gupta, P., Christopher, S. A., Wang, J., Gehrig, R., Lee, Y. and Kumar, N. (2006) 'Satellite remote sensing of particulate matter and air quality assessment over global cities', *J. Atmos. Env.*, pp. 5880–5892. doi: 10.1016/j.atmosenv.2006.03.016.

Haibin, L. and Zhenling, L. (2010) 'Recycling utilization patterns of coal mining waste in China', *Resources, Conservation and Recycling*. Elsevier B.V., 54(12), pp. 1331–1340. doi: 10.1016/j.resconrec.2010.05.005.

Hansen, M. C. and Loveland, T. R. (2012) 'A review of large area monitoring of land cover change using Landsat data', *Remote Sensing of Environment*. Elsevier Inc., 122, pp. 66–74. doi: 10.1016/j.rse.2011.08.024.

He, C., Shi, P., Xie, D. and Zhao, Y. (2010) 'Improving the normalized difference built-up index to map urban built-up areas using a semiautomatic segmentation approach', *Remote Sensing Letters*, 1(4), pp. 213–221. doi: 10.1080/01431161.2010.481681.

Helldén, U. and Tottrup, C. (2008) 'Regional desertification: A global synthesis', *Global and Planetary Change*, 64(3–4), pp. 169–176. doi: 10.1016/j.gloplacha.2008.10.006.

Helmer, E. H. and Ruefenacht, B. (2005) 'Cloud-free satellite image mosaics with regression trees and histrogram matching', *Photogrammetric Engineering & Remote Sensing*, 71(9), pp. 1079–1089. doi: 10.14358/PERS.71.9.1079.

Hernandez, A. (no date) 'Landscape Metrics & Ecological Processes Concepts and

Applications', *Prenhall.Com*. Available at: http://www.prenhall.com/lo/c06/WebResources/FRWS7910_AHernadez.pdf.

Herold, M., Scepan, J. and Clarke, K. C. (2002) 'The use of remote sensing and landscape metrics to describe structures and changes in urban land uses', *Environment and Planning A*, 34(8), pp. 1443–1458. doi: 10.1068/a3496.

Herrmann, S. M., Anyamba, A. and Tucker, C. J. (2005) 'Recent trends in vegetation dynamics in the African Sahel and their relationship to climate', *Global Environmental Change*, 15(4), pp. 394–404. doi: 10.1016/j.gloenvcha.2005.08.004.

Hlatywayo, J. P. and Masvosve, T. (2015) 'Use of GIS and Orthophotos in spatio-temporal assessment of land uses and city expansion : A case of Pietermaritzburg , Kwazulu-Natal, South Africa', *South African Journal of Geomatics*, 4(4), pp. 526–547.

Hlavac, V. (2011) 'Fundamentals of Image Processing', *Optical and Digital Image Processing: Fundamentals and Applications*, pp. 71–96. doi: 10.1002/9783527635245.ch4.

Ho, L. T. K., Umitsu, M. and Yamaguchi, Y. (2010) 'Flood hazard mapping by satellite images and SRTM DEM in the Vu Gia-Thu Bon alluvial plain, Central Vietnam', *International Archives of the Photogrammetry, Remote Sensing and Spatial Information Science*, XXXVIII(part8), pp. 275–280. doi: 10.1016/j.apgeog.2011.01.005.

Hodgson, M. E., Jensen, J. R., Tullis, J. a, Riordan, K. D. and Archer, C. M. (2003) 'Synergistic Use of Lidar and Color Aerial Photography for Mapping Urban Parcel Imperviousness', *Photogrammetric Engineering & Remote Sensing*, 69(9), pp. 973–980. doi: 10.14358/PERS.69.9.973.

Hoffmann, J. and Sander, P. (2006) 'Remote sensing and GIS in hydrogeology', *Hydrogeology Journal*, 15(1), pp. 1–3. doi: 10.1007/s10040-006-0140-2.

Hollmann, R., Merchant, C. J., Saunders, R., Downy, C., Buchwitz, M., Cazenave, A., Chuvieco, E., Defourny, P., De Leeuw, G., Forsberg, R., Holzer-Popp, T., Paul, F., Sandven, S., Sathyendranath, S., Van Roozendael, M. and Wagner, W. (2013) 'The ESA climate change initiative: Satellite data records for essential climate variables', *Bulletin of the American Meteorological Society*, 94(10), pp. 1541–1552. doi: 10.1175/BAMS-D-11-00254.1.

Hsu, C. and Lin, C. (2002) 'A comparison of methods for multiclass support vector machines', *Neural Networks, IEEE Transactions on*, 13(2), pp. 415–425. doi: 10.1109/TNN.2002.1021904.

Huang, C., Davis, L. S. and Townshend, J. R. G. (2002) 'An assessment of support vector machines for land cover classification', *International Journal of Remote Sensing*, 23(4), pp. 725–749. doi: 10.1080/01431160110040323.

Huang, L. ;, Fang, Y., Zuo, X. ;, Yu, X., Huang, L., Zuo, X. and Tai, X. C. (2015) 'Table of contents 1. Automatic Change Detection Method of Multitemporal Remote Sensing Images Based on 2D-Otsu Automatic Change Detection Method of Multitemporal Remote Sensing Images Based on 2D-Otsu Algorithm Improved by Firefly Algorithm', 2015. doi: 10.1155/2015/327123.

Hubert-Moy, L., Cotonnec, A., Le Du, L., Chardin, A. and Perez, P. (2001) 'A comparison of

parametric classification procedures of remotely sensed data applied on different landscape units', *Remote Sensing of Environment*, 75(2), pp. 174–187. doi: 10.1016/S0034-4257(00)00165-6.

Huete, A., Didan, K., Miura, T., Rodriguez, E. P., Gao, X. and Ferreira, L. G. (2002) 'Overview of the radiometric and biophysical performance of the MODIS vegetation indices', *Remote Sensing of Environment*, 83(1–2), pp. 195–213. doi: 10.1016/S0034-4257(02)00096-2.

Hussain, M., Chen, D., Cheng, A., Wei, H. and Stanley, D. (2013) 'Change detection from remotely sensed images: From pixel-based to object-based approaches', *ISPRS Journal of Photogrammetry and Remote Sensing*. International Society for Photogrammetry and Remote Sensing, Inc. (ISPRS), 80, pp. 91–106. doi: 10.1016/j.isprsjprs.2013.03.006.

Hyde, P., Dubayah, R., Walker, W., Blair, J. B., Hofton, M. and Hunsaker, C. (2006) 'Mapping forest structure for wildlife habitat analysis using multi-sensor (LiDAR, SAR/InSAR, ETM+, Quickbird) synergy', *Remote Sensing of Environment*, 102(1–2), pp. 63–73. doi: 10.1016/j.rse.2006.01.021.

Hyyppa, J., Hyyppa, H., Inkinen, M., Engdahl, M., Linko, S. and Zhu, Y. H. (2000) 'Accuracy comparison of various remote sensing data sources in the retrieval of forest stand attributes', *Forest Ecology and Management*, 128(1–2), pp. 109–120. doi: 10.1016/S0378-1127(99)00278-9.

Idol, T., Haack, B. and Mahabir, R. (2015) 'Comparison and integration of spaceborne optical and radar data for mapping in Sudan', *International Journal of Remote Sensing*, 36(6), pp. 1551–1569. doi: Doi 10.1080/01431161.2015.1015659.

Ikeda, H., Okamoto, K. and Fukuhara, M. (1999) 'Estimation of aboveground grassland phytomass with a growth model using Landsat TM and climate data', *International Journal of Remote Sensing*, 20(11), pp. 2283–2294. doi: 10.1080/014311699212254.

İlsever, M. and Ünsalan, C. (2012) 'Pixel-Based Change Detection Methods', *Two-Dimensional Change Detection Methods*, pp. 7–22. doi: 10.1007/978-1-4471-4255-3.

Im, J., Jensen, J. R. J. and Tullis, J. A. J. (2008) 'Object-based change detection using correlation image analysis and image segmentation', *International Journal of Remote Sensing*, 29(March 2015), pp. 423, 399. doi: 10.1080/01431160601075582.

Inoue, Y., Kurosu, T., Maeno, H., Uratsuka, S., Kozu, T., Dabrowska-Zielinska, K. and Qi, J. (2002) 'Season-long daily measurements of multifrequency (Ka, Ku, X, C, and L) and full-polarization backscatter signatures over paddy rice field and their relationship with biological variables', *Remote Sensing of Environment*, 81(2–3), pp. 194–204. doi: 10.1016/S0034-4257(01)00343-1.

Jackson, T. J., Chen, D., Cosh, M., Li, F., Anderson, M., Walthall, C., Doriaswamy, P. and Hunt, E. R. (2004) 'Vegetation water content mapping using Landsat data derived normalized difference water index for corn and soybeans', *Remote Sensing of Environment*, 92(4), pp. 475–482. doi: 10.1016/j.rse.2003.10.021.

Vander Jagt, B. J., Durand, M. T., Margulis, S. A., Kim, E. J. and Molotch, N. P. (2015) 'On the characterization of vegetation transmissivity using LAI for application in passive microwave remote sensing of snowpack', *Remote Sensing of Environment*. Elsevier Inc., 156,

pp. 310–321. doi: 10.1016/j.rse.2014.09.001.

Janzen, D. T., Fredeen, A. L. and Wheate, R. D. (2006) 'Radiometric correction techniques and accuracy assessment for Landsat TM data in remote forested regions', *Canadian Journal of Remote Sensing*, 32(5), pp. 330–340. doi: 10.5589/m06-028.

Ji, L., Wylie, B. K., Brown, D. R. N., Peterson, B., Alexander, H. D., Mack, M. C., Rover, J., Waldrop, M. P., McFarland, J. W., Chen, X. and Pastick, N. J. (2015) 'Spatially explicit estimation of aboveground boreal forest biomass in the Yukon River Basin, Alaska', *International Journal of Remote Sensing*, 36(4), pp. 939–953. doi: 10.1080/01431161.2015.1004764.

Jia, K., Li, Q., Tian, Y., Wu, B., Zhang, F. and Meng, J. (2012) 'Crop classification using multi-configuration SAR data in the North China Plain', *International Journal of Remote Sensing*, 33(1), pp. 170–183. doi: 10.1080/01431161.2011.587844.

Jia, X. and Richards, J. A. (1994) 'Efficient maximum likelihood classification for imaging spectrometer data sets', *IEEE Transactions on Geoscience and Remote Sensing*, 32(2), pp. 274–281. doi: 10.1109/36.295042.

Jiang, Z., Huete, A. R., Chen, J., Chen, Y., Li, J., Yan, G. and Zhang, X. (2006) 'Analysis of NDVI and scaled difference vegetation index retrievals of vegetation fraction', *Remote Sensing of Environment*, 101(3), pp. 366–378. doi: 10.1016/j.rse.2006.01.003.

Jiang, Z., Huete, A. R., Didan, K. and Miura, T. (2008) 'Development of a two-band enhanced vegetation index without a blue band', *Remote Sensing of Environment*, 112(10), pp. 3833–3845. doi: 10.1016/j.rse.2008.06.006.

Jobin, B., Labrecque, S., Grenier, M. and Falardeau, G. (2008) 'Object-based classification as an alternative approach to the traditional pixel-based classification to identify potential habitat of the Grasshopper Sparrow', *Environmental Management*, 41(1), pp. 20–31. doi: 10.1007/s00267-007-9031-0.

Jonard, F., Weihermüller, L., Schwank, M., Jadoon, K. Z., Vereecken, H. and Lambot, S. (2015) 'Estimation of Hydraulic properties of a sandy soil using ground-based active and passive microwave remote sensing', *IEEE Transactions on Geoscience and Remote Sensing*, 53(6), pp. 3095–3109. doi: 10.1109/TGRS.2014.2368831.

Jones, D. A., Hansen, A. J., Bly, K., Doherty, K., Verschuyl, J. P., Paugh, J. I., Carle, R. and Story, S. J. (2009) 'Monitoring land use and cover around parks: A conceptual approach', *Remote Sensing of Environment*. Elsevier Inc., 113(7), pp. 1346–1356. doi: 10.1016/j.rse.2008.08.018.

Joyce, K. E., Belliss, S. E., Samsonov, S. V., McNeill, S. J. and Glassey, P. J. (2009) 'A review of the status of satellite remote sensing and image processing techniques for mapping natural hazards and disasters', *Progress in Physical Geography*, 33(2), pp. 183–207. doi: 10.1177/0309133309339563.

Jung, M. and Chang, E. (2015) 'International Journal of Remote Sensing NDVI-based land-cover change detection using harmonic analysis NDVI-based land-cover change detection using harmonic analysis', *International Journal of Remote Sensing*, 36(4), pp. 1097–1113. doi: 10.1080/01431161.2015.1007252.

Kalnay, E. and Cai, M. (2003) 'Impact of urbanization and land-use change on climate', *Nature*, 423(May), pp. 528–531. doi: 10.1038/nature01649.1.

Kamusoko, C. and Aniya, M. (2009) 'Hybrid classification of Landsat data and GIS for land use/cover change analysis of the Bindura district, Zimbabwe', *International Journal of Remote Sensing*, 30(1), pp. 97–115. doi: 10.1080/01431160802244268.

Kavzoglu, T. and Colkesen, I. (2009) 'A kernel functions analysis for support vector machines for land cover classification', *International Journal of Applied Earth Observation and Geoinformation*, 11(5), pp. 352–359. doi: 10.1016/j.jag.2009.06.002.

Kavzoglu, T. and Mather, P. M. (2003) 'The use of backpropagating artificial neural networks in land cover classification', *International Journal of Remote Sensing*, 24(23), pp. 4907–4938. doi: 10.1080/0143116031000114851.

Kennedy, R. E., Townsend, P. A., Gross, J. E., Cohen, W. B., Bolstad, P., Wang, Y. Q. and Adams, P. (2009) 'Remote sensing change detection tools for natural resource managers: Understanding concepts and tradeoffs in the design of landscape monitoring projects', *Remote Sensing of Environment*. Elsevier Inc., 113(7), pp. 1382–1396. doi: 10.1016/j.rse.2008.07.018.

Kerr, J. T. and Ostrovsky, M. (2003) 'From space to species: Ecological applications for remote sensing', *Trends in Ecology and Evolution*, 18(6), pp. 299–305. doi: 10.1016/S0169-5347(03)00071-5.

Keuchel, J., Naumann, S., Heiler, M. and Siegmund, A. (2003) 'Automatic land cover analysis for Tenerife by supervised classification using remotely sensed data', *Remote Sensing of Environment*, 86(4), pp. 530–541. doi: 10.1016/S0034-4257(03)00130-5.

Khaing, M. M., Htun, K. Z. and Lwin, Z. M. (2016) 'Land Use / Land Cover Change Mapping of Mandalay City'.

Kim, M. (2013) 'Semi-supervised learning of hidden conditional random fields for time-series classification', *Neurocomputing*, 119, pp. 339–349. doi: 10.1016/j.neucom.2013.03.024.

Kim, Y., Evans, R. G. and Iversen, W. M. (2008) 'Remote Sensing and Control of an Irrigation System Using a Distributed Wireless Sensor Network', *IEEE Transactions on Instrumentation and Measurement*, 57(7), pp. 1379–1387. doi: 10.1109/TIM.2008.917198.

Kleyn, L., Mangara, P. and Remas, H. (no date) 'Implementation of automatic spectral rule-based preliminary mapping for enhanced object-based classification of South African land cover classes'.

Kuemmerle, T., Radeloff, V. C., Perzanowski, K. and Hostert, P. (2006) 'Cross-border comparison of land cover and landscape pattern in Eastern Europe using a hybrid classification technique', *Remote Sensing of Environment*, 103(4), pp. 449–464. doi: 10.1016/j.rse.2006.04.015.

Kumar, P., Gupta, D. K., Mishra, V. N. and Prasad, R. (2015) 'Comparison of support vector machine, artificial neural network, and spectral angle mapper algorithms for crop classification using LISS IV data', *International Journal of Remote Sensing*, 36(6), pp. 1604–1617. doi: 10.1080/2150704X.2015.1019015.

Kumar, Y. and Sahoo, G. (2012) ‘Analysis of Parametric & Non Parametric Classifiers for Classification Technique using WEKA’, *Information Technology and Computer Science*, 7(7), pp. 43–49. doi: 10.5815/ijitcs.2012.07.06.

Lasanta, T. and Vicente-Serrano, S. M. (2012) ‘Complex land cover change processes in semiarid Mediterranean regions: An approach using Landsat images in northeast Spain’, *Remote Sensing of Environment*. Elsevier Inc., 124, pp. 1–14. doi: 10.1016/j.rse.2012.04.023.

Latham, J. (2008) ‘FAO Land cover mapping initiatives’, *North America Land Cover Summit*, pp. 75–96. Available at: http://www.aag.org/galleries/nalcs/CH6.pdf.

Latham, J., Cumani, R., Rosati, I. and Bloise, M. (2014) ‘FAO Global Land Cover SHARE’, *Database Beta-Release Verion 1.0*, p. 40. Available at: http://www.glcn.org/downs/prj/glcshare/GLC_SHARE_beta_v1.0_2014.pdf.

Lawrence, P. J., Feddema, J. J., Bonan, G. B., Meehl, G. A., O’Neill, B. C., Oleson, K. W., Levis, S., Lawrence, D. M., Kluzek, E., Lindsay, K. and Thornton, P. E. (2012) ‘Simulating the biogeochemical and biogeophysical impacts of transient land cover change and wood harvest in the Community Climate System Model (CCSM4) from 1850 to 2100’, *Journal of Climate*, 25(9), pp. 3071–3095. doi: 10.1175/JCLI-D-11-00256.1.

Lentile, L. B., Smith, A. M. S., Hudak, A. T., Morgan, P., Bobbitt, M. J., Lewis, S. A. and Robichaud, P. R. (2009) ‘Remote sensing for prediction of 1-year post-fire ecosystem condition’, *International Journal of Wildland Fire*, 18(5), pp. 594–608. doi: 10.1071/WF07091.

Li, J., Xu, B., Yang, X., Jin, Y., Zhao, L., Zhao, F., Chen, S., Guo, J., Qin, Z. and Ma, H. (2015) ‘Characterizing changes in grassland desertification based on Landsat images of the Ongniud and Naiman Banners, Inner Mongolia’, *International Journal of Remote Sensing*, 36(19–20), pp. 5137–5149. doi: 10.1080/01431161.2015.1029596.

Li, P., Jiang, L. and Feng, Z. (2013) ‘Cross-comparison of vegetation indices derived from landsat-7 enhanced thematic mapper plus (ETM+) and landsat-8 operational land imager (OLI) sensors’, *Remote Sensing*, 6(1), pp. 310–329. doi: 10.3390/rs6010310.

Li, S. and Chen, X. (2014) ‘A new bare-soil index for rapid mapping developing areas using landsat 8 data’, *International Archives of the Photogrammetry, Remote Sensing and Spatial Information Sciences - ISPRS Archives*, 40(4), pp. 139–144. doi: 10.5194/isprsarchives-XL-4-139-2014.

Li, X., Shen, H., Zhang, L. and Li, H. (2015) ‘Sparse-based reconstruction of missing information in remote sensing images from spectral/temporal complementary information’, *ISPRS Journal of Photogrammetry and Remote Sensing*. International Society for Photogrammetry and Remote Sensing, Inc. (ISPRS), 106, pp. 1–15. doi: 10.1016/j.isprsjprs.2015.03.009.

Li, X. and Yeh, A. G.-O. (2004) ‘Analyzing spatial restructuring of land use patterns in a fast growing region using remote sensing and GIS’, *Landscape and Urban Planning*, 69(4), pp. 335–354. doi: 10.1016/j.landurbplan.2003.10.033.

Liu, K., Shi, W. and Zhang, H. (2011) ‘A fuzzy topology-based maximum likelihood classification’, *ISPRS Journal of Photogrammetry and Remote Sensing*. Elsevier B.V., 66(1), pp. 103–114. doi: 10.1016/j.isprsjprs.2010.09.007.

Liu, Q., Liu, G., Huang, C. and Xie, C. (2015) 'Comparison of tasselled cap transformations based on the selective bands of Landsat 8 OLI TOA reflectance images', *International Journal of Remote Sensing*, 36(2), pp. 417–441. doi: 10.1080/01431161.2014.995274.

Lu, D., Mausel, P., Brondizio, E. and Moran, E. F. (2004a) 'Change detection techniques', *International Journal of Remote Sensing*, 25(March 2015), pp. 2365–2407. doi: 10.1080/0143116031000139863.

Lu, D., Mausel, P., Brondizio, E. and Moran, E. F. (2004b) 'Change detection techniques', *International Journal of Remote Sensing*, 25(June 2015), pp. 2365–2407. doi: 10.1080/0143116031000139863.

Lunetta, R. S., Knight, J. F., Ediriwickrema, J., Lyon, J. G. and Worthy, L. D. (2006) 'Land-cover change detection using multi-temporal MODIS NDVI data', *Remote Sensing of Environment*, 105(2), pp. 142–154. doi: 10.1016/j.rse.2006.06.018.

Lyle, G., Lewis, M. and Ostendorf, B. (2013) 'Testing the temporal ability of landsat imagery and precision agriculture technology to provide high resolution historical estimates of wheat yield at the farm scale', *Remote Sensing*, 5(4), pp. 1549–1567. doi: 10.3390/rs5041549.

De Maesschalck, R., Jouan-Rimbaud, D. and Massart, D. L. L. (2000) 'The Mahalanobis distance', *Chemometrics and Intelligent Laboratory Systems*, 50(1), pp. 1–18. doi: 10.1016/S0169-7439(99)00047-7.

Mahavir (2000) 'High (Spatial) resolution vs. Low resolution images: A planner's view point', *International Archives of Photogrammetry and Remote Sensing*, XXXIII, pp. 127–132.

Mallinis, G., Koutsias, N., Tsakiri-Strati, M. and Karteris, M. (2008) 'Object-based classification using Quickbird imagery for delineating forest vegetation polygons in a Mediterranean test site', *ISPRS Journal of Photogrammetry and Remote Sensing*, 63(2), pp. 237–250. doi: 10.1016/j.isprsjprs.2007.08.007.

Manandhar, R., Odeh, I. O. a. and Ancev, T. (2009) 'Improving the Accuracy of Land Use and Land Cover Classification of Landsat Data Using Post-Classification Enhancement', *Remote Sensing*, 1(3), pp. 330–344. doi: 10.3390/rs1030330.

Mares, C., Mares, I., Mihailescu, M., Stanciu, A. and Cubasch, U. (2015) 'Trends Of Climate Extreme Indices In The 21 st Century In The Danube Middle And Lower Basin', (October), pp. 1–12.

Marghany, M. and Hashim, M. (2011) 'Comparison between Mahalanobis classification and neural network for oil spill detection using RADARSAT-1 SAR data', 6(3), pp. 566–576. doi: 10.5897/IJPS11.004.

Markham, B. L., Storey, J. C., Williams, D. L. and Irons, J. R. (2004) 'Landsat sensor performance: history and current status', *IEEE Transactions on Geoscience and Remote Sensing*, 42(12), pp. 2691–2694. doi: 10.1109/TGRS.2004.840720.

Martin, B. . . and John, I. (1983) 'Some partial indicators of scientific progress in radio astronomy of innovation in selected European grammes', *Research Policy*, 12(2), pp. 61–90.

Martinuzzi, S., Gould, W. A. and Ramos González, O. M. (2007) 'Land development, land use, and urban sprawl in Puerto Rico integrating remote sensing and population census data',

Landscape and Urban Planning, 79(3–4), pp. 288–297. doi: 10.1016/j.landurbplan.2006.02.014.

Mas, J.-F. (1999a) 'Monitoring land-cover changes: a com parison of change detection techniques', *International Journal of Remote Sensing*, 20(1), pp. 139–152. doi: 10.1080/014311699213659.

Mas, J.-F. (1999b) 'Monitoring land-cover changes: A comparison of change detection techniques', *International Journal of Remote Sensing*, 20(1), pp. 139–152. doi: 10.1080/014311699213659.

Mas, J. F. and Flores, J. J. (2008) 'The application of artificial neural networks to the analysis of remotely sensed data sensed data', *International Journal of Remote Sensing*, 29(3), pp. 617–663. doi: 10.1080/01431160701352154.

Matsushita, B., Yang, W., Chen, J., Onda, Y. and Qiu, G. (2007) 'Sensitivity of the Enhanced Vegetation Index (EVI) and Normalized Difference Vegetation Index (NDVI) to Topographic Effects: A Case Study in High-density Cypress Forest', *Sensors*, 7(11), pp. 2636–2651. doi: 10.3390/s7112636.

Maulik, U. and Bandyopadhyay, S. (2002) 'Performance evaluation of some clustering algorithms and validity indices', *IEEE Transactions on Pattern Analysis and Machine Intelligence*, 24(12), pp. 1650–1654. doi: 10.1109/TPAMI.2002.1114856.

McAlpine, C. A., Syktus, J., Ryan, J. G., Deo, R. C., McKeon, G. M., McGowan, H. A. and Phinn, S. R. (2009) 'A continent under stress: Interactions, feedbacks and risks associated with impact of modified land cover on Australia's climate', *Global Change Biology*, 15(9), pp. 2206–2223. doi: 10.1111/j.1365-2486.2009.01939.x.

McCray, W. P. (2000) 'Large Telescopes and the Moral of Economy of Recent Astronomy', *Social Studies of Science*, 30(5), pp. 685–711.

Mcgarigal, K. (2001) 'Landscape metrics for categorical map aatterns', 2001(Chapter 5), pp. 1–77. doi: 10.1007/BF00162741.

McIver, D. K. and Friedl, M. A. (2001) 'Estimating pixel-scale land cover classification confidence using nonparametric machine learning methods', *IEEE Transactions on Geoscience and Remote Sensing*, 39(9), pp. 1959–1968. doi: 10.1109/36.951086.

Meek, D. W. and Hatfield, J. L. (1994) 'Data quality checking for single station meteorological databases', *Agricultural and Forest Meteorology*, 69(1–2), pp. 85–109. doi: 10.1016/0168-1923(94)90083-3.

Mellor, A., Boukir, S., Haywood, A. and Jones, S. (2015) 'Exploring issues of training data imbalance and mislabelling on random forest performance for large area land cover classification using the ensemble margin', *ISPRS Journal of Photogrammetry and Remote Sensing*. International Society for Photogrammetry and Remote Sensing, Inc. (ISPRS), 105, pp. 155–168. doi: 10.1016/j.isprsjprs.2015.03.014.

Mercier, G., Derrode, E., Trouve, E. and Bombrun, L. (2012) 'Change detection in remote sensing observation', p. Chapter 4.

Metternicht, G., Hurni, L. and Gogu, R. (2005) 'Remote sensing of landslides: An analysis of the potential contribution to geo-spatial systems for hazard assessment in mountainous

environments', *Remote Sensing of Environment*, 98(2–3), pp. 284–303. doi: 10.1016/j.rse.2005.08.004.

Minale, A. S. and Kameswara Rao, K. (2012) 'Impacts of land cover/use dynamics of Gilgel Abbay catchment of Lake Tana on climate variability, Northwestern Ethiopia', *Applied Geomatics*, 4(3), pp. 155–162. doi: 10.1007/s12518-012-0092-2.

Miura, T., Huete, A. R., Yoshioka, H. and Holben, B. N. (2001) 'An error and sensitivity analysis of atmospheric resistant vegetation indices derived from dark target-based atmospheric correction', *Remote Sensing of Environment*, 78(3), pp. 284–298. doi: 10.1016/S0034-4257(01)00223-1.

Modarres, R. and de Paulo Rodrigues da Silva, V. (2007) 'Rainfall trends in arid and semi-arid regions of Iran', *Journal of Arid Environments*, 70(2), pp. 344–355. doi: 10.1016/j.jaridenv.2006.12.024.

Mondal, A., Kundu, S., Chandniha, S. K., Shukla, R. and Mishra, P. K. (2012) 'Comparison of Support Vector Machine and Maximum Likelihood Classification Technique using Satellite Imagery', *International Journal of Remote Sensing and GIS*, 1(2), pp. 116–123.

Mountrakis, G., Im, J. and Ogole, C. (2011a) 'Support vector machines in remote sensing: A review', *ISPRS Journal of Photogrammetry and Remote Sensing*. Elsevier B.V., 66(3), pp. 247–259. doi: 10.1016/j.isprsjprs.2010.11.001.

Mountrakis, G., Im, J. and Ogole, C. (2011b) 'Support vector machines in remote sensing: A review', *ISPRS Journal of Photogrammetry and Remote Sensing*, 66(3), pp. 247–259. doi: 10.1016/j.isprsjprs.2010.11.001.

Mulder, V. L., de Bruin, S., Schaepman, M. E. and Mayr, T. R. (2011) 'The use of remote sensing in soil and terrain mapping - A review', *Geoderma*. Elsevier B.V., 162(1–2), pp. 1–19. doi: 10.1016/j.geoderma.2010.12.018.

Muller-karger, F. E. and Andre, S. (2001) 'Change detection in shallow coral reef environments using Landsat 7 ETM + data . Remote Sens Environ Change detection in shallow coral reef environments using Landsat 7 ETM + data', 78(OCTOBER), pp. 150–162. doi: 10.1016/S0034-4257(01)00256-5.

Mumby, P. J. and Edwards, A. J. (2002) 'Mapping marine environments with IKONOS imagery: Enhanced spatial resolution can deliver greater thematic accuracy', *Remote Sensing of Environment*, 82(2–3), pp. 248–257. doi: 10.1016/S0034-4257(02)00041-X.

Muñoz-Villers, L. E. and López-Blanco, J. (2008) 'Land use/cover changes using Landsat TM/ETM images in a tropical and biodiverse mountainous area of central-eastern Mexico', *International Journal of Remote Sensing*, 29(1), pp. 71–93. doi: 10.1080/01431160701280967.

Munyati, C. (2000) 'Wetland change detection on the Kafue Flats, Zambia, by classification of a multitemporal remote sensing image dataset', *International Journal of Remote Sensing*, 21(9), pp. 1787–1806. doi: 10.1080/014311600209742.

Munyati, C. (2004) 'Use of Principal Component Analysis (PCA) of Remote Sensing Images in Wetland Change Detection on the Kafue Flats, Zambia', *Geocarto International*, 19(3), pp. 11–22. doi: 10.1080/10106040408542313.

Muttitanon, W. and Tripathi, N. K. (2005) ‘Land use/land cover changes in the coastal zone of Ban Don Bay, Thailand using Landsat 5 TM data’, *International Journal of Remote Sensing*, 26(11), pp. 2311–2323. doi: 10.1080/01431160512331326666.

Myint, S. W., Gober, P., Brazel, A., Grossman-Clarke, S. and Weng, Q. (2011) ‘Per-pixel vs. object-based classification of urban land cover extraction using high spatial resolution imagery’, *Remote Sensing of Environment*. Elsevier Inc., 115(5), pp. 1145–1161. doi: 10.1016/j.rse.2010.12.017.

Nagendra, H., Munroe, D. K. and Southworth, J. (2004) ‘From pattern to process: Landscape fragmentation and the analysis of land use/land cover change’, *Agriculture, Ecosystems and Environment*, 101(2–3), pp. 111–115. doi: 10.1016/j.agee.2003.09.003.

Nagendra, H., Pareeth, S. and Ghate, R. (2006) ‘People within parks - Forest villages, land-cover change and landscape fragmentation in the Tadoba Andhari Tiger Reserve, India’, *Applied Geography*, 26(2), pp. 96–112. doi: 10.1016/j.apgeog.2005.11.002.

Nairobi, I. (2012) ‘Remote sensing land-cover change in Port Elizabeth during South Africa ’ s democratic transition’, 108, pp. 1–7.

Nemani, R. R., Keeling, C. D., Hashimoto, H., Jolly, W. M., Piper, S. C., Tucker, C. J., Myneni, R. B. and Running, S. W. (2003) ‘Climate-driven increases in global terrestrial net primary production from 1982 to 1999.’, *Science (New York, N.Y.)*, 300(5625), pp. 1560–3. doi: 10.1126/science.1082750.

Neuenschwander, A. L. (2007) ‘Remote sensing of vegetation dynamics in response to flooding and fire in the Okavango Delta, Botswana’.

Nie, Q. and Xu, J. (2013) ‘The relationship between vegetation coverage and climate elements in Yellow River Basin, China’, (3). doi: 10.7287/peerj.preprints.153v1.

Ning, S. K., Chang, N. Bin, Jeng, K. Y. and Tseng, Y. H. (2006) ‘Soil erosion and non-point source pollution impacts assessment with the aid of multi-temporal remote sensing images’, *Journal of Environmental Management*, 79(1), pp. 88–101. doi: 10.1016/j.jenvman.2005.05.019.

Nsubuga, F. W., Olwoch, J. M. and Rautenbach, H. (2014) ‘Variability properties of daily and monthly observed near-surface temperatures in Uganda: 1960-2008’, *International Journal of Climatology*, 34(2), pp. 303–314. doi: 10.1002/joc.3686.

Nutini, F., Boschetti, M., Brivio, P. A., Bocchi, S. and Antoninetti, M. (2013) ‘Land-use and land-cover change detection in a semi-arid area of Niger using multi-temporal analysis of Landsat images’, *International Journal of Remote Sensing*, 34(13), pp. 4769–4790. doi: 10.1080/01431161.2013.781702.

Nyamadzawo, G., Gwenzi, W., Kanda, A., Kundhlande, A. and Masona, C. (2013) ‘Understanding the causes, socio-economic and environmental impacts, and management of veld fires in tropical Zimbabwe’, *Fire Science Reviews*, 2(1), p. 2. doi: 10.1186/2193-0414-2-2.

Otukei, J. R. and Blaschke, T. (2010) ‘Land cover change assessment using decision trees, support vector machines and maximum likelihood classification algorithms’, *International Journal of Applied Earth Observation and Geoinformation*, 12(SUPPL. 1), pp. 27–31. doi:

10.1016/j.jag.2009.11.002.

Otunga, C., Odindi, J. and Mutanga, O. (2014) 'Land Use Land Cover Change in the fringe of eThekwini Municipality: Implications for urban green spaces using remote sensing', 3(2), pp. 145–162.

Pal, M. and Mather, P. M. (2005) 'Support vector machines for classification in remote sensing', *International Journal of Remote Sensing*, 26(5), pp. 1007–1011. doi: 10.1080/01431160512331314083.

Pal, M., Maxwell, A. E. and Warner, T. A. (2013) 'Kernel-based extreme learning machine for remote-sensing image classification', *Remote Sensing Letters*, 4(9), pp. 853–862. doi: 10.1080/2150704X.2013.805279.

Paola, J. D. and Schowengerdt, R. A. (1995) 'A detailed comparison of backpropagation neural network and maximum-likelihood classifiers for urban land use classification', *Geoscience and Remote Sensing, IEEE Transactions on*, 33(4), pp. 981–996. doi: 10.1109/36.406684.

Papers, H. W. (2007) 'Application of FAO / UNEP Land Cover Classification System (LCCS) for study of land cover dynamics in SNPBZ Workshop Report', *Group*, (April), pp. 1–21.

Parker, D. C., Manson, S. M., Janssen, M. A., Hoffmann, M. J. and Deadman, P. (2003) 'Multi-agent systems for the simulation of land-use and land-cover change: A review', *Annals of the Association of American Geographers*, 93(2), pp. 314–337. doi: 10.1111/1467-8306.9302004.

Perumal, K. and Bhaskaran, R. (2010) 'Supervised classification performance of multispectral images', *Journal of Computing*, 2(2), pp. 124–129. Available at: http://arxiv.org/abs/1002.4046.

Peters, A. J., WalterShea, E. A., Lel JI, A. V., Hayes, M. and Svoboda, M. D. (2002) 'Drought monitoring with NDVI-based standardized vegetation index', *American Society for Photogrammetry and remote sensing*, 68(1), pp. 71–75. Available at: http://www.asprs.org/a/publications/pers/2002journal/january/2002_jan_71-75.pdf.

Peterson, T. C., Easterling, D. R., Karl, T. R., Groisman, P., Nicholls, N., Plummer, N., Torok, S., Auer, I., Boehm, R., Gullett, D., Vincent, L., Heino, R., Tuomenvirta, H., Mestre, O., Szentimrey, T., Salinger, J., Forland, E. J., Hanssen-Bauer, I., Alexandersson, H., Jones, P. and Parker, D. (1998) 'Homogeneity Adjustsments of in situ Atmospheric Climate Data: A Review', *International Journal of Climatology*, 18, pp. 1493–1517. doi: 10.1002/(SICI)1097-0088(19981115)18:13<1493::AID-JOC329>3.0.CO;2-T.

Pettorelli, N., Vik, J. O., Mysterud, A., Gaillard, J. M., Tucker, C. J. and Stenseth, N. C. (2005) 'Using the satellite-derived NDVI to assess ecological responses to environmental change', *Trends in Ecology and Evolution*, 20(9), pp. 503–510. doi: 10.1016/j.tree.2005.05.011.

Pinstrup-Andersen, P. (2009) 'Food Security: Definition and Measurement', *Food Security*, 1, pp. 5–7. doi: 10.1007/s12571-008-0002-y.

'Pixel-based image classification What is image classification or pattern recognition' (2008).

Potapov, P. V., Turubanova, S. A., Hansen, M. C., Adusei, B., Broich, M., Altstatt, A., Mane, L. and Justice, C. O. (2012) 'Quantifying forest cover loss in Democratic Republic of the Congo, 2000-2010, with Landsat ETM+ data', *Remote Sensing of Environment*. Elsevier Inc., 122, pp. 106–116. doi: 10.1016/j.rse.2011.08.027.

Pradhan, S. (2001) 'Crop Area Estimation Using GIS, Remote Sensing and Area Frame Sampling', *International Journal of Applied Earth Observation and Geoinformation*, 3(1), pp. 86–92. doi: 10.1016/S0303-2434(01)85025-X.

Quigley, J. M. (1998) 'Urban Diversity and Economic Growth', *Journal of Economic Perspectives*, 12(2), pp. 127–138. doi: 10.1257/jep.12.2.127.

Quincey, D. J., Lucas, R. M., Richardson, S. D., Glasser, N. F., Hambrey, M. J. and Reynolds, J. M. (2005) 'Optical remote sensing techniques in high-mountain environments: application to glacial hazards', *Progress in Physical Geography*, 29(4), pp. 475–505. doi: 10.1191/0309133305pp456ra.

Rahman, M., Ullah, R., Lan, M., Sri Sumantyo, J. T., Kuze, H. and Tateishi, R. (2013) 'Comparison of Landsat image classification methods for detecting mangrove forests in Sundarbans', *International Journal of Remote Sensing*, 34(4), pp. 1041–1056. doi: 10.1080/01431161.2012.717181.

Raudsepp-Hearne, C., Peterson, G. D., Tengö, M., Bennett, E. M., Holland, T., Benessaiah, K., MacDonald, G. K. and Pfeifer, L. (2010) 'Untangling the Environmentalist's Paradox: Why Is Human Well-being Increasing as Ecosystem Services Degrade?', *BioScience*, 60(8), pp. 576–589. doi: 10.1525/bio.2010.60.8.4.

Riaño, D., Chuvieco, E., Salas, J. and Aguado, I. (2003) 'Assesment of Different Topographic Corrections in Landsat -TM Data for Mapping Vegetation Types', *IEEE Transactions on Geoscience and Remote Sensing*, 41(5), pp. 1056–1061. doi: 10.1109/TGRS.2003.811693.

Ridd, M. K. and Liu, J. (1998) 'A comparison of four algorithms for change detection in an urban environment', *Remote Sensing of Environment*, 63(2), pp. 95–100. doi: 10.1016/S0034-4257(97)00112-0.

Robert A. Schowengerdt (2012) *Remote Sensing: Models and Methods for Image Processing*, *Journal of environmental management*. doi: 10.1016/j.jenvman.2011.10.007.

Rocchini, D. and Di Rita, A. (2005) 'Relief effects on aerial photos geometric correction', *Applied Geography*, 25(2), pp. 159–168. doi: 10.1016/j.apgeog.2005.03.002.

Röder, A., Udelhoven, T., Hill, J., del Barrio, G. and Tsiourlis, G. (2008) 'Trend analysis of Landsat-TM and -ETM+ imagery to monitor grazing impact in a rangeland ecosystem in Northern Greece', *Remote Sensing of Environment*, 112(6), pp. 2863–2875. doi: 10.1016/j.rse.2008.01.018.

De Roeck, E. R., Verhoest, N. E. C., Miya, M. H., Lievens, H., Batelaan, O., Thomas, A. and Brendonck, L. (2008) 'Remote sensing and wetland ecology: A South African case study', *Sensors*, 8(5), pp. 3542–3556. doi: 10.3390/s8053542.

Roerink, G. J., Menenti, M., Soepboer, W. and Su, Z. (2003) 'Assessment of climate impact on vegetation dynamics by using remote sensing', *Physics and Chemistry of the Earth*, 28(1–

3), pp. 103–109. doi: 10.1016/S1474-7065(03)00011-1.

Rogan, J., Franklin, J., Stow, D., Miller, J., Woodcock, C. and Roberts, D. (2008) 'Mapping land-cover modifications over large areas: A comparison of machine learning algorithms', *Remote Sensing of Environment*, 112(5), pp. 2272–2283. doi: 10.1016/j.rse.2007.10.004.

Rogerson, P. (2002) 'Change detection thresholds for remotely sensed images', *Journal of Geographical Systems*, 4(1), pp. 85–97. doi: 10.1007/s101090100076.

Rokni, K., Ahmad, A., Solaimani, K. and Hazini, S. (2015) 'A new approach for surface water change detection: Integration of pixel level image fusion and image classification techniques', *International Journal of Applied Earth Observation and Geoinformation*. Elsevier B.V., 34(1), pp. 226–234. doi: 10.1016/j.jag.2014.08.014.

Romero-Ruiz, M. H., Flantua, S. G. A., Tansey, K. and Berrio, J. C. (2012) 'Landscape transformations in savannas of northern South America: Land use/cover changes since 1987 in the Llanos Orientales of Colombia', *Applied Geography*. Elsevier Ltd, 32(2), pp. 766–776. doi: 10.1016/j.apgeog.2011.08.010.

Rosin, P. L. (2002) 'Thresholding for Change Detection', *Computer Vision and Image Understanding*, 86(2), pp. 79–95. doi: 10.1006/cviu.2002.0960.

Roy, D. P., Wulder, M. A., Loveland, T. R., C.E., W., Allen, R. G., Anderson, M. C., Helder, D., Irons, J. R., Johnson, D. M., Kennedy, R., Scambos, T. A., Schaaf, C. B., Schott, J. R., Sheng, Y., Vermote, E. F., Belward, A. S., Bindschadler, R., Cohen, W. B., Gao, F., Hipple, J. D., Hostert, P., Huntington, J., Justice, C. O., Kilic, A., Kovalskyy, V., Lee, Z. P., Lymburner, L., Masek, J. G., McCorkel, J., Shuai, Y., Trezza, R., Vogelmann, J., Wynne, R. H. and Zhu, Z. (2014) 'Landsat-8: Science and product vision for terrestrial global change research', *Remote Sensing of Environment*. Elsevier B.V., 145, pp. 154–172. doi: 10.1016/j.rse.2014.02.001.

Rozenstein, O. and Karnieli, A. (2011) 'Comparison of methods for land-use classification incorporating remote sensing and GIS inputs', *Applied Geography*. Elsevier Ltd, 31(2), pp. 533–544. doi: 10.1016/j.apgeog.2010.11.006.

Ruelland, D., Levavasseur, F. and Tribotté, A. (2010) 'Patterns and dynamics of land-cover changes since the 1960s over three experimental areas in Mali', *International Journal of Applied Earth Observation and Geoinformation*, 12(SUPPL. 1). doi: 10.1016/j.jag.2009.10.006.

Ruelland, D., Tribotte, A., Puech, C. and Dieulin, C. (2011) 'Comparison of methods for LUCC monitoring over 50 years from aerial photographs and satellite images in a Sahelian catchment', *International Journal of Remote Sensing*, 32(6), pp. 1747–1777. doi: 10.1080/01431161003623433.

Sakai, T., Hatta, S., Okumura, M., Hiyama, T., Yamaguchi, Y. and Inoue, G. (2015) 'Use of Landsat TM/ETM+ to monitor the spatial and temporal extent of spring breakup floods in the Lena River, Siberia', *International Journal of Remote Sensing*, 36(May), pp. 719–733. doi: 10.1080/01431161.2014.995271.

Santillan, J., Makinano, M. and Paringit, E. (2011) 'Integrated landsat image analysis and hydrologic modeling to detect impacts of 25-year land-cover change on surface runoff in a Philippine watershed', *Remote Sensing*, 3(6), pp. 1067–1087. doi: 10.3390/rs3061067.

Sawaya, K. E., Olmanson, L. G., Heinert, N. J., Brezonik, P. L. and Bauer, M. E. (2003) 'Extending satellite remote sensing to local scales: Land and water resource monitoring using high-resolution imagery', *Remote Sensing of Environment*, 88(1–2), pp. 144–156. doi: 10.1016/j.rse.2003.04.006.

Schneider, A. and Woodcock, C. E. (2008) 'Compact, Dispersed, Fragmented, Extensive? A Comparison of Urban Growth in Twenty-five Global Cities using Remotely Sensed Data, Pattern Metrics and Census Information', *Urban Studies*, 45(3), pp. 659–692. doi: 10.1177/0042098007087340.

Schroeder, T. A., Cohen, W. B., Song, C., Canty, M. J. and Yang, Z. (2006) 'Radiometric correction of multi-temporal Landsat data for characterization of early successional forest patterns in western Oregon', *Remote Sensing of Environment*, 103(1), pp. 16–26. doi: 10.1016/j.rse.2006.03.008.

Schueler, V., Kuemmerle, T. and Schröder, H. (2011) 'Impacts of surface gold mining on land use systems in Western Ghana', *Ambio*, 40(5), pp. 528–539. doi: 10.1007/s13280-011-0141-9.

Serpico, S. B., Bruzzone, L. and Roli, F. (1996a) 'An experimental comparison of neural and statistical non-parametric algorithms for supervised classification of remote-sensing images', *Pattern Recognition Letters*, 17(13), pp. 1331–1341. doi: 10.1016/S0167-8655(96)00090-6.

Serpico, S. B., Bruzzone, L. and Roli, F. (1996b) 'An experimental comparison of neural and statistical non-parametric algorithms for supervised classification of remote sensing images', *Pattern Recognition Letters*, 17(3), pp. 1331–1341.

Serra, P., Pons, X. and Saur??, D. (2008) 'Land-cover and land-use change in a Mediterranean landscape: A spatial analysis of driving forces integrating biophysical and human factors', *Applied Geography*, 28(3), pp. 189–209. doi: 10.1016/j.apgeog.2008.02.001.

Sesnie, S. E., Dickson, B. G., Rosenstock, S. S. and Rundall, J. M. (2011) 'A comparison of Landsat TM and MODIS vegetation indices for estimating forage phenology in desert bighorn sheep (Ovis canadensis nelsoni) habitat in the Sonoran Desert, USA', *International Journal of Remote Sensing*, 33(1), pp. 276–286. doi: 10.1080/01431161.2011.592865.

Shalaby, A. and Tateishi, R. (2007) 'Remote sensing and GIS for mapping and monitoring land cover and land-use changes in the Northwestern coastal zone of Egypt', *Applied Geography*, 27(1), pp. 28–41. doi: 10.1016/j.apgeog.2006.09.004.

Sharma, L., Pandey, P. C. and Nathawat, M. S. (2012) 'Assessment of land consumption rate with urban dynamics change using geospatial techniques', *Journal of Land Use Science*, 7(2), pp. 135–148. doi: 10.1080/1747423x.2010.537790.

Shevyrnogov, A., Trefois, P. and Vysotskaya, G. (2000) 'Multi-satellite data merge to combine NOAA AVHRR efficiency with landsat-6 MSS spatial resolution to study vegetation dynamics', *Advances in Space Research*, 26(7), pp. 1131–1133. doi: 10.1016/S0273-1177(99)01130-8.

Shuying, J., Deren, L. and Jingwen, W. (2005) 'A Comparison of Support Vector Machine with Maximum Likelihood Classification Algorithms on Texture Features', *Spectrum*, 00(Idm), pp. 3717–3720.

Si, H., Bi, H., Li, X. and Yang, C. (2010) 'Environmental evaluation for sustainable development of coal mining in Qijiang, Western China', *International Journal of Coal Geology*. Elsevier B.V., 81(3), pp. 163–168. doi: 10.1016/j.coal.2009.11.004.

Singh, A. (1989) 'Review Article: Digital change detection techniques using remotely-sensed data', *International Journal of Remote Sensing*, 10(6), pp. 989–1003. doi: 10.1080/01431168908903939.

Skelsey, C., Law, a. N. R., Winter†, M., Lishman, J. R. and Winter, M. (2003) 'A system for monitoring land cover', *International Journal of Remote Sensing*, 24(23), pp. 4853–4869. doi: 10.1080/0143116031000101585.

Small, C. (2006) 'Comparative analysis of urban reflectance and surface temperature', *Remote Sensing of Environment*, pp. 168–189. doi: DOI 10.1016/j.rse.2005.10.029.

Song, C., Woodcock, C. E., Seto, K. C., Lenney, M. P. and Macomber, S. A. (2001) 'Classification and change detection using Landsat TM data: When and how to correct atmospheric effects?', *Remote Sensing of Environment*, 75(2), pp. 230–244. doi: 10.1016/S0034-4257(00)00169-3.

Southworth, J. (2004) 'An assessment of Landsat TM band 6 thermal data for analysing land cover in tropical dry forest regions.', *International Journal of Remote Sensing*, 25(4), pp. 689–706. doi: 10.1080/0143116031000139917.

Southworth, J., Nagendra, H. and Tucker, C. (2002) 'Fragmentation of a landscape: Incorporating landscape metrics into satellite analyses of land-cover change', *Landscape Research*, 27(3), pp. 253–269. doi: 10.1080/01426390220149511.

Stefanov, W. L. (2001) 'Monitoring urban land cover change: An expert system approach to land cover classification of semiarid to urban centers', *Remote Sensing of Environment*, 77, pp. 173–185. doi: 10.1016/S0034-4257(01)00204-8.

Sterling, S. M., Ducharne, A. and Polcher, J. (2013) 'The impact of global land-cover change on the terrestrial water cycle', *Nature Climate Change*. Nature Publishing Group, 3(4), pp. 385–390. doi: Doi 10.1038/Nclimate1690.

Strahler, A. H. (1980) 'The use of prior probabilities in maximum likelihood classification of remotely sensed data.', *Remote Sensing of Environment*, 10(2), pp. 135–163. doi: 10.1016/0034-4257(80)90011-5.

Stroppiana, D., Bordogna, G., Carrara, P., Boschetti, M., Boschetti, L. and Brivio, P. A. (2012) 'A method for extracting burned areas from Landsat TM/ETM+ images by soft aggregation of multiple Spectral Indices and a region growing algorithm', *ISPRS Journal of Photogrammetry and Remote Sensing*. International Society for Photogrammetry and Remote Sensing, Inc. (ISPRS), 69, pp. 88–102. doi: 10.1016/j.isprsjprs.2012.03.001.

Sun, J., Yang, J., Zhang, C., Yun, W. and Qu, J. (2013) 'Automatic remotely sensed image classification in a grid environment based on the maximum likelihood method', *Mathematical and Computer Modelling*. Elsevier Ltd, 58(3–4), pp. 573–581. doi: 10.1016/j.mcm.2011.10.063.

Sutton, P., Elvidge, C. and Ghosh, T. (2007) 'Estimation of gross domestic product at sub-national scales using nighttime satellite imagery', *International Journal of Ecological*

Economics & Statistics, 8(S07), pp. 5–21. Available at: http://urizen-geography.nsm.du.edu/~psutton/AAA_Sutton_WebPage/Sutton/Publications/Sut_Pub_13.pdf .

Swetnam, R. D., Fisher, B., Mbilinyi, B. P., Munishi, P. K. T., Willcock, S., Ricketts, T., Mwakalila, S., Balmford, A., Burgess, N. D., Marshall, A. R. and Lewis, S. L. (2011) 'Mapping socio-economic scenarios of land cover change: A GIS method to enable ecosystem service modelling', *Journal of Environmental Management*. Elsevier Ltd, 92(3), pp. 563–574. doi: 10.1016/j.jenvman.2010.09.007.

Taylor, P., Pohl, C. and Genderen, J. L. Van (2010) *Review article Multisensor image fusion in remote sensing : Concepts , methods and applications*, *International Journal of Remote Sensing*. doi: 10.1080/014311698215748.

Telcan (2013) 'Remote sensing', *Remote Sensing Tutorial*, p. 337. doi: 10.1109/6.367967.

Tewkesbury, A. P., Comber, A. J., Tate, N. J., Lamb, A. and Fisher, P. F. (2015) 'A critical synthesis of remotely sensed optical image change detection techniques', *Remote Sensing of Environment*. Elsevier Inc., 160, pp. 1–14. doi: 10.1016/j.rse.2015.01.006.

Tilahun, A. (2015) 'Accuracy Assessment of Land Use Land Cover Classification using Google Earth', *American Journal of Environmental Protection*, 4(4), p. 193. doi: 10.11648/j.ajep.20150404.14.

Toth, D. and Aach, T. (2001) 'Improved minimum distance classification with Gaussian outlier detection for industrial inspection', *Proceedings - 11th International Conference on Image Analysis and Processing, ICIAP 2001*, pp. 584–588. doi: 10.1109/ICIAP.2001.957073.

Townsend, P. A., Helmers, D. P., Kingdon, C. C., McNeil, B. E., de Beurs, K. M. and Eshleman, K. N. (2009) 'Changes in the extent of surface mining and reclamation in the Central Appalachians detected using a 1976-2006 Landsat time series', *Remote Sensing of Environment*. Elsevier Inc., 113(1), pp. 62–72. doi: 10.1016/j.rse.2008.08.012.

Turner II, B. ., Lambin, E. F. and Reenberg, A. (2007) 'The emergence of land change science for global environmental change and sustainability', 104(128), pp. 20666–20671.

Uuemaa, E., Antrop, M., Marja, R., Roosaare, J. and Mander, Ü. (2009) 'Landscape Metrics and Indices : An Overview of Their Use in Landscape Research Imprint / Terms of Use', *Living Reviews in Landscape Research*, 3, pp. 1–28. doi: 10.12942/lrlr-2009-1.

Vancutsem, C., Ceccato, P., Dinku, T. and Connor, S. J. (2010) 'Evaluation of MODIS land surface temperature data to estimate air temperature in different ecosystems over Africa', *Remote Sensing of Environment*. Elsevier Inc., 114(2), pp. 449–465. doi: 10.1016/j.rse.2009.10.002.

Vicente-Serrano, S. M., Pérez-Cabello, F. and Lasanta, T. (2008) 'Assessment of radiometric correction techniques in analyzing vegetation variability and change using time series of Landsat images', *Remote Sensing of Environment*, 112(10), pp. 3916–3934. doi: 10.1016/j.rse.2008.06.011.

Villamuelas, M., Fernández, N., Albanell, E., Gálvez-Cerón, A., Bartolomé, J., Mentaberre, G., López-Olvera, J. R., Fernández-Aguilar, X., Colom-Cadena, A., López-Martín, J. M., Pérez-Barbería, J., Garel, M., Marco, I. and Serrano, E. (2016) 'The Enhanced Vegetation

Index (EVI) as a proxy for diet quality and composition in a mountain ungulate', *Ecological Indicators*. Elsevier Ltd, 61, pp. 658–666. doi: 10.1016/j.ecolind.2015.10.017.

Vinukollu, R. K., Wood, E. F., Ferguson, C. R. and Fisher, J. B. (2011) 'Global estimates of evapotranspiration for climate studies using multi-sensor remote sensing data: Evaluation of three process-based approaches', *Remote Sensing of Environment*. Elsevier Inc., 115(3), pp. 801–823. doi: 10.1016/j.rse.2010.11.006.

Vogelmann, J. E., Helder, D., Morfitt, R., Choate, M. J., Merchant, J. W. and Bulley, H. (2001) 'Effects of Landsat 5 Thematic Mapper and Landsat 7 Enhanced Thematic Mapper plus radiometric and geometric calibrations and corrections on landscape characterization', *Remote Sensing of Environment*, 78(1–2), pp. 55–70. doi: 10.1016/S0034-4257(01)00249-8.

Waqar, M. M., Mirza, J. F., Mumtaz, R. and Hussain, E. (2012) 'Development of New Indices for Extraction of Built-Up Area & Bare Soil', *Open Access Scientific Reports*, 1(1), pp. 1–4. doi: 10.4172/scientificreports.13.

Ward, D., Phinn, S. R. and Murray, A. T. (2000) 'Monitoring Growth in Rapidly Urbanizing Areas Using Remotely Sensed Data', *The Professional Geographer*, 52(3), pp. 371–386. doi: 10.1111/0033-0124.00232.

Wasige, J. E., Groen, T. A., Smaling, E. and Jetten, V. (2012) 'Monitoring basin-scale land cover changes in Kagera Basin of Lake Victoria using: Ancillary data and remote sensing', *International Journal of Applied Earth Observation and Geoinformation*. Elsevier B.V., 21(1), pp. 32–42. doi: 10.1016/j.jag.2012.08.005.

Wedderburn-bisshop, A. G., Walls, J., Senarath, U. and Stewart, A. (2001) 'Methodology for mapping change in woody landcover over Queensland from 1999 to 2001 using Landsat ETM + .', pp. 1–10.

Weiss, J. L., Gutzler, D. S., Coonrod, J. E. A. and Dahm, C. N. (2004) 'Long-term vegetation monitoring with NDVI in a diverse semi-arid setting, central New Mexico, USA', *Journal of Arid Environments*, 58(2), pp. 249–272. doi: 10.1016/j.jaridenv.2003.07.001.

Weng, Q. (2002) 'Land use change analysis in the Zhujiang Delta of China using satellite remote sensing, GIS and stochastic modelling.', *Journal of environmental management*, 64(3), pp. 273–284. doi: 10.1006/jema.2001.0509.

Weng, Q., Lu, D. and Schubring, J. (2004) 'Estimation of land surface temperature-vegetation abundance relationship for urban heat island studies', *Remote Sensing of Environment*, 89(4), pp. 467–483. doi: 10.1016/j.rse.2003.11.005.

Weyerhaeuser, H., Wilkes, A. and Kahrl, F. (2005) 'Local impacts and responses to regional forest conservation and rehabilitation programs in China's northwest Yunnan province', *Agricultural Systems*, 85(3 SPEC. ISS.), pp. 234–253. doi: 10.1016/j.agsy.2005.06.008.

Whiteside, T. G., Boggs, G. S. and Maier, S. W. (2011) 'Comparing object-based and pixel-based classifications for mapping savannas', *International Journal of Applied Earth Observation and Geoinformation*. Elsevier B.V., 13(6), pp. 884–893. doi: 10.1016/j.jag.2011.06.008.

Wilson, E. H. and Sader, S. A. (2002) 'Detection of forest harvest type using multiple dates of Landsat TM imagery . Remote Sens Environ Detection of forest harvest type using

multiple dates', 80(October 2015), pp. 385–396. doi: 10.1016/S0034-4257(01)00318-2.

Wu, C. (2004) 'Normalized spectral mixture analysis for monitoring urban composition using ETM+ imagery', *Remote Sensing of Environment*, 93(4), pp. 480–492. doi: 10.1016/j.rse.2004.08.003.

Wu, J. (2008) 'The magazine of food, farm, and resource issues Land Use Changes: Economic, Social, and Environmental Impacts', *CHOICES 4th Quarter*, 23(4).

Wu, Z., Hu, Z. and Fan, Q. (2012) 'Superpixel-Based Unsupervised Change Detection Using Multi-Dimensional Change Vector Analysis and Svm-Based Classification', *ISPRS Annals of Photogrammetry, Remote Sensing and Spatial Information Sciences*, I-7(September), pp. 257–262. doi: 10.5194/isprsannals-I-7-257-2012.

Wulder, M. A., White, J. C., Goward, S. N., Masek, J. G., Irons, J. R., Herold, M., Cohen, W. B., Loveland, T. R. and Woodcock, C. E. (2008) 'Landsat continuity: Issues and opportunities for land cover monitoring', *Remote Sensing of Environment*, 112(3), pp. 955–969. doi: 10.1016/j.rse.2007.07.004.

Xian, G., Homer, C. and Fry, J. (2009) 'Updating the 2001 National Land Cover Database land cover classification to 2006 by using Landsat imagery change detection methods', *Remote Sensing of Environment*. Elsevier Inc., 113(6), pp. 1133–1147. doi: 10.1016/j.rse.2009.02.004.

Xiang, S., Nie, F. and Zhang, C. (2008) 'Learning a Mahalanobis distance metric for data clustering and classification', *Pattern Recognition*, 41(12), pp. 3600–3612. doi: 10.1016/j.patcog.2008.05.018.

Xiao, H. and Weng, Q. (2007) 'The impact of land use and land cover changes on land surface temperature in a karst area of China', *Journal of Environmental Management*, 85(1), pp. 245–257. doi: 10.1016/j.jenvman.2006.07.016.

Xiuwan, C. (2002) 'Using remote sensing and GIS to analyse land cover change and its impacts on regional sustainable development', *International Journal of Remote Sensing*, 23(1), pp. 107–124. doi: 10.1080/01431160010007051.

Xu, H. (2006) 'Modification of normalised difference water index (NDWI) to enhance open water features in remotely sensed imagery', *International Journal of Remote Sensing*, 27(14), pp. 3025–3033. doi: 10.1080/01431160600589179.

Xu, H. (2007) 'Extraction of urban built-up land features from Landsat imagery using a thematic-oriented index combination technique', *Photogrammetric Engineering and Remote Sensing*, 73(12), pp. 1381–1391. doi: 10.14358/PERS.73.12.1381.

Xu, M. and Wei, C. (2012) 'Remotely sensed image classification by complex network eigenvalue and connected degree', *Computational and Mathematical Methods in Medicine*, 2012. doi: 10.1155/2012/632703.

Yan, G., Mas, J. -F., Maathuis, B. H. P., Xiangmin, Z. and Van Dijk, P. M. (2006) 'Comparison of pixel-based and object-oriented image classification approaches—a case study in a coal fire area, Wuda, Inner Mongolia, China', *International Journal of Remote Sensing*, 27(18), pp. 4039–4055. doi: 10.1080/01431160600702632.

Yang, J., Weisberg, P. J. and Bristow, N. A. (2012) 'Landsat remote sensing approaches for

monitoring long-term tree cover dynamics in semi-arid woodlands: Comparison of vegetation indices and spectral mixture analysis', *Remote Sensing of Environment*, pp. 62–71. doi: 10.1016/j.rse.2011.12.004.

Yang, X. and Lo, C. P. (2002) 'Using a time series of satellite imagery to detect land use and land cover changes in the Atlanta, Georgia metropolitan area', *International Journal of Remote Sensing*, 23(9), pp. 1775–1798. doi: 10.1080/01431160110075802.

Yousefi, S., Khatami, R., Mountrakis, G., Mirzaee, S., Pourghasemi, H. R. and Tazeh, M. (2015) 'Accuracy assessment of land cover/land use classifiers in dry and humid areas of Iran', *Environmental Monitoring and Assessment*, 187(10). doi: 10.1007/s10661-015-4847-1.

Yu, L. and Gong, P. (2012) 'Google Earth as a virtual globe tool for Earth science applications at the global scale: progress and perspectives', *International Journal of Remote Sensing*, 33(12), pp. 3966–3986. doi: 10.1080/01431161.2011.636081.

Yuan, F., Sawaya, K. E., Loeffelholz, B. C. and Bauer, M. E. (2005) 'Land cover classification and change analysis of the Twin Cities (Minnesota) metropolitan area by multitemporal Landsat remote sensing', *Remote Sensing of Environment*, 98(2–3), pp. 317–328. doi: 10.1016/j.rse.2005.08.006.

Zha, Y., Gao, J. and Ni, S. (2003) 'Use of normalized difference built-up index in automatically mapping urban areas from TM imagery', *International Journal of Remote Sensing*, 24(3), pp. 583–594. doi: 10.1080/01431160304987.

Zhang, D., Chen, S. and Zhou, Z. H. (2006) 'Learning the kernel parameters in kernel minimum distance classifier', *Pattern Recognition*, 39(1), pp. 133–135. doi: 10.1016/j.patcog.2005.08.001.

Zhao, H. Z. H. and Chen, X. C. X. (2005) 'Use of normalized difference bareness index in quickly mapping bare areas from TM/ETM+', *Proceedings. 2005 IEEE International Geoscience and Remote Sensing Symposium, 2005. IGARSS '05.*, 3, pp. 1666–1668. doi: 10.1109/IGARSS.2005.1526319.

Zhou, Q., Li, B. and Kurban, a. (2008) 'Trajectory analysis of land cover change in arid environment of China', *International Journal of Remote Sensing*, 29(4), pp. 1093–1107. doi: 10.1080/01431160701355256.

Zhou, Y., Yang, G., Wang, S., Wang, L., Wang, F. and Liu, X. (2014) 'A new index for mapping built-up and bare land areas from Landsat-8 OLI data', *Remote Sensing Letters*. Taylor & Francis, 5(10), pp. 862–871. doi: 10.1080/2150704X.2014.973996.

Zhu, G. and Blumberg, D. G. (2002) 'Classification using ASTER data and SVM algorithms';, *Remote Sensing of Environment*, 80(2), pp. 233–240. doi: 10.1016/S0034-4257(01)00305-4.

Zhu, Z. and Woodcock, C. E. (2014) 'Continuous change detection and classification of land cover using all available Landsat data', *Remote Sensing of Environment*. Elsevier Inc., 144, pp. 152–171. doi: 10.1016/j.rse.2014.01.011.

Zhu, G. and Blumberg, D. G. (2002) 'Classification using ASTER data and SVM algorithms';, *Remote Sensing of Environment*, 80(2), pp. 233–240. doi: 10.1016/S0034-4257(01)00305-4.

Zhu, Z. and Woodcock, C. E. (2014) ‘Continuous change detection and classification of land cover using all available Landsat data’, *Remote Sensing of Environment*. Elsevier Inc., 144, pp. 152–171. doi: 10.1016/j.rse.2014.01.011.